CHEMICAL COMPOSITION OF SATURN'S

RINGS AND ICY SATELLITES

by

LARRY ALLEN LEBOFSKY

B.S., Caltech, Pasadena, California (1969)

SUBMITTED IN PARTIAL FULFILLMENT OF THE

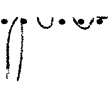REQUIREMENTS FOR THE

DEGREE OF (DOCTOR OF SCIENCE)
Ph. D.

at the
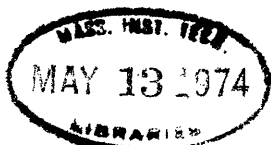
MASSACHUSETTS INSTITUTE OF TECHNOLOGY

December, 1973, *i.e. February 1974*

SIGNATURE OF AUTHOR ... ...
                                Department of Earth and
                                Planetary Sciences,
                                December, 1973

CERTIFIED BY ... ...
                                        Thesis Supervisor

ACCEPTED BY ... ...
                                Chairman, Departmental
                            Committee on Graduate Students

CHEMICAL COMPOSITION OF SATURN'S
RINGS AND ICY SATELLITES

by

LARRY ALLEN LEBOFSKY

SUBMITTED TO THE DEPARTMENT OF EARTH AND PLANETARY SCIENCES

IN PARTIAL FULFILLMENT OF THE REQUIREMENTS FOR THE

DEGREE OF DOCTOR OF SCIENCE

ABSTRACT: The spectral reflectivities of the surfaces of solar system bodies have been studied and compared with laboratory studies of various frosts. Calculations on the stability (against evaporation) of the surface frosts of these bodies were also carried out. These results have been combined to determine the composition of the surfaces of icy satellites and Saturn's rings. The surfaces of the Galilean satellites of Jupiter and Saturn's rings are composed of water frost contaminated with solar ultraviolet irradiated NH_3 and H_2S frosts producing decreased reflectivities shortward of 0.5μ. It is also concluded that the surfaces of Saturn's satellites are probably composed mainly of ammonium hydrates.

Thesis supervisor: John S. Lewis
Title: Associate Professor of Geochemistry and Chemistry

ACKNOWLEDGEMENTS

I wish to thank Dr. John Lewis, my thesis advisor, for the guidance provided throughout the completion of this work.

I also thank Lawrence Bass and Bruce Fegley for their invaluable help in computer programing and helpful discussions.

I finally thank the members of my committee: Professors J. S. Lewis, R. G. Burns, S. G. Kleinmann, T. B. McCord and R. G. Prinn for constructive conversations.

But, my greatest and warmest thanks goes to my wife Marcia for her encouragement and advice while I worked on this thesis.

TABLE OF CONTENTS

LIST OF TABLES

Table II-1:

The characteristics of the visible filter set used for all ring and star runs.

Table II-2:

The normalized fluxes of the standard stars, the sun and the rings.

Table III-1:

Wavelengths of observed absorption bands (Figure III-6) and their assigned vibrational modes.

Table A-1:

The calculated data for the determination of vapor pressures.

CRC   Handbook of Chemistry and Physics, 197]
M   Miller, 1961
ICT   International Critical Tables, 1929
LAL   Values calculated by the author in Appendix A
CRC uses the formula: $\log P_{mm} = 0.2185/T + B$
All others: $\log P_{mm} = A/T + B$
Where P_{mm} is the vapor pressure of the gas over the solid in millimeters of mercury (Torr).

Table B-1:

Several examples of the data used to make Table B-2. The
second line for each number represents the exponent, eg.:

   0.101744   0.101744X10$^{-3.00}$
     -3.00

Table B-2:

Table B-2 summarizes the results of our calculations. The
table contains the evaporation rates of the frosts from
Appendix A. The numbers represent $\log_{10}$(cm) of the evapora-
tion rate per billion years (eg. 10^5 cm/10^9 years = 5).
Evaporation rates greater than 10^8 cm/10^9 years are labeled
U (unstable) and less than 10^0 cm/10^9 years 0 (no evaporation).
Note that for Saturn's rings anything over tens of meters is
probably unstable since the particles are about that size.
For a given planet, four numbers are given which represent
0° (equator) and 60° latitude for albedoes of 0.7 and 0.5.
Eg:

<div align="center">

JUPITER

   0°   60°

A=0.7   A=0.5   A=0.7   A=0.5

</div>

The third column for Saturn assumes a rapidly rotating body
which may be valid for the ring particles.

I. Introduction

The determination of the composition of the surfaces
of solar system bodies has generally been limited to
silicate surfaces (McCord and Adams,1969; McCord, Adams and
Johnson, 1970; McCord and Johnson, 1970; Chapman, 1971;
Huguenin, 1973; Gaffey, 1973). Only in the last four years
have visible and infrared reflection spectra of bodies with
icy surfaces (satellites of Jupiter and Saturn and Saturn's
rings) been detailed enough to begin to determine the possible
composition of the surfaces. For several bodies (Galilean
satellites and Saturn's rings) infrared spectra have shown
the presence of water frost (Pilcher, et al., 1970; Pilcher,
et al., 1973; Fink, et al., 1973). Visible spectra of these
icy bodies have complicated the problem. Two types of spectra
have been seen: flat, featureless spectra (Saurn's satellites;
McCord, Johnson and Elias, 1971) and spectra that show blue
and ultraviolet decreases in reflectivity (Galilean satellites,
Johnson and McCord, 1970; Saturn's rings, Lebofsky, et al.,
1970). The second set of objects have had water frost iden-
tified on their surfaces and so the water frost must be
contaminated by some as yet unknown coloring agent.

This work was originally intended to be a study of the
spectral reflectance properties of Saturn's rings in an
attempt to determine the composition of the ring particles.
But, when an attempt was made to compare the telescopic
results with laboratory visible spectra of frosts,it was

found that no relevant laboratory spectra existed. The scope of this thesis was therefore expanded to encompass a study of frosts in the laboratory and to investigate the stability of these frosts in the solar system. Since the surfaces of atmosphereless satellites are exposed to solar ultraviolet radiation, the frosts investigated in the laboratory are also exposed to ultraviolet radiation to examine the reflectance properties of the resultant irradiated frosts.

This work thus presents an investigation of the spectral reflectance properties of frosts and the likelihood of finding these frosts on the surfaces of satellites and in Saturn's rings, and compares these results with known reflection spectra in an attempt to determine the chemical composition of the surfaces of these bodies.

II. Telescopic Observations

a) Introduction

The rings of Saturn have fascinated scientists since they were first observed by Galileo in the seventeenth century. Early studies of the rings were limited to purely observational investigations, in an attempt to determine their size, shape and general structure. The introduction of micrometric, photographic and photometric techniques and attempts to determine theoretically the structure of the rings have greatly increased our knowledge of the rings. As these rings are unique in the solar system, any theory which accounts for the formation of the solar system must also explain the rings. The problem of their formation and present state has been approached from several directions with little agreement among astronomers as to the answers.

There are three rings: A, B and C ("Crepe" ring). Ring B is the brightest, ring A is next in brightness and somewhat transparent. Ring C is the faintest ring and is noticeably transparent as seen when the rings are projected against the planet.

From our position on Earth we can study the rings through only reflected and radiated energy. The wavelength dependence of the reflection spectrum of a surface is determined primarily by the composition, mineralogy and particle size of the surface materials. Investigations in the IR region ($1.2-2.5\mu$) have shown that the reflection spectrum of the rings most closely resembles laboratory IR spectra of water frost (Pilcher,

et al., 1970). In compiling the literature on the rings, it soon became clear that more work was needed to determine the chemical composition of Saturn's rings. The lack of any intensive investigations of the visible (0.3-1.1μ) reflection spectrum of the rings led the author to make this study in the hope of better defining their chemical composition.

For detailed reviews concerning Saturn's rings see Alexander (1962), Moroz (1963), Bobrov (1970) and Cook and Franklin (1973).

b) Observations

During the 1969 and 1970 apparitions of Saturn, a photometric study of the rings was carried out. The 60-inch (152 cm) telescopes at Mt. Wilson, California and Cerro Tololo, Chile, and the 24-inch (61 cm) telescope at Mt. Wilson, California were used. Most of the work was done ith an ITT FW-118 (S-1) photomultiplier tube, though some of the observations were made using an ITT FW-130 (S-20) photomultiplier tube. A double beam photometer (McCord, 1968) was used with the second beam set for detailed subtraction of the sky background and light from the disk of Saturn scattered in the earth's atmosphere.

A standard star of known spectral flux was measured at frequent intervals during the observing periods as a calibration. For this program ξ^2 Ceti and 29 Piscium were used as standards. The wavelength dependence of atmospheric extinction was eliminated by comparing the object flux and the standard star flux at the same air mass. Knowing the stellar spectral flux and the solar spectral flux, the spectral

reflectivity of the object can be found. From these obser-
vations, the ring/star ratio is determined and then is multi-
plied by the known star/sun flux ratio. The derived curve is
scaled to a value of 1.0 at $\lambda = 0.564\mu$. Relative stellar
spectral flux/solar spectral flux ratios and the effective
band centers for the filters used in these observations were
obtained from Elias (1972); see Tables II-1 and II-2. For
more detailed discussions of observational techniques see
McCord (1968), Johnson (1969) and Chapman (1971).

The first beam was positioned on the ring ansa (either
east or west). The second beam was positioned either north
or south of the rings at about the same angular distance from
the center of Saturn as the first beam. Aperature sizes used
were 3.5, 1.75 and 1.4 arc seconds on the 60-inch telescopes
and 3.6 arc seconds on the 24-inch telescope.

Ring B is broader (4.0 at mean opposition) than either of
the other rings and is also brighter. Since very good seeing
is needed to measure the A or C ring, most of the data presented
and the subsequent discussion concern ring B.

TABLE II-1

NOMINAL WAVELENGTH (μ)	EFFECTIVE WAVELENGTH	BANDWIDTH (at half max)	TRANSMISSION (at peak)
0.32	0.3263	.016	.19
0.34	0.3428	.022	.14
0.36	0.3602	.014	.18
0.38	0.3827	.013	.23
0.40	0.4034	.028	.48
0.43	0.4346	.028	.42
0.47	0.4686	.033	.49
0.50	0.5002	.029	.56
0.53	0.5337	.033	.46
0.57	0.5663	.029	.55
0.60	0.5994	.032	.54
0.63	0.6327	.032	.56
0.67	0.6650	.027	.50
0.70	0.6993	.026	.54
0.73	0.7302	.033	.51
0.77	0.7638	.031	.57
0.80	0.8057	.049	.46
0.85	0.8550	.047	.48
0.90	0.9046	.048	.58
0.95	0.9467	.051	.59
1.00	1.0023	.050	.53
1.05	1.0520	.050	.55
1.10	1.0979	.049	.44

TABLE II-2

NOMINAL WAVELENGTH	ξ^2CETI/SUN	29 PSC/SUN	RING A	RING B	RING C
0.32	2.9462	5.5115	0.448	0.355	0.575
0.34	2.3463	4.3779	0.440	0.389	0.637
0.36	2.1913	3.9059	0.469	0.435	0.574
0.38	3.3094	4.8084	0.598	0.516	0.728
0.40	2.8154	3.1201	0.699	0.578	0.630
0.43	2.0985	2.2356	0.723	0.668	0.786
0.47	1.5447	1.6200	0.855	0.785	0.914
0.50	1.2952	1.3375	0.875	0.872	0.837
0.53	1.1733	1.1854	1.000	0.937	0.915
0.57	1.0000	1.0000	1.000	1.000	1.000
0.60	0.8576	0.8576	1.013	1.012	1.154
0.63	0.7706	0.7583	1.038	1.038	0.953
0.67	0.6781	0.6618	1.065	1.107	0.956
0.70	0.6418	0.6315	1.077	1.111	1.076
0.73	0.6076	0.5994	1.087	1.137	1.136
0.77	0.5719	0.5614	1.091	1.151	1.163
0.80	0.5313	0.5216	1.043	1.155	1.185
0.85	0.5251	0.5101	1.085	1.191	1.239
0.90	0.5072	0.4795	1.121	1.180	1.246
0.95	0.4791	0.4368	1.047	1.123	1.129
1.00	0.4525	0.4165	1.005	1.127	1.158
1.05	0.4241	0.4011	0.994	1.131	1.191
1.10	0.3884	0.3791	0.992	1.041	1.285

c) Results

The normalized reflection spectrum of ring B appears in Figure II-1 (see Table II-1). The points represent averages of the runs taken with Mt. Wilson and Cerro Tololo telescopes. The standard deviation of the average value is shown as an error bar. Figure II-2 compares these results with those of Shain (1935), Franklin and Cook (1965), Younkin and Münch, (1965), Münch (1971), and Irvine and Lane (1973) as scaled to the narrowband interference filter reflectivity curve of the rings obtained by us. The comparisons are made difficult by the fact that Franklin and Cook used wide band filters. We used narrowband filters, Irvine and Lane used narrowband filters, and Shain and Younkin and Münch used spectral scans of higher resolution.

The open triangles represent the centers of the band passes of the B and V filters of Franklin and Cook. The V filter value was rescaled to fall on the curve of the narrowband filters. As can be seen, the B filter value falls very close to our curve, in fairly good agreement with our data. (The close agreement is aided by the fact that there is no change in slope of the reflectivity curve over this region which might adversely affect the effective wavelengths of the much wider band widths of the B and V filters.)

The crosses represent the values derived from Shain's magnitude variation measurements. Here, Shain's values are rescaled to a value of 1.0 at 0.564μ. Shain's curve also
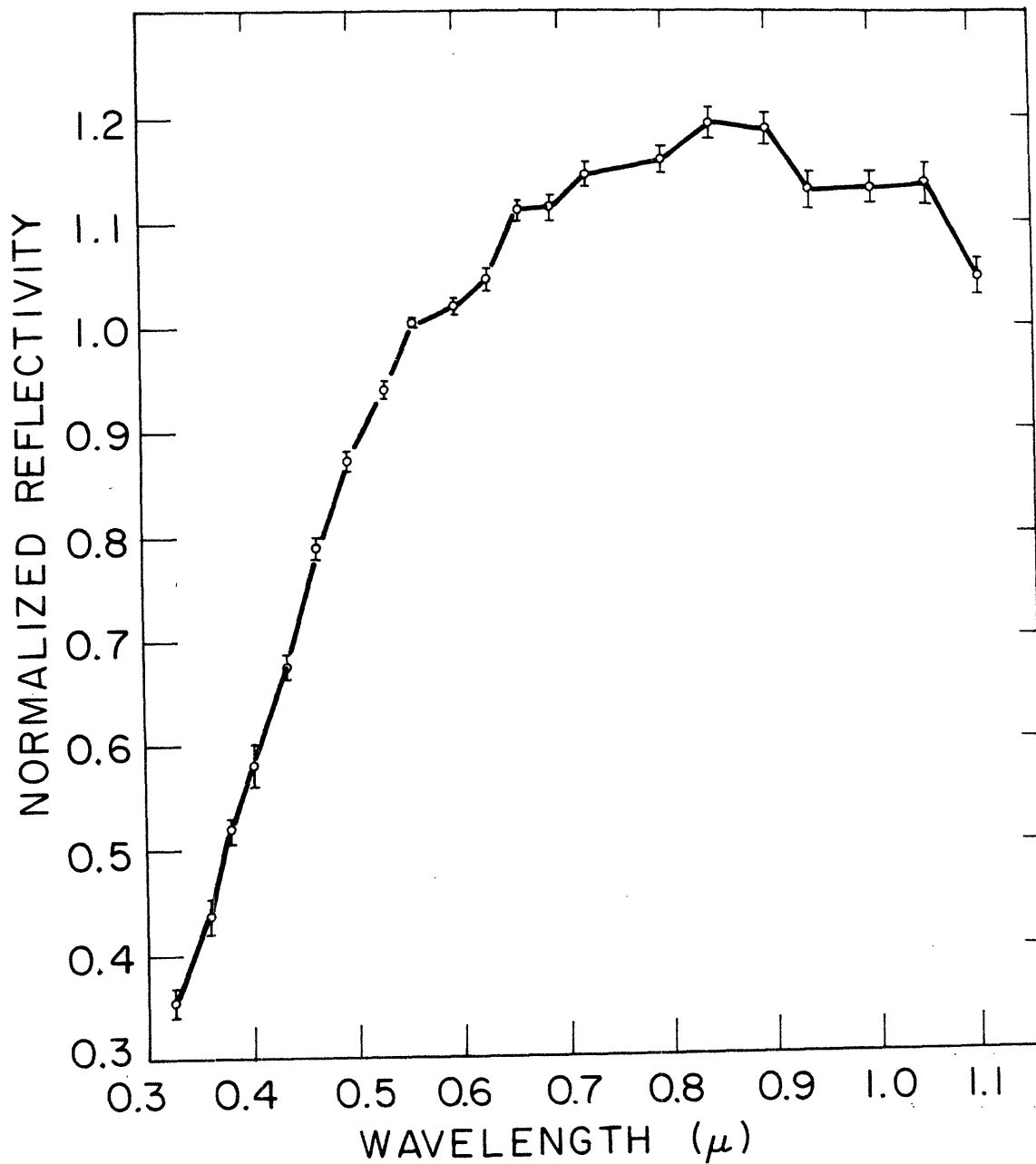
Figure II-1. The normalized reflectivity (scaled to 1.0 at 0.564μ) of Saturn's ring B as a function of wavelength. Each point represents an average of measurements through one interference filter. The deviation of the average value is shown as an error bar. A curve is drawn through the data points.
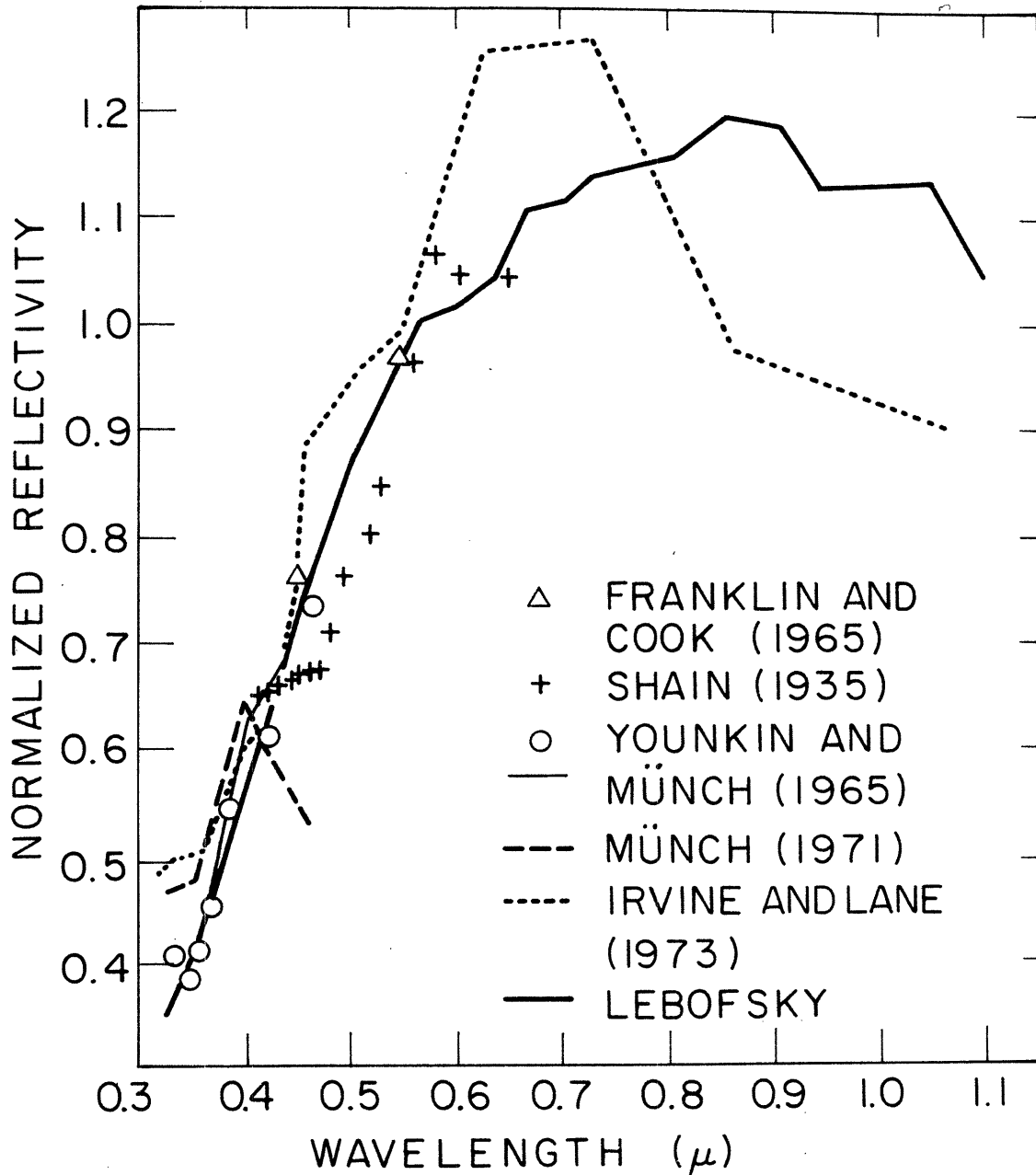
Figure II-2. The normalized spectral reflectivities of the rings obtained by Shain (1933), Younkin and Münch (1965; Münch, 1971) and Irvine and Lane (1973). The ring B normalized reflectivity is shown for comparison.

shows a significant falloff of the reflectivity of the rings with decreasing wavelength, but the match with the other data presented is not very good.

The open circles, the solid line and the dashed line represent the data of Younkin and Münch. The scaling point of the Younkin and Münch curves was 0.5µ which was set equal to our 0.5µ value. The open circles represent the original photoelectric data (Younkin and Münch, 1965); the light solid line, photoelectric, and the dashed line, photographic measurements done as ring vs. planet (Münch, 1971). The fit of the photoelectric data to our data is much better than that of Shain.

The short dashes represent the work of Irvine and Lane (1973). The general slope of the curves match below 0.6µ, but beyond this, the match is poor. In the region 0.6 to 0.7µ their curve is much higher, and beyond 0.7µ, much lower than our curve. Irvine and Lane obtained the reflection spectra of the rings plus Saturn over a three year period. Since during this period the inclination of the rings changed, they extrapolated their data to 0° inclination, thus obtaining separate ring and Saturn spectra. This indirect method for determining the reflection spectrum of the rings may account for the large discrepency between our results and theirs, the difference being greatest in a region where the reflectivity of the planet is lowest. A comparison of our Saturn ring curve and their Saturn ring curve with two spectral curves of Saturn's disk (McCord, Johnson and Elias, 1971; Irvine and Lane, 1973) shows that

their ring curve matches the disk curves better than our Saturn ring curve, implying that their derived Saturn ring reflection spectrum is still contaminated by light from the disk of Saturn.

We can conclude that the reflectivity of Saturn's rings decreases shortward of about 0.5μ. Five investigations, using several different methods of data analysis, are in fairly close agreement.

Several features can be noted in the ring B reflection spectrum (Figure II-1). The reflection curve decreases sharply toward the blue at wavelengths shorter than about 0.6μ. There is a shoulder between 0.5 and 0.7μ.

The curve then flattens out to 0.9μ, decreasing toward longer wavelengths. Several other (Fredrick, 1963; Owen, 1965) have identified a 1.05 to 1.1μ feature in the ring spectrum, in agreement with our results.

Franklin and Cook (1965) and Irvine and Lane (1973) have found a phase dependent color variation for the rings. In reduced form, we have data at phase angles of 3°.5, 4°.5, 5°.5 and 5°.5 (after quadrature). Any variation of color with phase angle is unfortunately lost within the error of our measurements. This does not exclude the possibility of a phase variation since our results are probably too far from opposition and over too small a range of phase angles to show any opposition or phase angle effect.

The reflection spectra of rings A and C are compared in Figure II-3 with the reflection spectrum of ring B. There appears to be a variation of the reflectivity from ring to ring. Greater difficulty in guiding on the smaller rings and the poorer statistics due to fewer runs and lower signals
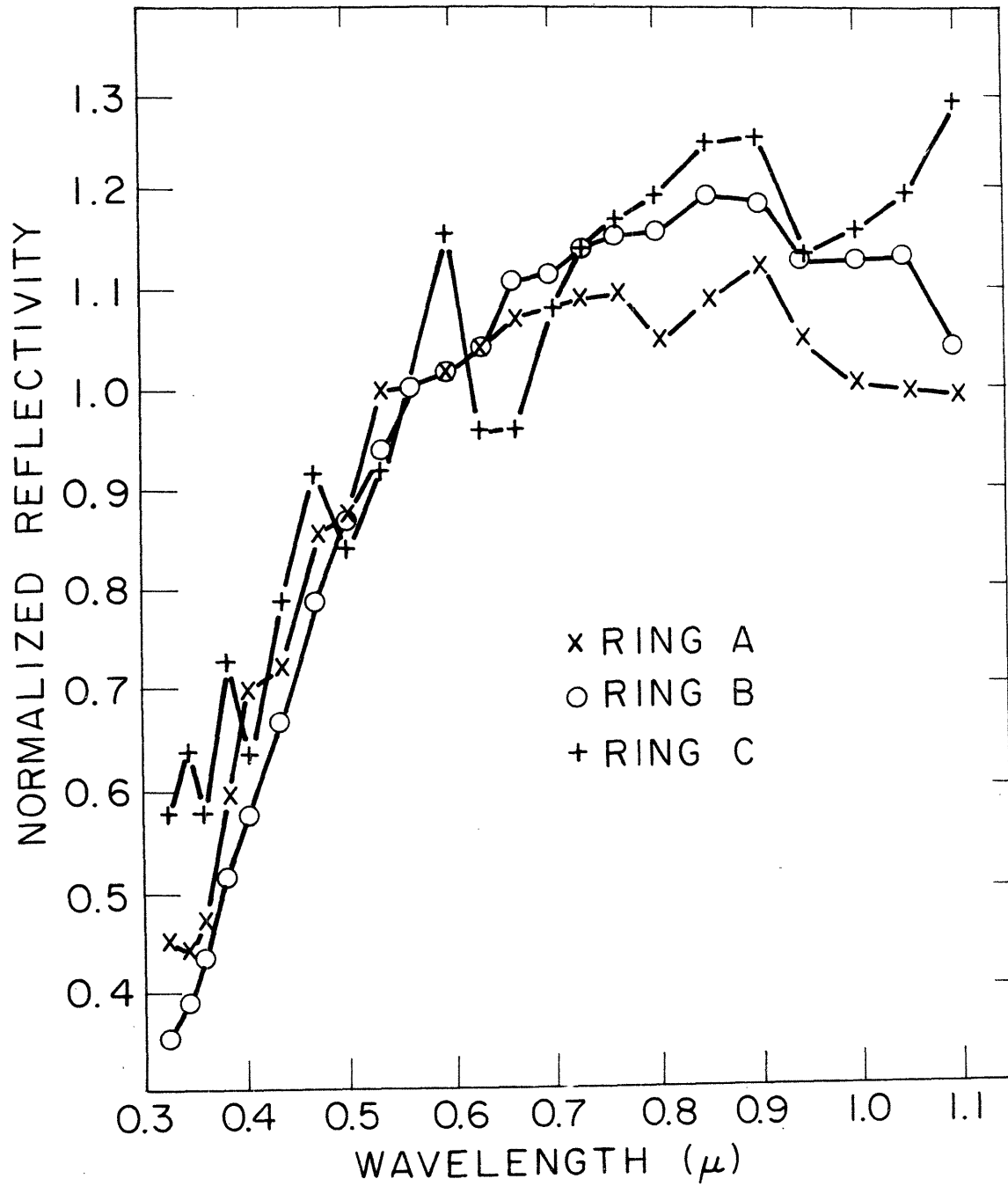
Figure II-3. The normalized spectral reflectivities of rings A and C. The ring B normalized reflectivity is shown for comparison.

have contributed to the large scatter of the data for rings A and C.
Scattered light from Saturn does not appear to be a problem. We would ex-
pect to see absorption bands due to methane in the spectrum of the rings
if any significant amount of light were scattered from the planet.

The dropoff in reflectivity of ring A is less than the dropoff in
ring B. Also, around 0.8 and 1.1μ the normalized reflectivity of ring A
is lower than that of ring B. Very little can be said about
ring C because of the large scatter in the data.

Of all the Solar System bodies that have been investigated, the visible
reflection spectrum of the rings most closely resembles the spectra of the
Galilean satellites (Figure II-4). The reflection spectra of J1 and J2 are
shown, J3 and J4 visible spectra are similar to J2's spectrum. J1 has a
steeper decrease in reflectivity than does ring B at short wavelengths. At
wavelengths longer than 0.5μ the match to J1's curve is better. The match
with the curve of J1 is better than the match between J1 and the other
Galilean satellites. It should be noted that the rings do not look like any
of the satellites of Saturn whose reflection spectra tend to be flat in the
visible and ultraviolet region (McCord, Johnson and Elias, 1970). (See
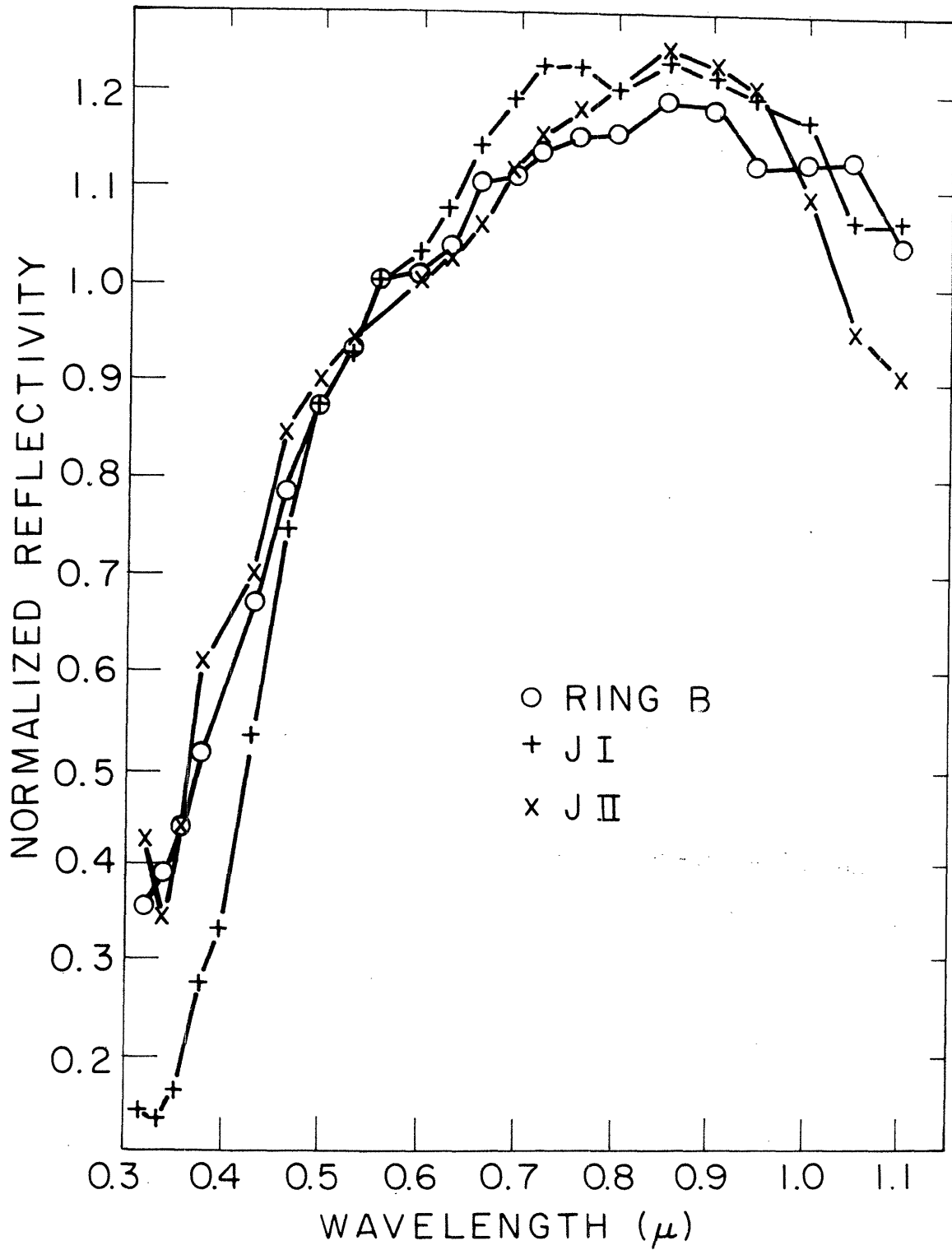Figure V-1).

Figure II-4. The spectral reflectivities of the Galilean satellites, J1 and J2. Ring B is shown for comparison.

d) Conclusions

The wavelength dependence of the reflection spectrum of a surface is determined primarily by the chemical composition and mineralogy of the surface. Where distinctive solid absorption bands are present, such as in the spectra of the moon (McCord and Johnson, 1970), Mars (McCord and Adams, 1969; Huguenin, 1973) and asteroids (Gaffey, 1973), identification of surface materials is possible. However, the reflection spectrum of ring B contains no distinctive absorption bands over the spectral region studied here (0.3 to 1.1μ).

Absorption bands do exist in the rings' spectrum at longer wavelengths (Pilcher, et al., 1970; Kuiper, et al., 1970) (see Figure II-5, indicating the probable presence of water frost. The rings appear to have an absorption (Ockman, 1958; see also Vanderberg, 1954; Ockman, 1957). A pure water frost, however, would be expected to have a flat reflection spectrum (white), in the visible region, in contrast to the spectrum shown in Figure II-1. Franklin and Cook (1965) and Irvine and Lane (1973) have also pointed out this problem.

All evidence indicates that the rings do not seem to be composed of pure water frost. The major alternative materials and mixtures of materials (silicates, frosts and silicates, and altered frosts) will be discussed in relation to the known spectral characteristics of the rings.

(1) Silicates: Reflection spectra of powdered silicates characteristically exhibit a decrease in the blue and ultraviolet region which is in some ways similar to the decrease found in the ring spectrum. Hydrous silicates sometimes show water absorption bands in their infrared (1.0-2.5μ) spectra, but these bands are generally narrow with little or no broadening (Adams and Filice, 1967; Hunt and Salisbury, 1970) unlike the ring spectrum. The
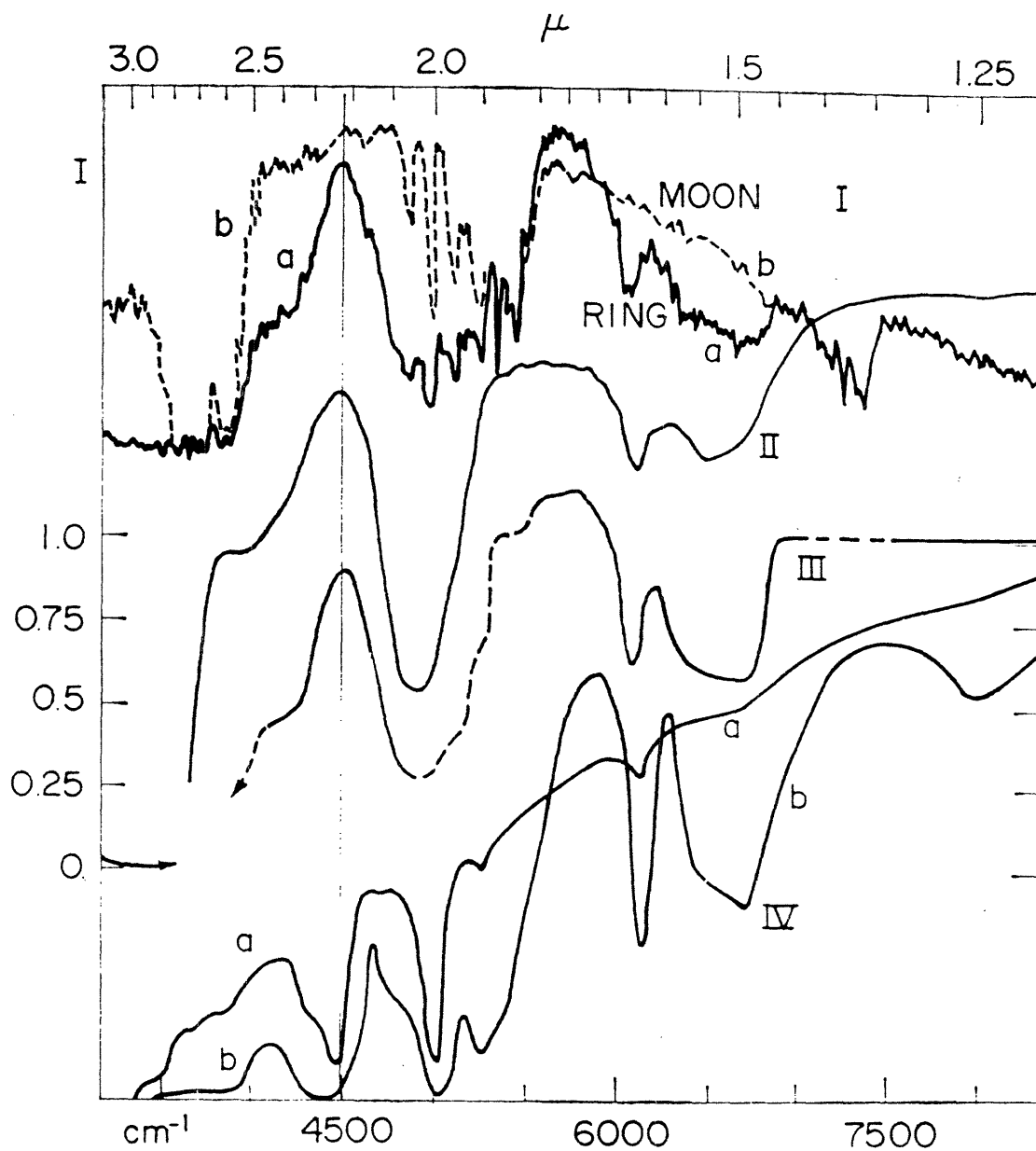
Fig. 1. Comparison of reflectance spectra for H_2O and NH_3 frosts and Saturn's rings. The major region of disagreement between the ring and NH_3 frost spectra is indicated by a vertical line at 2.22 μ (4500 cm^{-1}). With the exception of curve III, the vertical axis is not calibrated and sloping trends can be ignored for purposes of comparison. The vertical calibration for curve III is along the left side of the figure. (Curve Ia) The new Saturn ring spectrum of Kuiper et al. (1). (Curve Ib) Lunar comparison spectrum. (Curve II) Fine-grained H_2O frost spectrum of Kieffer (4); $\Delta\lambda \approx 0.05$ μ, $\lambda < 1.58$ μ; $\Delta\lambda \approx 0.03$ μ, $\lambda > 1.58$ μ. (Curve III) Normalized Saturn ring spectrum (Ia divided by Ib); the dashed portions of the curve indicate regions affected by telluric absorption. There is a gap in the curve near the saturated 2.7-μ telluric band. (Curve IV) Kieffer's preliminary NH_3 frost spectra: (IVa) fine-grained frost, (IVb) coarse-grained frost; same resolution as in curve II.

Figure II-5. Comparison of a ring infrared spectrum with laboratory spectra of frosts. From Pilcher, et al., 1970.

ring spectrum and the spectra of laboratory frosts (Kieffer, 1968, 1970, 1973) show broadening of infrared absorption bands due to the lengthening of the O-H bonds in the crystal structure of the water frost. Also, iron silicates generally exhibit electronic transition absorption bands in the $0.9-1.1\mu$ region; none are evident in the ring B spectrum to the precision of the measurements. Finally, the albedo of the ring particles is probably too high for any expected silicate (Bobrov, 1970; Franklin and Cook, 1965; Lumme, 1970; Berge and Read, 1968; Allen and Murdock, 1971; Adams and Filice, 1967; Hunt and Salisbury, 1970; Gaffey, 1973).

(2) Mixtures of frosts and silicates: If the mixture is of individual frost and silicate particles, the the light received from each component would be in proportion to the exposed surface area and the albedo of each component. Since water frost absorption bands in the infrared spectrum of the rings reach at least 70% (Pilcher, et al., 1970) either the silicate component reflects very little radiation of the exposed area of the silicate particles is very small. At visible wavelengths the ring spectrum decreases 70% between 0.8 and 0.3μ, similar to what is found in many silicates. Thus, at visible wavelengths, in this model, most of the reflected radiation must be coming from the silicate-like particles. However, water frost has a nearly constant high (60-90%) spectral reflectivity at visible wavelengths (Krinov, 1947; Veverka, 1970). Also, laboratory studies of silicates show that most have high infrared reflectivities (Adams and Filice, 1967; Hunt and Salisbury, 1970; Gaffey, 1973). This suggests that a mixture of frost and sili-

cate particles is not a satisfactory model.

Kieffer (1968) has shown that only a very thin layer of water frost ($0.007 gm/cm^2$) is needed to mask CO_2 frost below it. It would therefore be possible to have a silicate particle covered by a very thin layer of water frost whose infrared reflection spectrum would be similar to that of pure water frost. In the UV-visible region of the spectrum, the water frost would be transparent and the reflectivity would be indicative of the silicate particle, ie. a decrease in reflectivity in the UV. This too fails. The two layered particle would have the generally low reflectivity of the silicate particle in the visible region, not what is observed in Saturn's rings.

(3) Altered frosts: There are several possible effects which might cause frosts to have a low reflectivity at short wavelengths. Irradiation of the frost by either high energy particles or solar ultraviolet radiation might cause physical or chemical changes in the water frost, particularly in the presence of other compounds. An example of a possible important minor component is H_2S, which, when irradiated, will break down into hydrogen and sulfur. The sulfur would cause a falloff in reflectivity in the blue and ultraviolet region. At low temperatures, gas hydrates are also possible. If formed in the primordial gas cloud, it is possible to have trapped gases in the crystal lattice structure of the ice. The altered frosts will be discussed in greater detail later.

III. LABORATORY SPECTRA

a) <u>Motivation</u>

As has been shown in the previous section, the rings of Saturn seem to be composed mainly of water frost, but have a reflectivity that decreases toward the ultraviolet. The same is true for the Galilean satellites. All four satellites have albedoes compatible with icy surfaces (Johnson and McCord, 1970). J 2 and J3 have been shown to have infrared spectra compatible with the presence of water frost and it is also probable that J1 has an icy surface. J 4 may also have a partially ice-covered surface (Pilcher, et al., 1972; Fink et al., 1973). These satellites, too, show decreases in reflectivity toward the ultraviolet (Johnson and McCord, 1970).

No laboratory visible reflection spectra of frosts existed previous to this investigation (except for Krinov, 1947) so that no comparisons could be made between the spectral reflectivities of the rings and the Galilean satellites and the reflectivities of known frosts. Therefore, a laboratory investigation was begun to study the spectral reflection properties of various frosts under conditions expected in the outer solar system.

The possible frost condensates of major importance in the solar system are H_2O, NH_3, H_2S and CH_4. Hydrates and NH_4SH are also expected (Miller, 1961; Delsemme and Miller, 1970; Delsemme and Wenger, 1970; Lewis, 1972). Solar UV radiation probably plays an important part in the chemical stability and formation of various frosts. Lewis and Prinn (1970) have proposed NH_4SH which has undergone solar UV photolysis to form ammonium polysulfide as the yellow coloring agent in the clouds of Jupiter. It is possible that ammonium polysulfides cause the colorations of the rings and the surfaces of Galilean satellites. For these reasons, studies were conducted to determine

the visible reflection spectra of frozen H_2O, NH_3, H_2S, mixtures of these and their UV irradiated products. Attempts were made to study the reflection spectrum of CH_4 frost, but CH_4 is not very stable at liquid nitrogen (LN_2) temperatures so no results were obtained. Special emphasis was placed on NH_3 and H_2S mixtures since they were already known to have, upon UV irradiation, low reflectivities in the blue region of the spectrum.

b) Apparatus and Procedure

The apparatus was set up to measure the spectral reflectivity of a standard surface (MgO), cool down the "cold finger", deposit a frost and irradiate the sample, measuring the spectral reflectivity of the un-irradiated and irradiated sample (see Figure III-1).

Most experiments were done using liquid nitrogen (LN_2) as a coolant (77°K). Several experiments were conducted using a dry ice-acetone mixture as a coolant (195°K).

A grating monochromator and detector were used to measure the spectral reflectivity of the sample (vs. the MgO standard) in the spectral region 0.18 to 1.03μ.

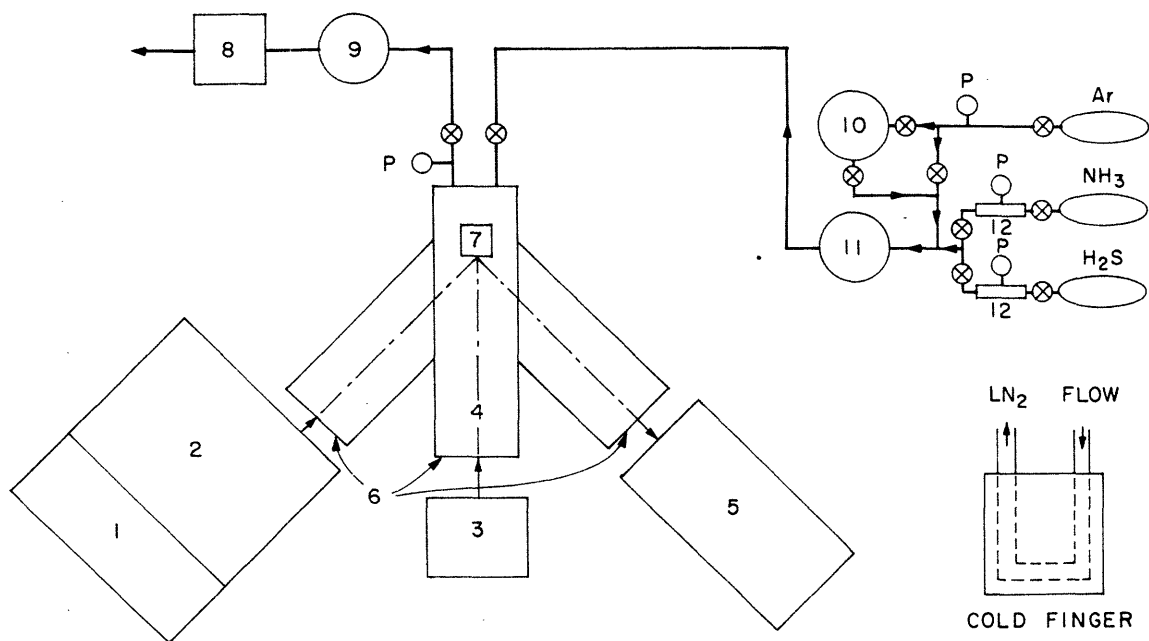For a detailed description of the apparatus and procedure see appendix C.

Figure III-1. Laboratory setup for the investigation of UV irradiated frosts.

1. Light source
2. Monochromator
3. Xenon arc lamp
4. Cold chamber
5. Photomultplier detector
6. Quartz window
7. Cold finger
8. Fore pump
9. Cold trap
10. Water chamber
11. Mixing chamber
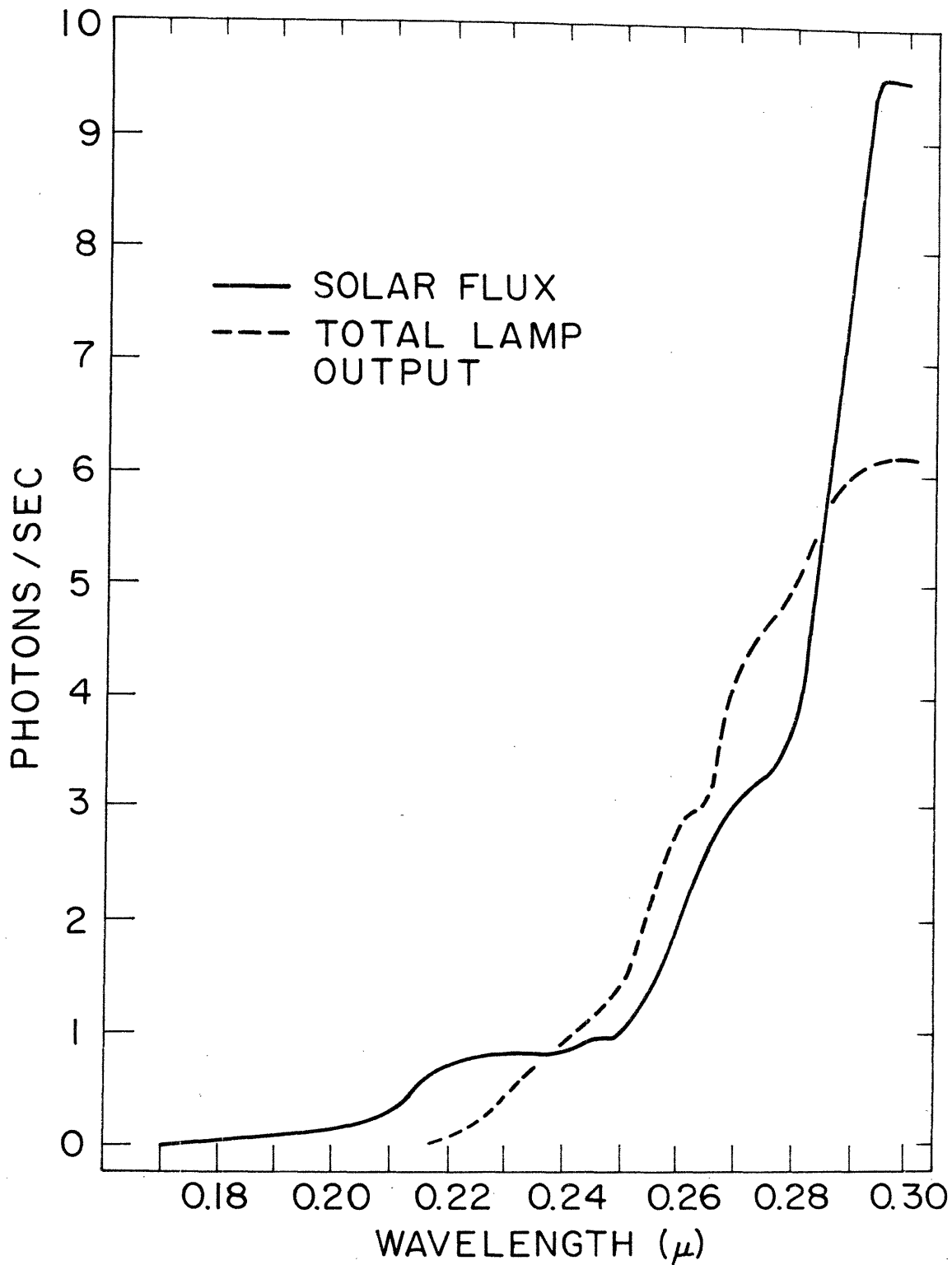12. Gas chamber of known volume
⊗   Valve
P   Pressure (vacuum) gauge

Figure III-2. A comparison of solar flux and lamp output. The solar flux is 10^{12} photons/cm^2/Å/sec at a distance of 1AU from the sun. The lamp flux is the total output in 10^{15} photons/Å/sec of the lamp. (Lens and window transmission taken into account.) The solar flux is taken from Schultz and Holland.

c) <u>Results</u>

For this investigation, the frosts studied were H_2O, NH_3, NH_3+H_2O, H_2S,NH_3+H_2S,H_2S+H_2O, and $NH_3+H_2S+H_2O$. An attempt was made to study the properties of CH_4, but it was impossible to obtain a frost layer so no results are presented. Figures III-3 and III-4 show the raw output of an MgO run and a frost (NH_3) run. The system response peak at about 0.73μ may cause false features around that wavelength due to small errors in the wavelength calibration (10-20Å) for a given run. As previously stated, dividing a frost curve (III-4) by a standard (III-3) gives the desired reflectivition curve, eg. Figure III-6A. The results are presented below.

H_2O: Figure III-5A shows the spectrum (0.3-1.03μ) of H_2O frost, un-irradiated. The curve is featureless, except for an increase in reflectivity toward the infrared. One hour of UV irradiation (Figure III-5B) did not produce any significant change in the reflection spectrum of the H_2O frost. The reason for the increase in reflectivity of the water frost toward longer wavelengths is unknown, but appears to be real, being based on two separate experiments.

NH_3: The reflection spectrum of unirradiated NH_3 frost (Figure III-6A) does show some spectral features in the near infrared, probably due to molecular vibrations. A comparison has been made between infrared spectra of ammonia gas (Hertzberg, 1966; American Petrolium Company, 1959) and frost (Kieffer and Smythe, 1974) (see Figure III-7). A similarity in the positions of absorption bands observed in both the gas and frost spectra justifies the extention of the comparison to the near infrared absorption bands observed in our ammonia frost spectra (Table III-1). Other than these absorption bands, the reflection spectrum of the ammonia frost is
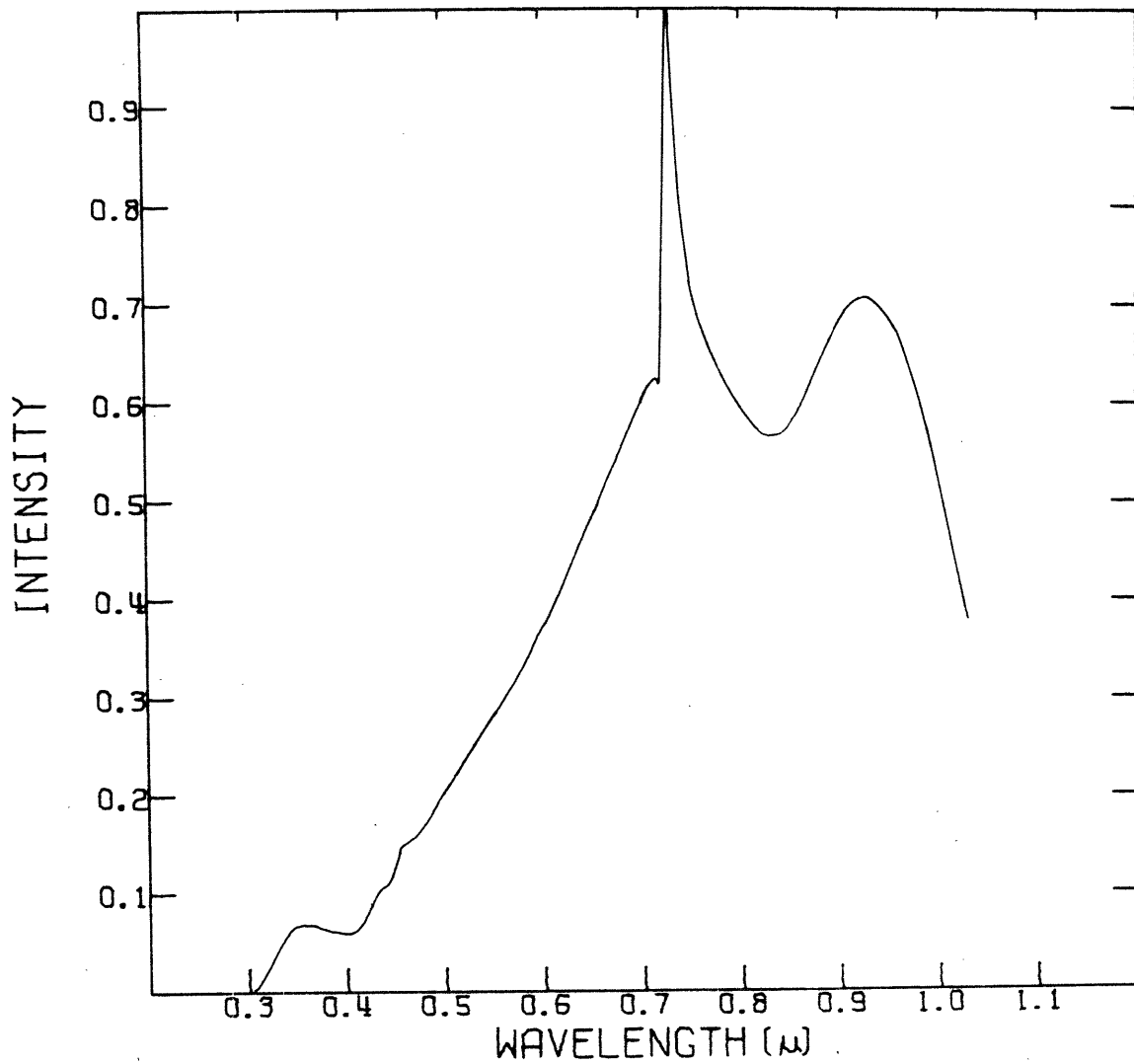
Figure III-3. * Raw photomultiplier output normalized to a maximum of 1.0.
An MgO "spectrum" is presented.
*As can be seen in Figures III-3,4, the signals are low below 0.5 , there-
fore the photon "noise" is higher in this region than at longer wave-
lengths. Error bars are given to represent the signal variation. No error
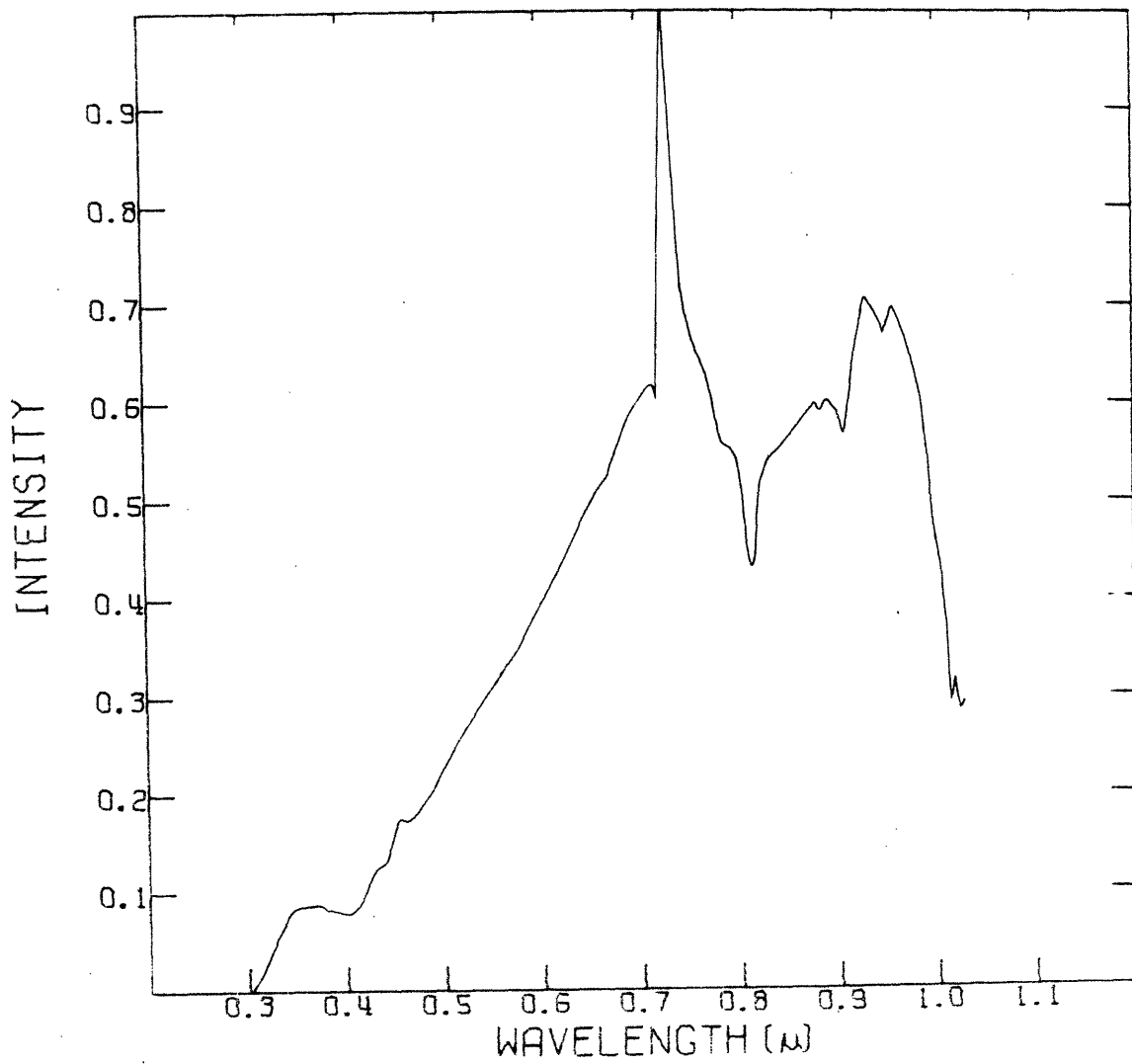bar implies error less than the thickness of the line.

Figure III-4. Output similar to Figure III-3 for an ammonia frost.
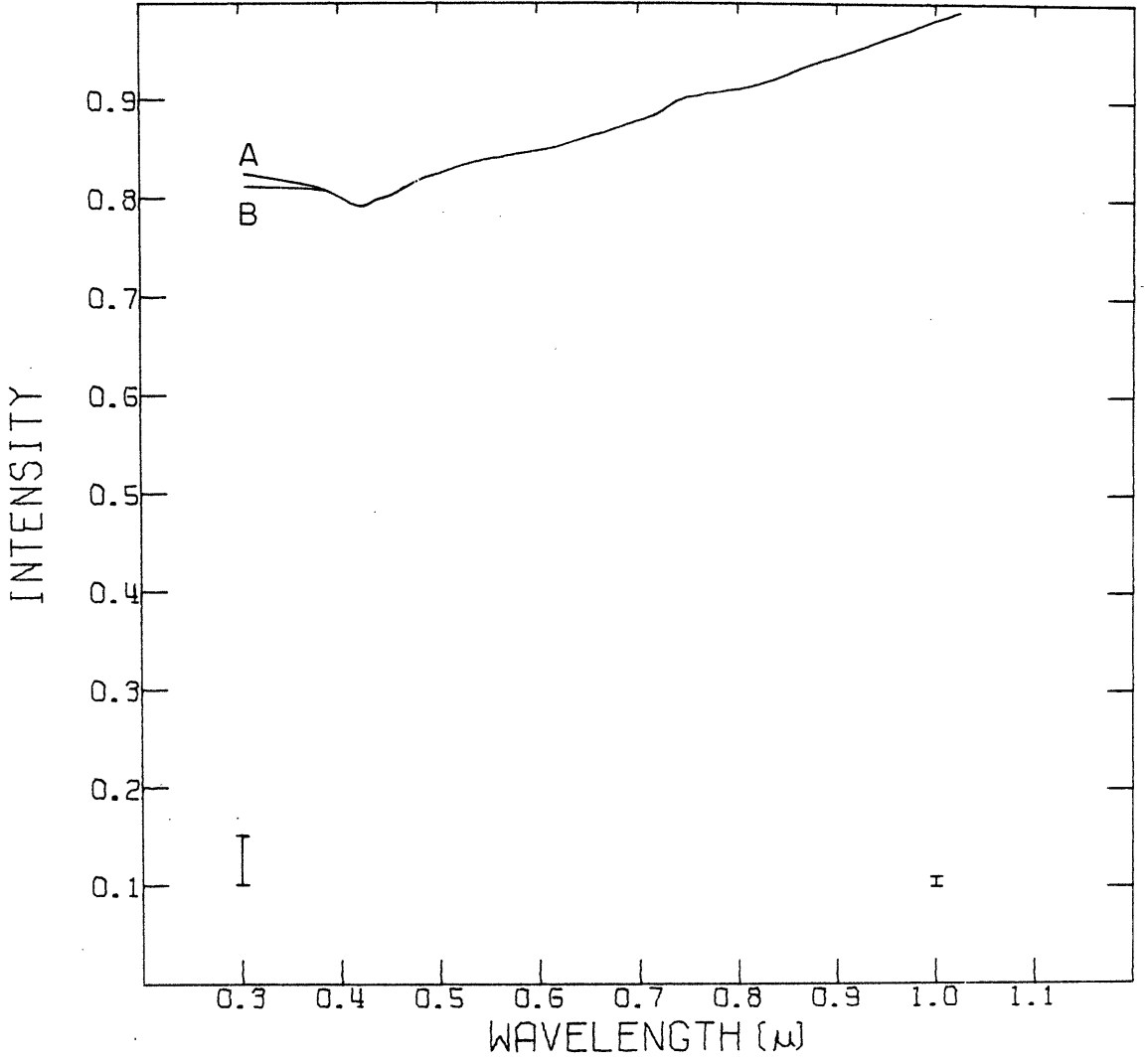
Figure III-5. H_2O frost reflection spectra

      A. unirradiated frost
      B. 1 hour irradiation

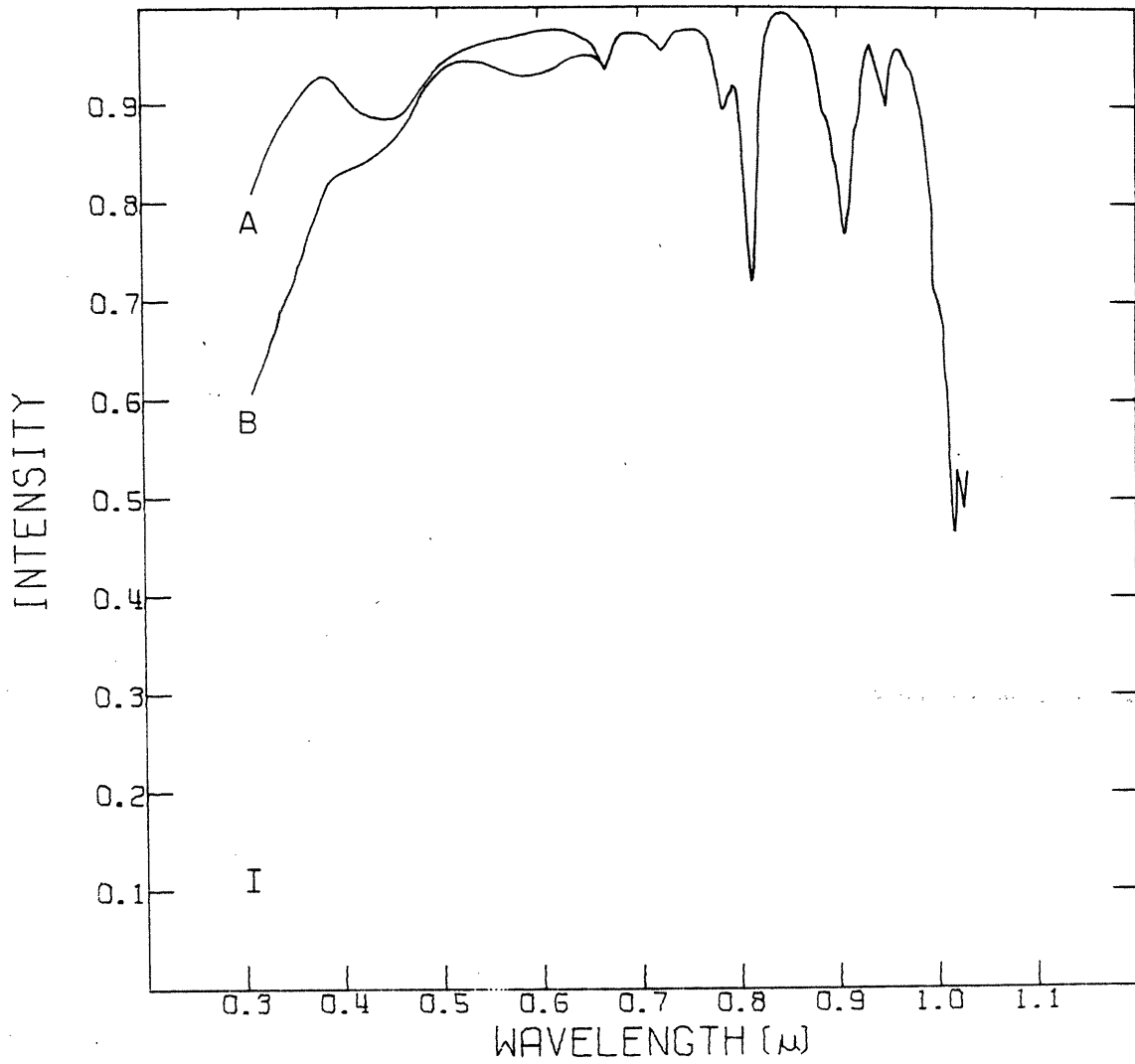Figure III-6. NH$_3$ frost reflection spectra

        A. unirradiated frost
        B. 1 hour irradiation

INFRARED SPECTRAL DATA
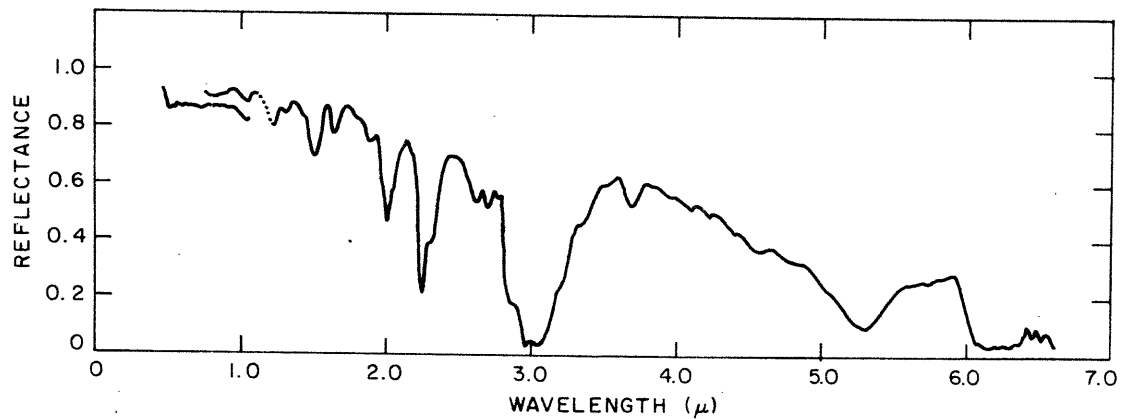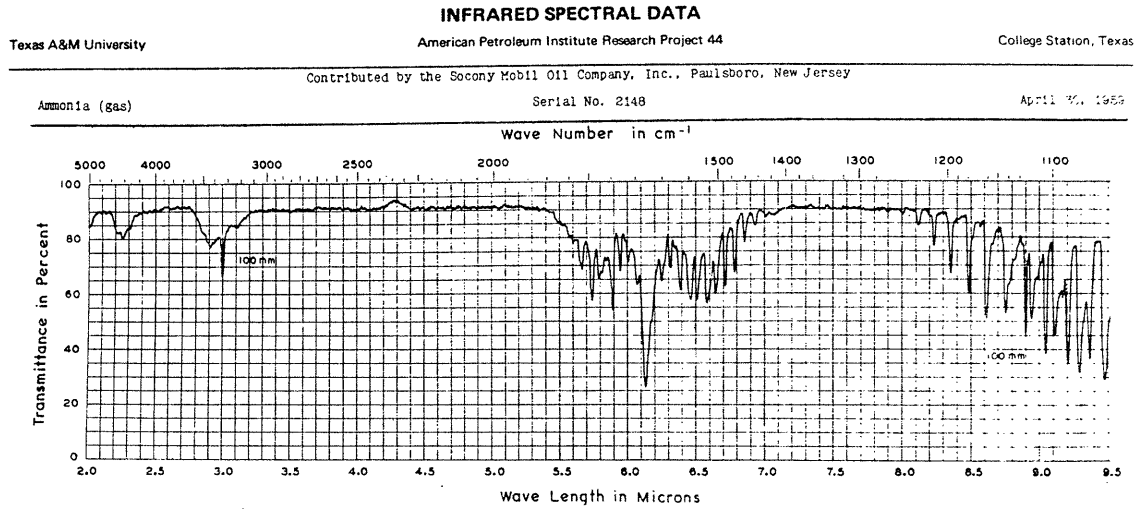
Figure III-7. A. gas absorption spectrum of ammonia
B. NH$_3$ frost reflection spectrum (Kieffer and Smythe, 1974)

TABLE III-1

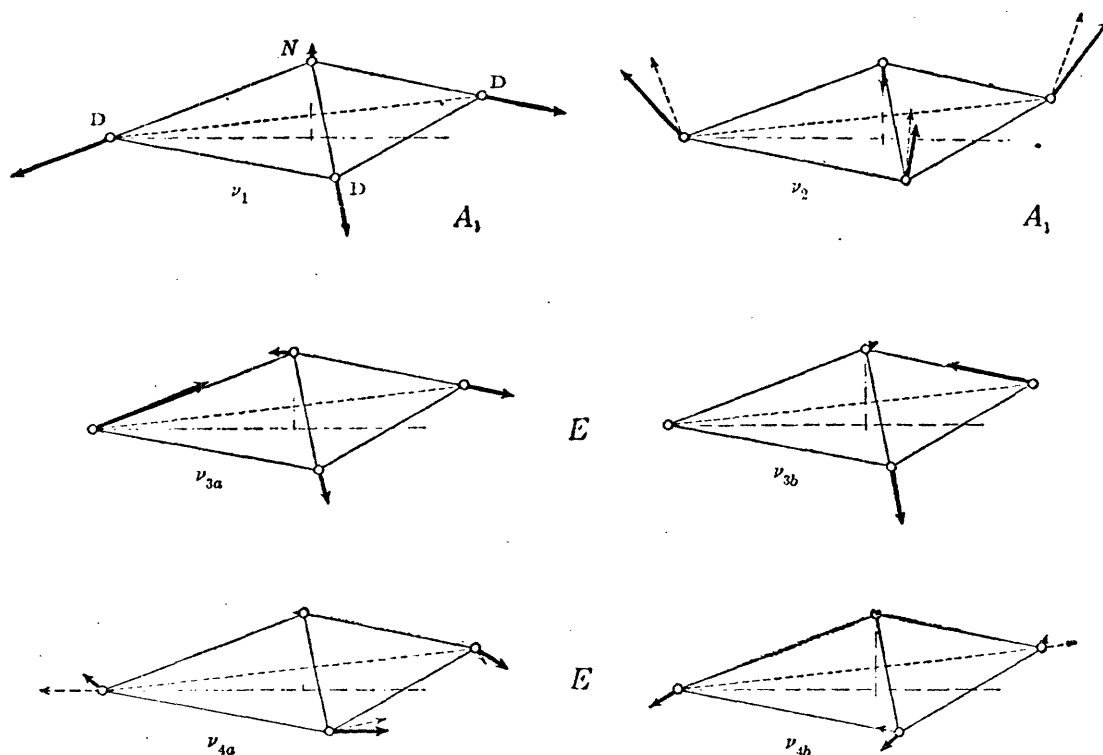| WAVELENGTH (μ)	ASSIGNMENT *
1.02	$3\nu_1$
0.95	$3\nu_1 + \nu_2$ (?)
0.90	$3\nu_1 + \nu_4$
0.82 $\Big\}$ 0.75	$4\nu_1, 2\nu_1, +2\nu_3$, etc.
1.00 (shoulder)	$2\nu_1 + \nu_3$

*See Figure III-8

FIG. 45. **Normal vibrations of the ND₃ molecule.**—The vibrations are drawn to scale for ND₃ (see p. 177) in oblique projection. (For NH₃ the large mass ratio of N to H would not have allowed the displacement vectors of N to be drawn to the same scale as those of H). Both components of the degenerate vibrations are shown. The broken-line arrows in ν_2 and ν_4 give the symmetry coordinates of Fig. 58 (see p. 155). They are added so that the form of the vibrations can be more clearly visualized. In ν_{3b} there is a very small displacement (too small to show in the scale of the diagram) of the left D nucleus parallel to the line connecting the two other D nuclei (see also the discussion of Fig. 60 on p. 171). It should be noted that ν_{3a} and ν_{4a} are symmetric, ν_{3b} and ν_{4b} antisymmetric with respect to the plane of symmetry through the left D nucleus, that is, the plane of the paper.

Figure III-8. Normal vibrations of NH_3 from Hertzberg (1966)

$$\nu_1 = 3335.9, \; 3337.5 \; \text{cm}^{-1}$$
$$\nu_2 = 931.58, \; 968.08 \; \text{cm}^{-1}$$
$$\nu_3 = 3414 \; \text{cm}^{-1}$$
$$\nu_4 = 1627.5 \; \text{cm}^{-1}$$

flat. Again, upon irradiation (1 hour) there is no significant change in the reflection spectrum (Figure III-6B).

$NH_3 + 10 \ H_2O$: As can be seen in the curve of the unirradiated frost (Figure III-9A), the reflection spectrum is flat and featureless. The bands that appeared in the pure NH_3 frost do not appear in the frost mixture. Irradiation (3 hours) of this frost does not significantly change its reflection spectrum.

H_2S: The reflection spectrum of the unirradiated H_2S frost is, as were the previous frost spectra, flat and featureless (Figure III-10A). But, upon irradiation, there is a significant change in the reflection spectrum of the frost. Curves B and C (Figure III-10) are for irradiation times of one and three hours respectively. There is a decrease in reflectivity below 0.5μ. There is also a broad absorption feature centered at 0.6μ which increases in strength with increased irradiation time. The next figure (Figure III-11) shows that with longer irradiation times, the 0.6μ feature appears to reach a maximum strength. The short-wavelength absorption feature also appears to be increasing in strength as the band edge shifts toward longer wavelengths. The spectral curves A, B and C are 3, 5 and 10 hours irradiation respectively. Experiments for longer irradiation times have not been conducted so that it is not known what happens to these longer irradiation times.
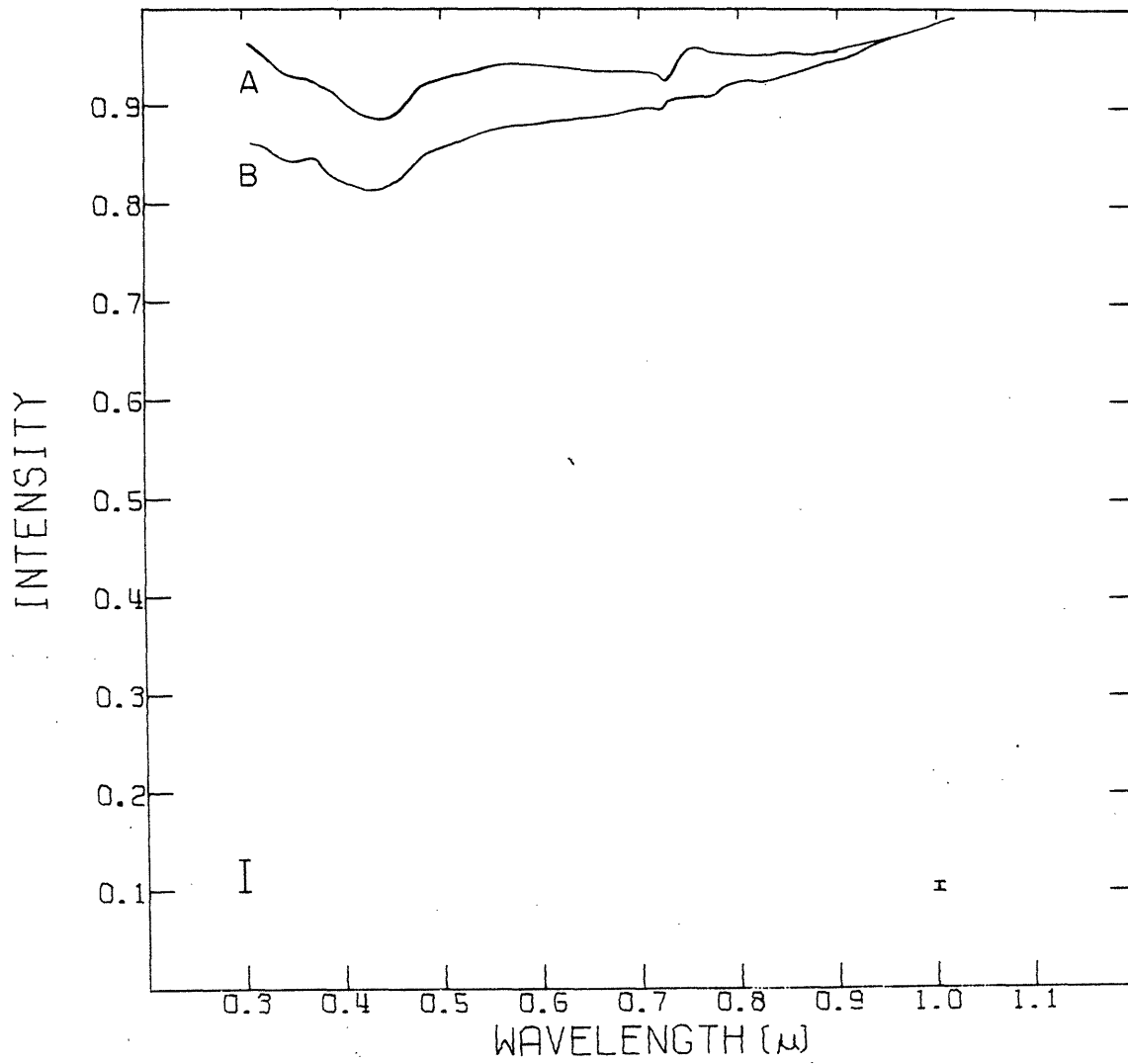
Figure III-9. NH$_3$ + 10H$_2$O frost reflection spectra
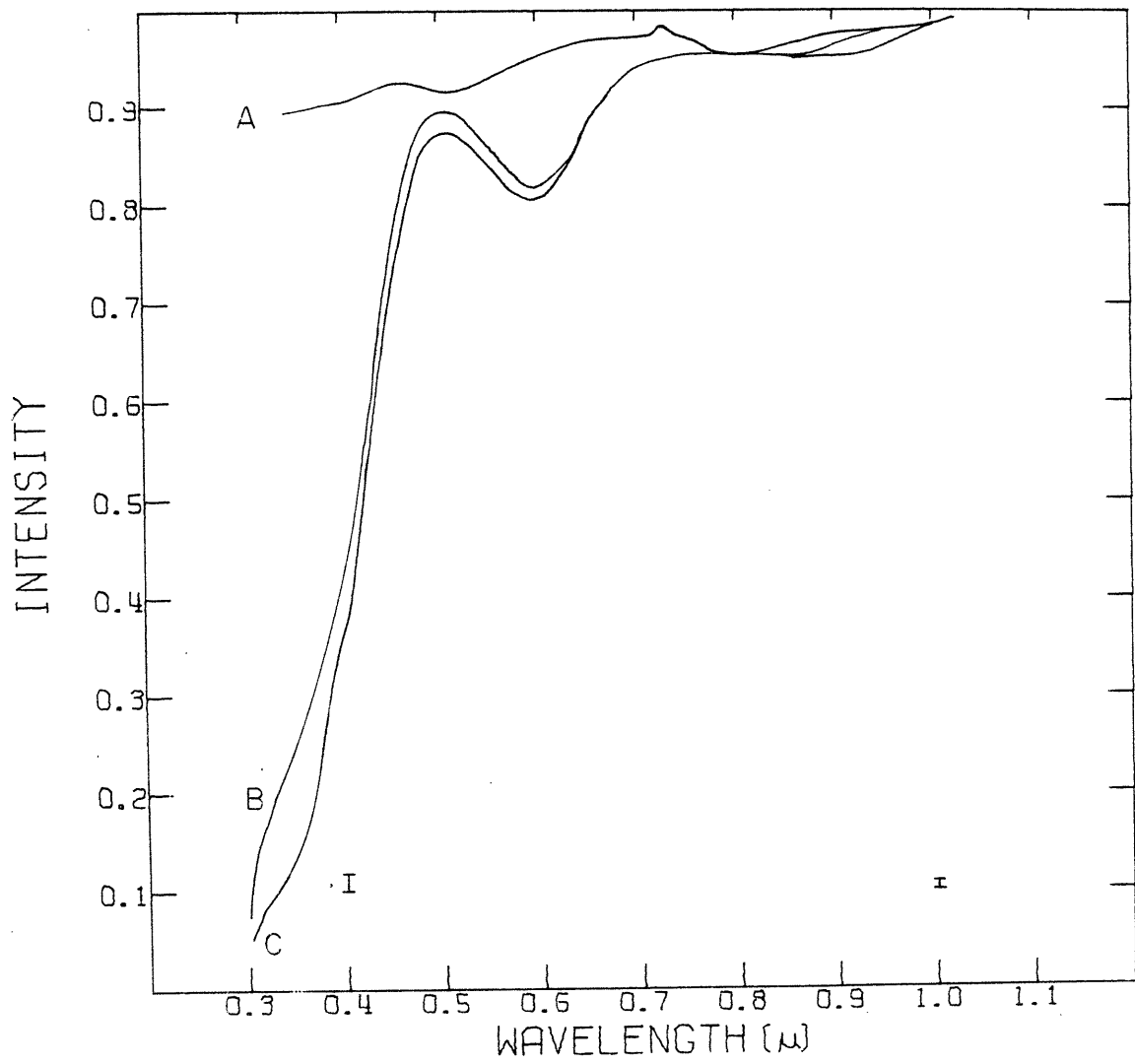   A. unirradiated frost
    B. 3 hours irradiation

Figure III-10. H$_2$S frost reflection spectra

A. unirradiated frost
B. 1 hour irradiation
C. 3 hours irradiation
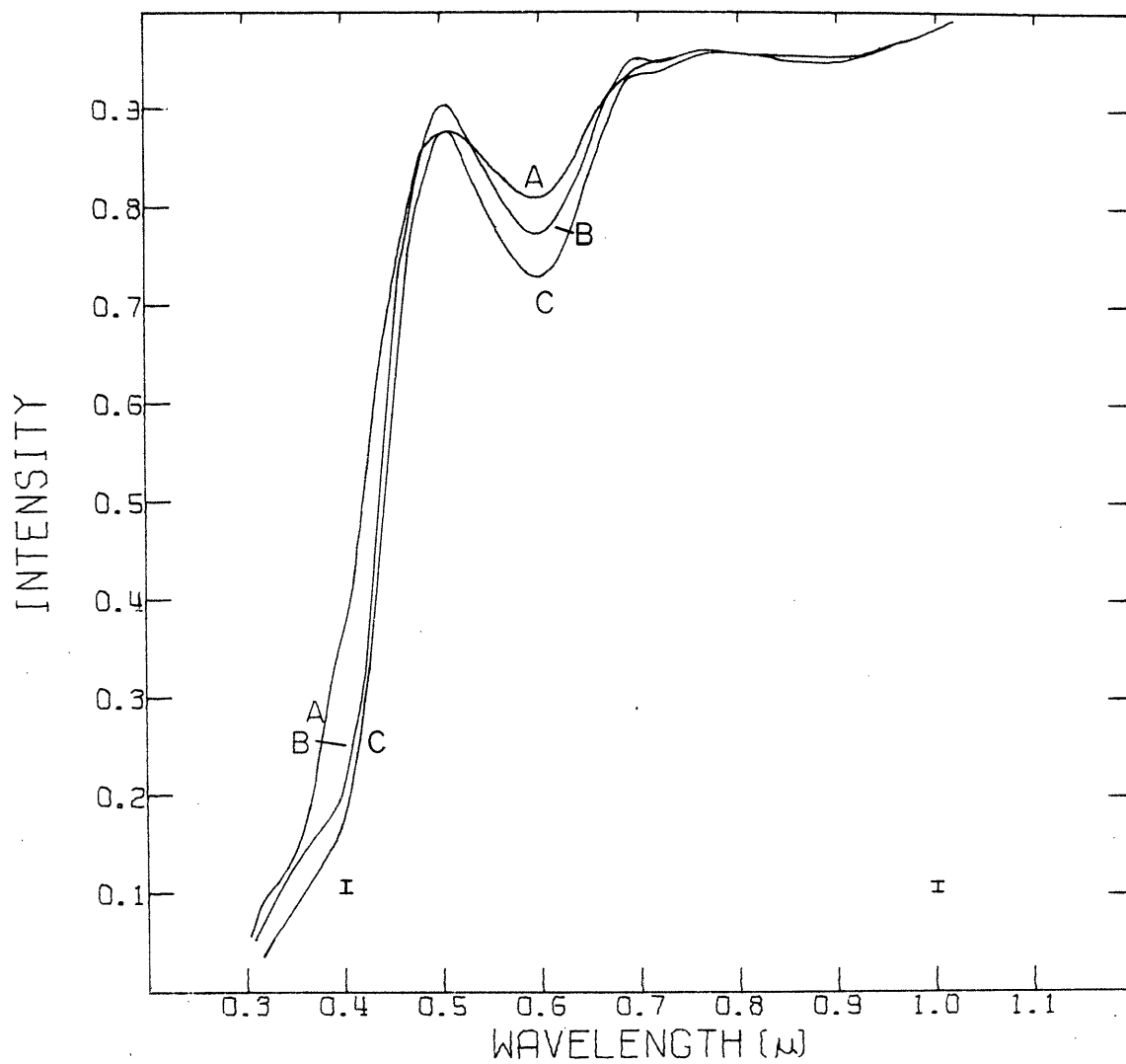
Figure III-11. H$_2$S frost reflection spectra

A. 3 hours irradiation
B. 5 hours irradiation
C. 10 hours irradiation

$H_2S + NH_3$:   The unirradiated $NH_3 + H_2S$ frost (NH_4SH) is flat and featureless (Figure III-12A). Upon irradiation (Figure III-12B), the spectrum appears to be similar to that obtained by the irradiation of pure H_2S frost. Again, with increasing irradiation time (Figures III-12C,D), the 0.6μ feature increases in depth and the short wavelength absorption feature moves toward longer wavelengths. In one experiment, the irradiation time was increased to 20 hours (Figure III-13). Note that the strength of the 0.6μ feature appears to be decreasing.

Several other types of experiments were conducted with the NH_4SH. A dry ice-acetone mixture was used as a coolant (Figure III-14). The absorption feature shortward of 0.5μ was decreased in strength and the 0.6μ feature all but disappeared. Several different cutoff filters were used to determine the wavelength dependence of the irradiation on the frost (Figure III-15). There is a definite weakening trend as one cuts off more and more of the UV radiation. Use of a pyrex filter, cutoff about 0.26μ (Figure III-15A), decreases somewhat the strength of the absorption feature shortward of 0.5μ and the 0.6μ feature. A glass filter (cutoff about 0.28μ) decreases the strengths even more, the 0.6μ band being almost completely eliminated (Figure III-15B). The 0.6μ band is eliminated and the short wavelength feature is significantly reduced with the use of a glass filter (cutoff about 0.3μ) (Figure III-15C).
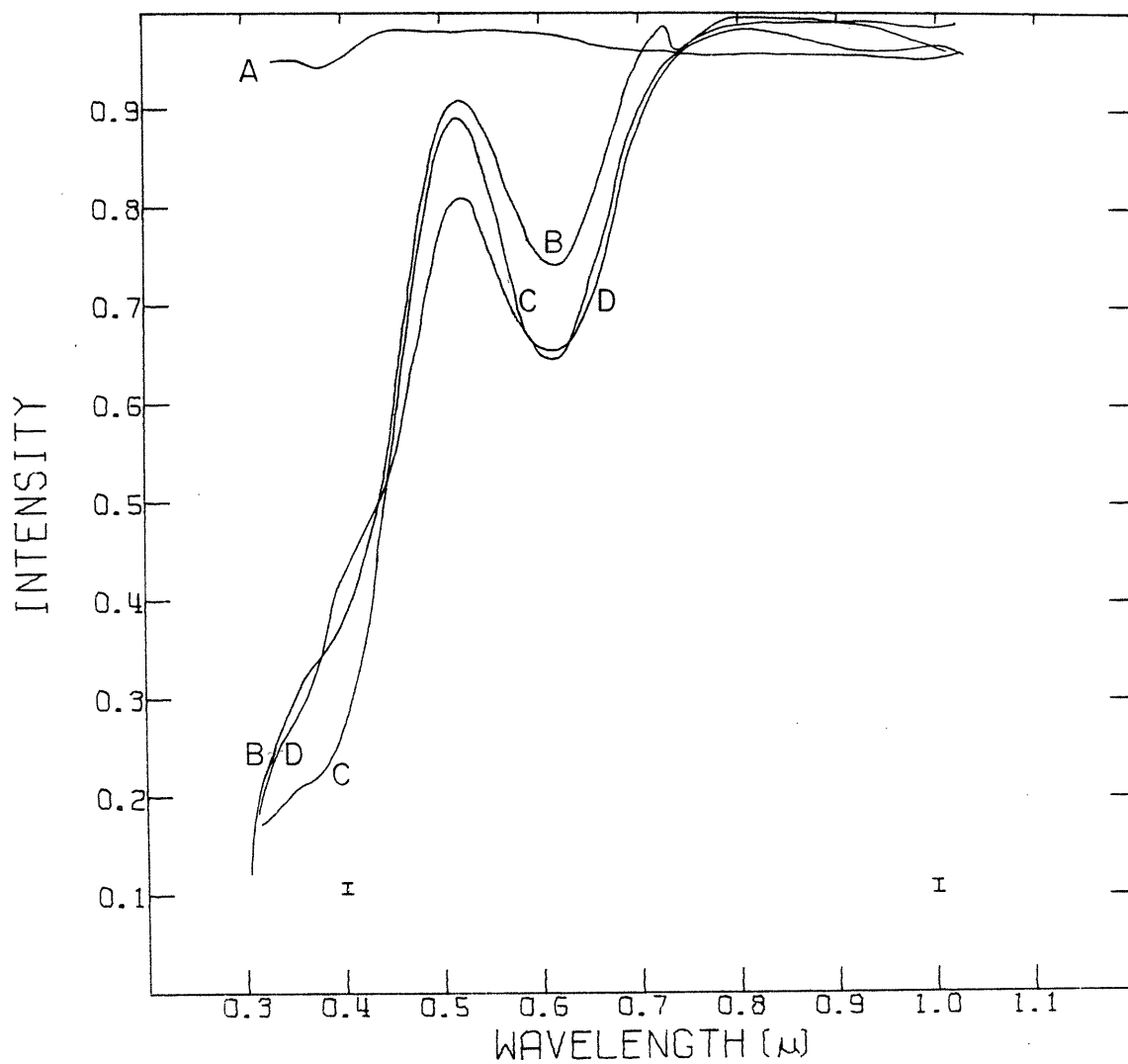
Figure III-12. NH_4SH frost reflection spectra
A.   unirradiated frost
B.   1 hour irradiation
C.   3 hours irradiation
D.   5 hours irradiation
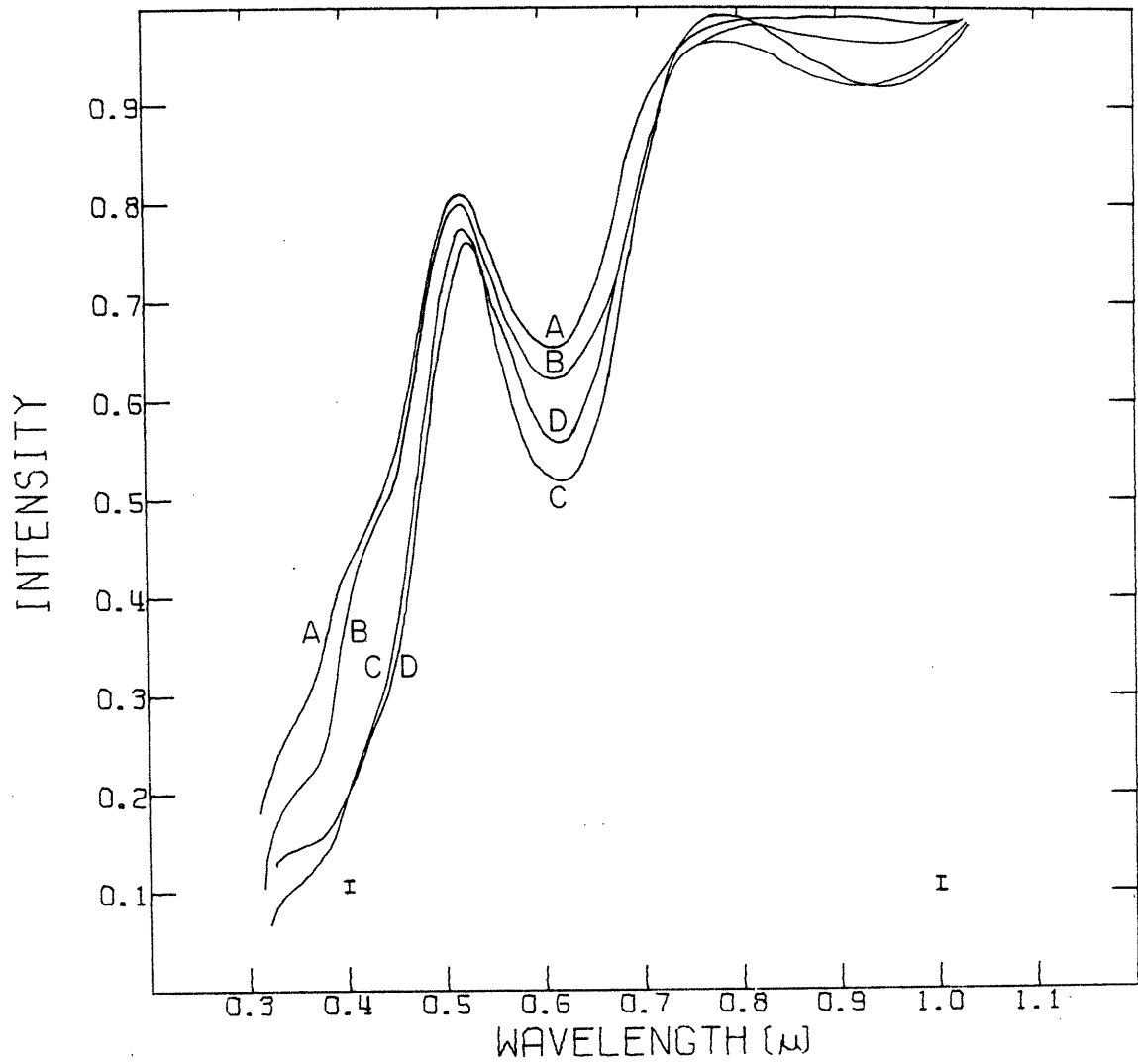
Figure III-13. NH$_4$SH frost reflection spectra

A. 5 hours irradiation
B. 10 hours irradiation
C. 15 hours irradiation
D. 20 hours irradiation

Figure III-14. NH$_4$SH frost cooled with a dry ice-acetone mixture

A. unirradiated frost
B. 1 hour irradiation
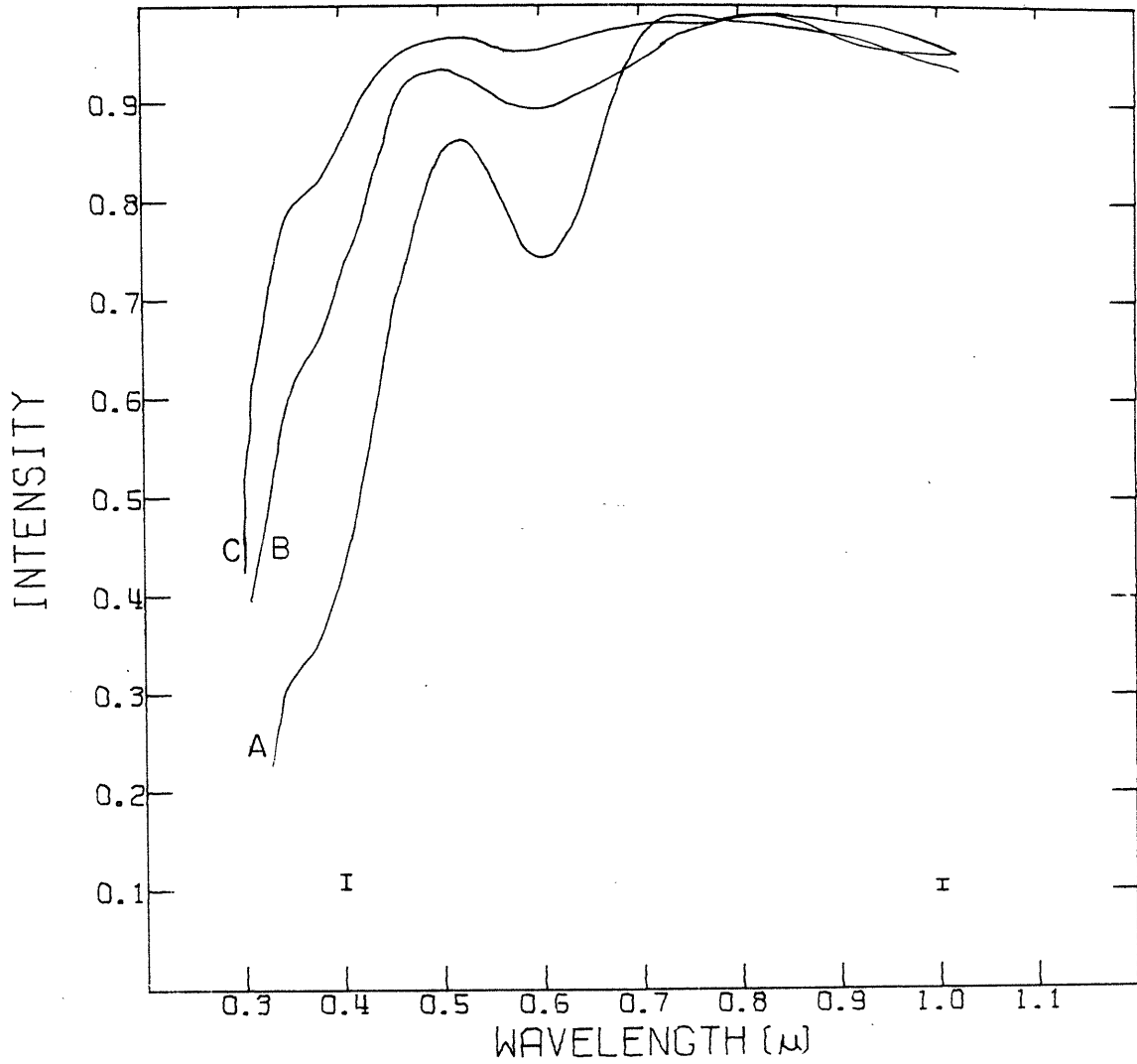
Figure III-15. NH$_4$SH frost reflection spectra

A. Pyrex filter (0.26μ cutoff) 3 hours irradiation
B. Glass filter (0.28μ cutoff) 3 hours irradiation
C. Glass filter (0.30μ cutoff) 3 hours irradiation

$NH_3 + 2H_2S$: As expected, the spectrum of the unirradi-
ated frost is featureless (Figure III-16A). Upon irradiation,
both the short wavelength absorption feature and the 0.6μ
feature appear. At longer irradiation (Figures III-16B,C),
the short wavelength absorption feature reaches a minimum at
about 0.4μ and flattens out shortward of that.

$5NH_3 + H_2S$: The unirradiated frost spectrum is feature-
less (Figure III-17A). The irradiated frost shows the 0.6μ
band and the shortwavelength absorption feature, but there
appears to be an absorption feature centered at 0.38μ.

$H_2S + 10H_2O$: To the naked eye, the frost is white, but
the reflection spectrum of the unirradiated frost is not
featureless (Figure III-18A). There is a decrease in reflec-
tivity longward of 0.85μ. The reflectivity decreases slowly
shortward of 0.7μ decreasing rapidly shortward of 0.35μ.
Irradiation tends to weaken the infrared absorption feature
but increases the strength of the short wavelength feature.

$NH_3 + H_2S + H_2O$: Similar to the $NH_3 + 10H_2O$, the unirra-
diated frost has a reflection spectrum which decreases toward
the IR and UV, though the UV absorption feature is much
weaker (Figure III-19A). Irradiation tends to strengthen
the UV absorption but the IR absorption remains about the same.
Also, a 0.6μ absorption band appears which gets stronger with
increasing irradiation (Figures III-19B,C).
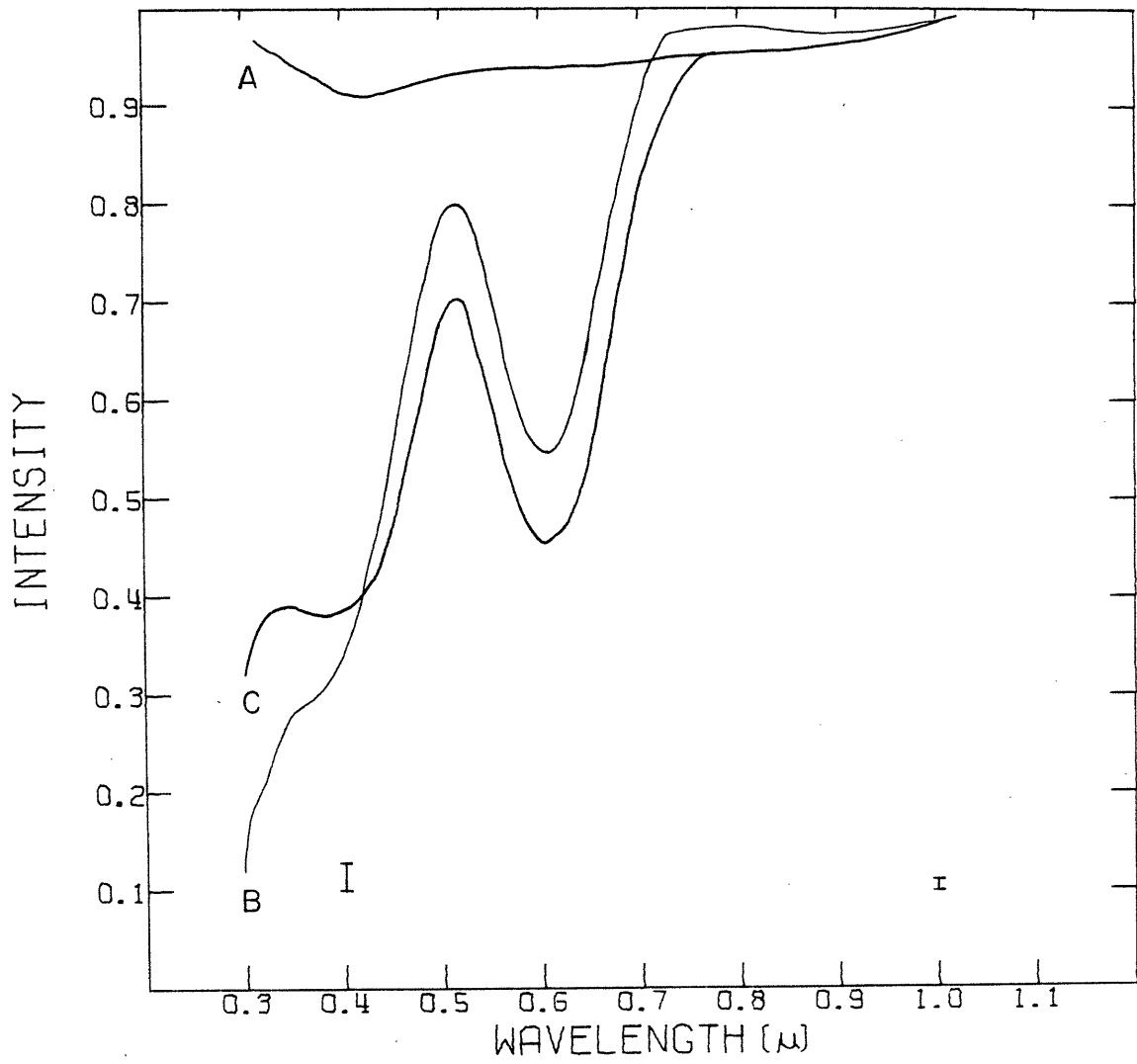
Figure III-16. $NH_3 + 2H_2S$ frost reflection spectra
A. unirradiated frost
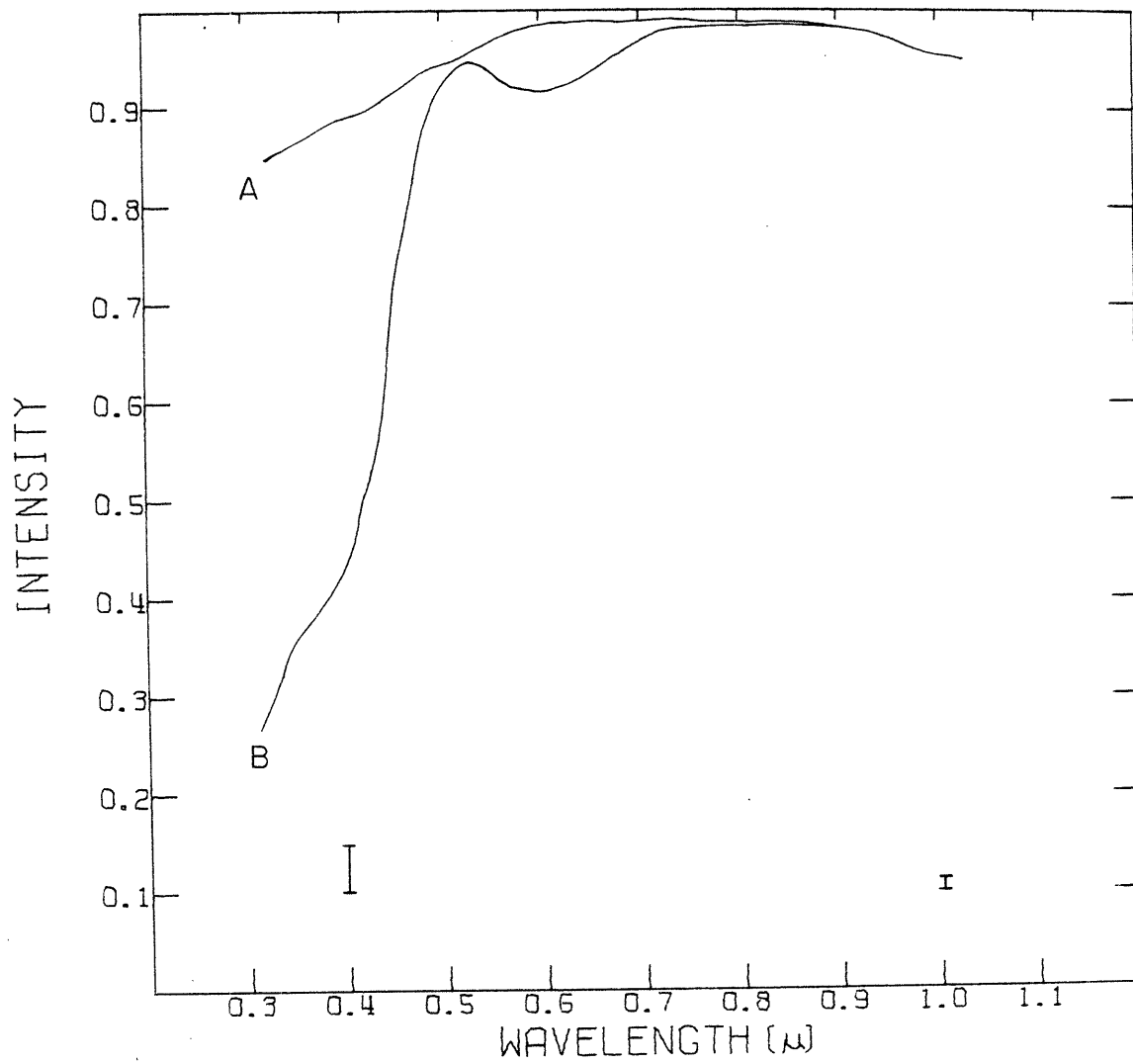B. 1 hour irradiation
C. 3 hours irradiation
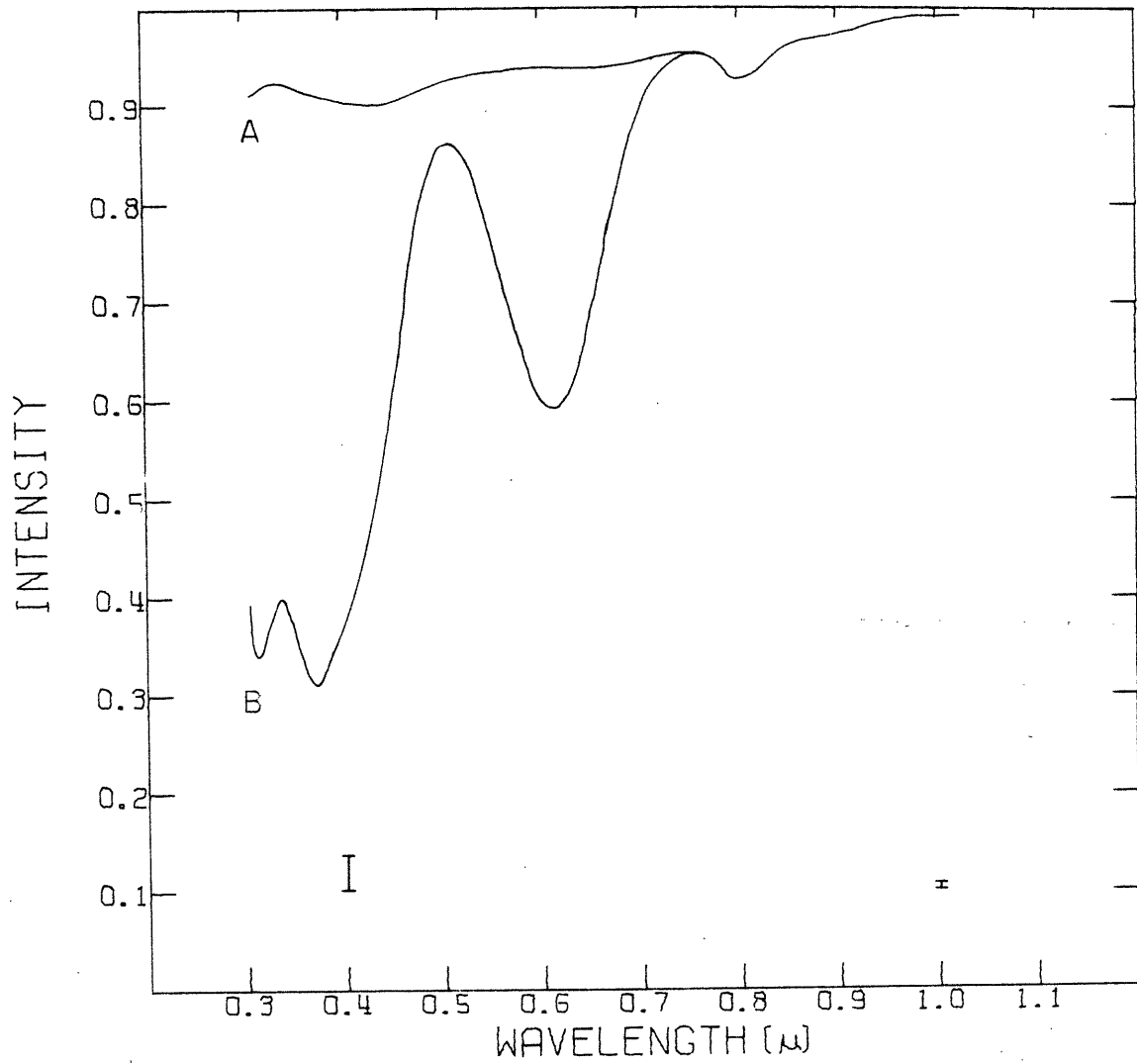
Figure III-17. 5NH$_3$ + H$_2$S frost reflection spectra

A. unirradiated frost
B. 1 hour irradiation
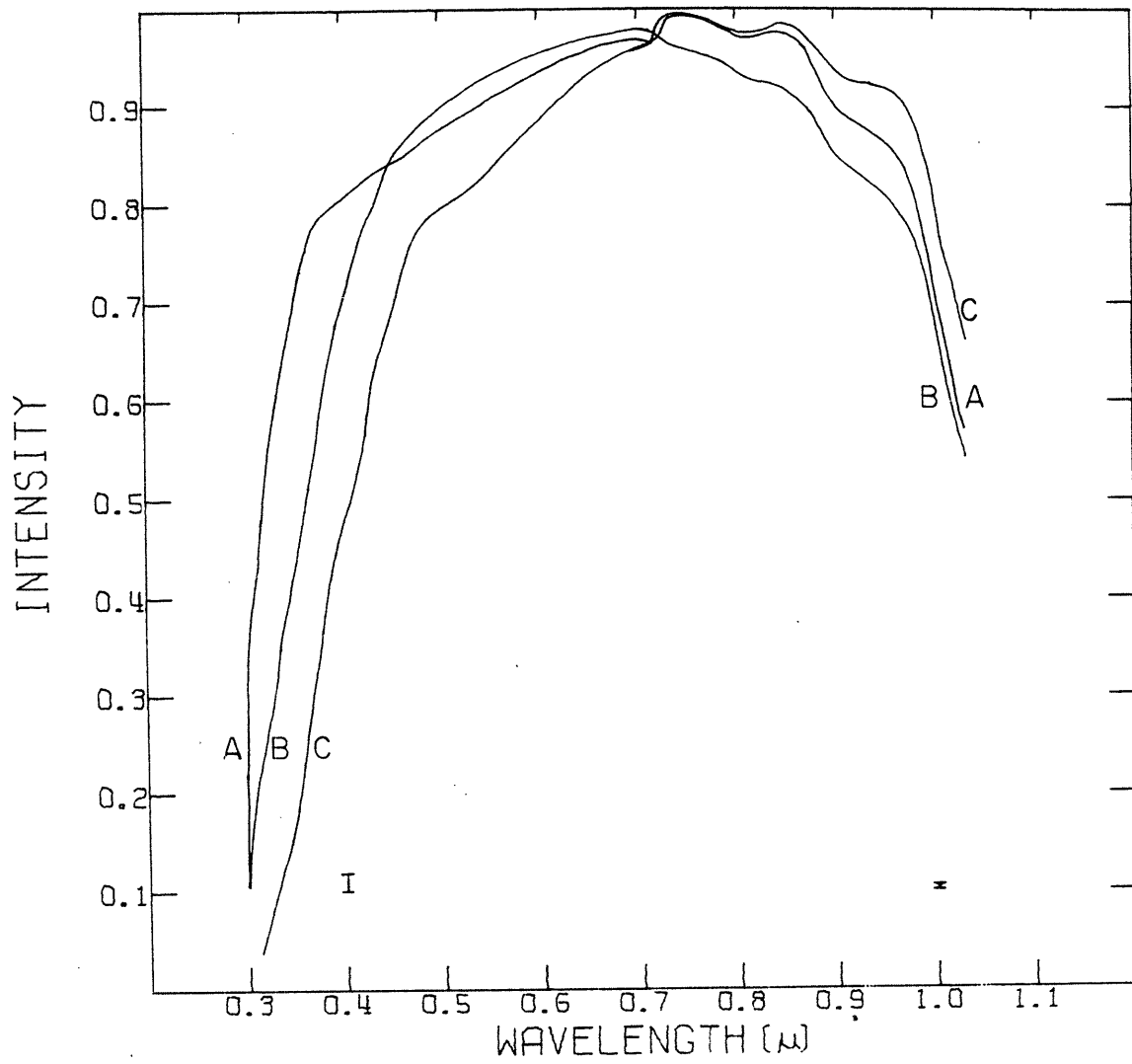
Figure III-18. $H_2S + 10H_2O$ frost reflection spectra

    A.   unirradiated frost
    B.   1 hour irradiation
    C.   3 hours irradiation
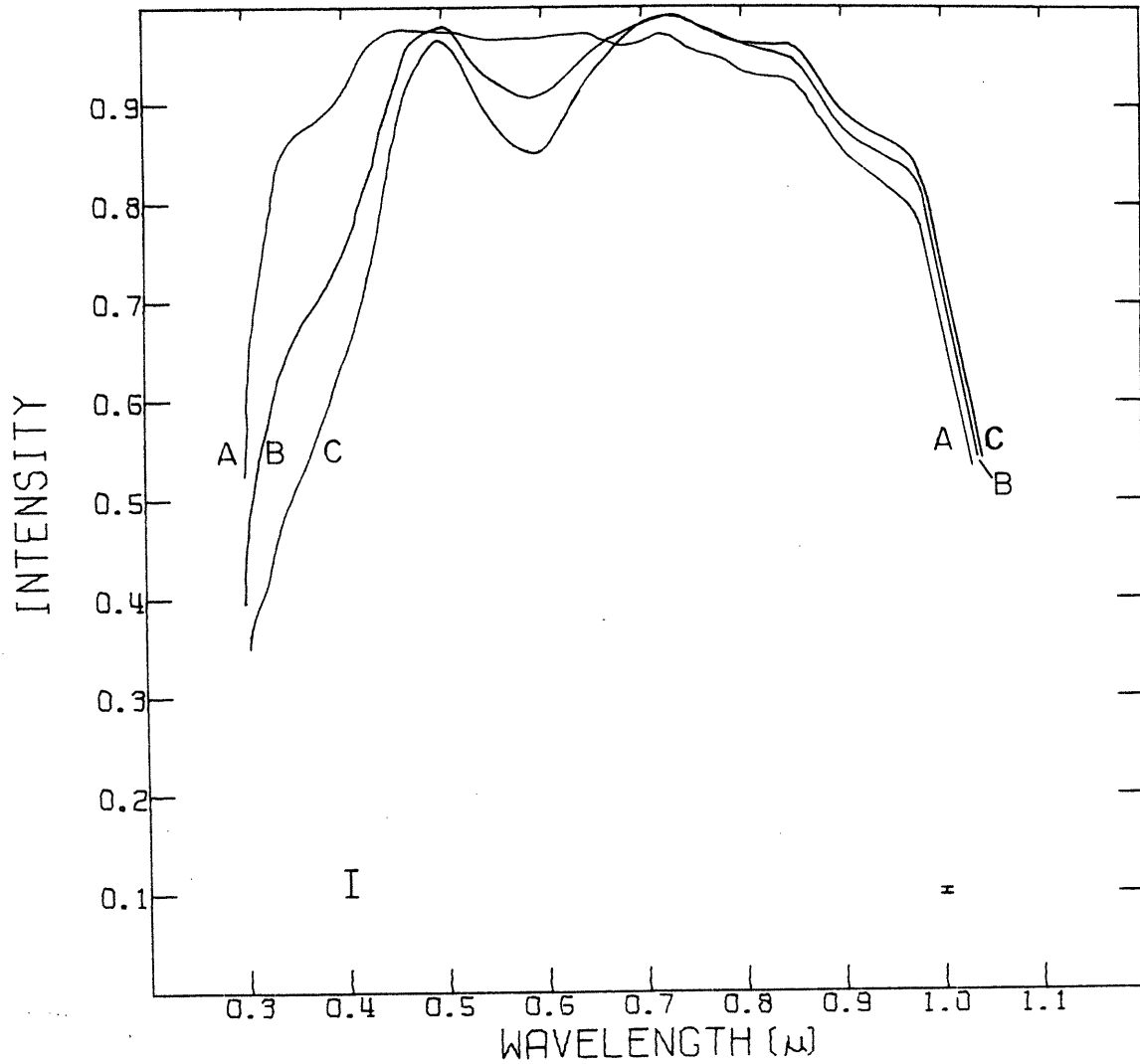
Figure III-19. $NH_4SH + H_2O$ frost reflection spectra

    A. unirradiated frost
    B. 1 hour irradiation
    C. 3 hours irradiation

d) Scope and Limitations

As can be seen from the data so far presented, the number of parameters that are involved in an experiment is quite large. The parameters investigated that may contribute to the spectral reflectivities of frosts were: original frost composition, irradiation time, irradiation intensity (see below), wavelength distribution of the irradiating light, final frost composition and possible contamination of the frost (see below). Another parameter that may affect the spectral reflectivity results is the particle size distribution in the frost. In this part of the thesis, we have limited our studies to the existence, positions and general trends of absorption features in the unirradiated and irradiated frosts being studied.

Changes in the particle size distribution will affect the strengths of absorption bands by changing the pathlength of the light before it is scattered out of the frost (Adams and Filice, 1968; Kieffer, 1968; Gaffey, 1973). Because of the setup of the cold chamber, it was impossible to examine the grain size of the frost without removing the cold finger from the cold chamber, so grain size measurements were carried out only a few times. By examination of several of the frosts under a microscope, it was found that the frosts were fine to medium grained (greater than 10μ in diameter). Kieffer (1968) found that the strengths of absorption features is very size dependent for medium and fine grained frosts. It is

therefore possible that the increase in the strengths of the absorptions bands may be due to an increase in grain size (due to energy input of the UV lamp). As can be seen in Figure III-6, one hour of irradiation does not affect the depth of the absorption features, so any change in grain size did not affect the strengths of the features. At these low temperatures, NH_3+H_2S and H_2S+H_2O are more stable than NH_3 and therefore less susceptible to changes in grain size, implying that the increase of absorption with increase in irradiation time is probably not due to an increase in particle size. Since H_2S is less stable than NH_3, it is not clear that we are not seeing any grain size effects, though, because of the similarity in the strengths of absorption features for a given amount of irradiation, it is again probable that what we are seeing is not a grain size effect.

Another limitation to the results of these experiments is the determination of the exact composition of the frosts formed by the irradiation of known parent frosts. Because of absorption by the surface layer, only a very thin layer of irradiated frost is formed. The majority of the frost on the cold finger remains unirradiated. Therefore no attempt was made to determine the composition of this frost layer by methods other than to compare reflection spectra of the frosts with spectra of known compounds (see below). From this, possible identifications can be made.

Finally, no attempt has been made to determine any wavelength-dependent phase angle effect (Figure III-1).

e) Conclusions

It is clear from the results presented in the chapter that of the frosts studied, only H_2S-bearing frost show any significant change in spectral reflectivity with UV irradiation. Methane frost may be affected by UV irradiation, but only radiation a wavelength less than 0.16μ is energetic enough to disrupt the CH_4 molecule. It is therefore unlikely that methane photodissociation by solar Uv radiation is of any significance because of the extremely low solar output below 0.16μ.

Figure III-20 shows the spectral reflectivity $(0.2-0.6\mu)$ of an NH_4SH frost. As with previous spectra of unirradiated frosts, the spectrum is flat beyond 0.3μ. But there is a significant decrease in reflectivity below about 0.27μ due to the breaking of the H-S bond. If this is true, it can be assumed that the frost should be unaffected by radiation longward of about 0.3μ. This is indeed the case (Figure III-15). The use of short wavelength cutoff filters greatly reduces the effects of the irradiation until, using a 0.3μ cutoff filter, the frost is almost unaffected by the irradiation.

The frost in Figure III-20 has been allowed to remain unirradiated in the chamber. As can be seen, there is no significant change in the frost spectrum after several hours. We can therefore conclude that all the results presented here represent UV irradiation of frosts and not secondary effects due to long-term contamination of the frost of the effects of visible light heating, etc. on the structure of the surface
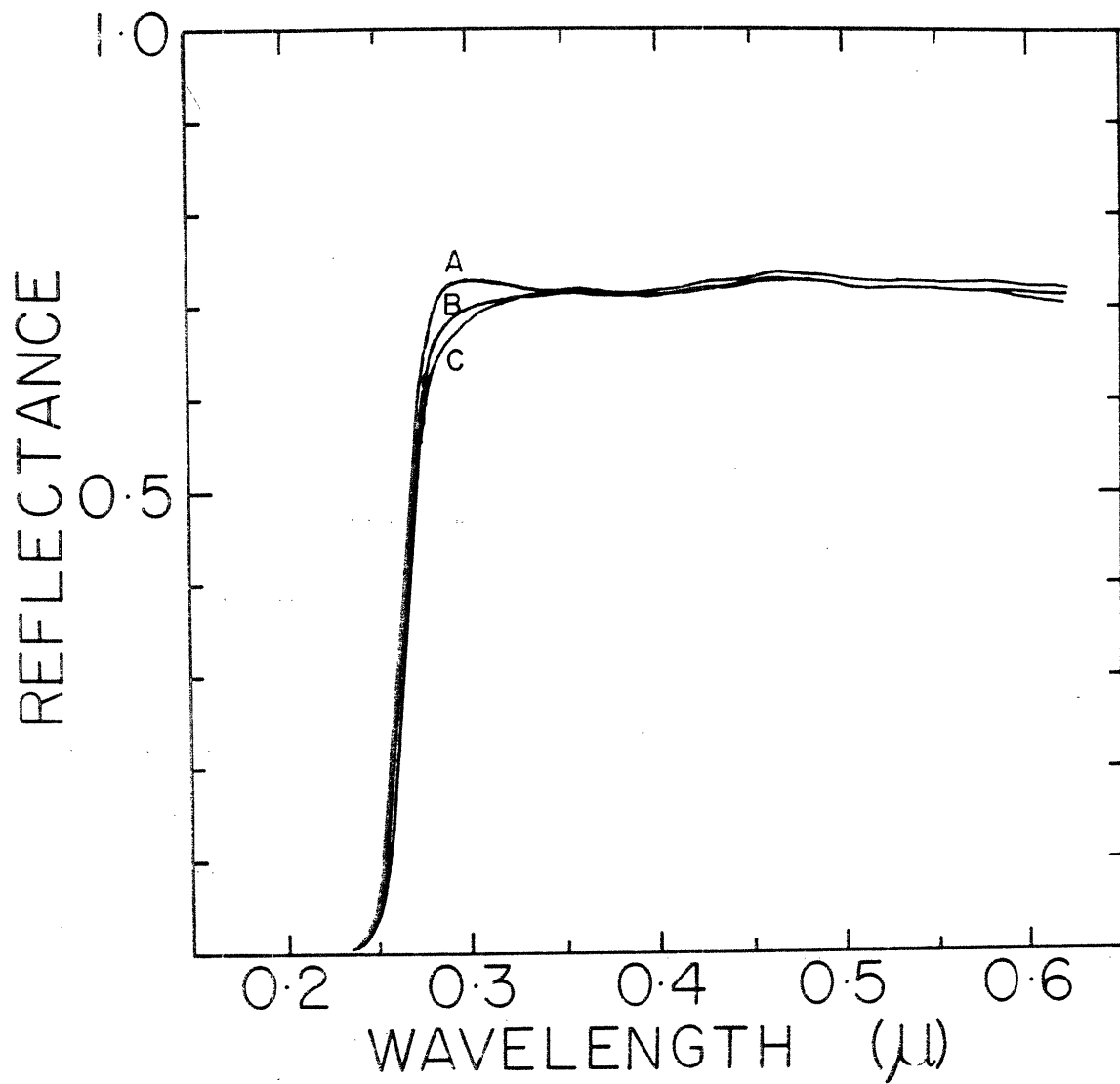
Figure III-20. NH$_4$SH frost reflection spectra

A. unirradiated frost, 1 hour
B. unirradiated frost, 3 hours
C. unirradiated frost, 5 hours
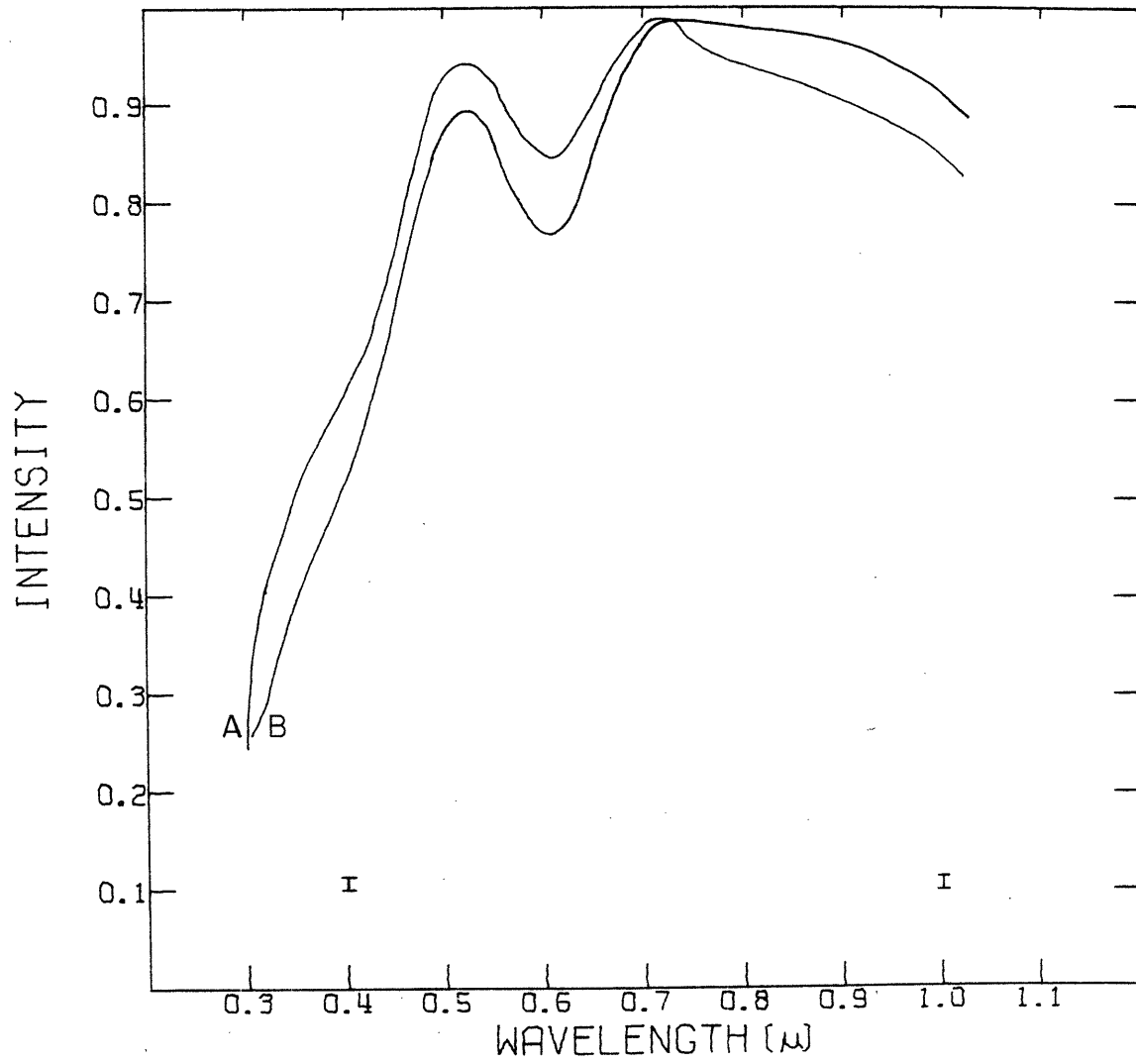
Figure III-21. NH$_4$SH frost reflection spectra

    A. 1/2 hour irradiation, no lens

    B. 1 hour irradiation, no lens

of the frost.

The effects of Uv irradiation on frost appears to be a very rapid process. Figure III-21 shows the effect of 0.5 and 1.0 hour irradiations on NH_4SH frost without the use of a lens to focus the light beam thereby reducing the irradiation rate by a factor of about 100 from the rate used in all other experiments. Comparison of these curves with a normal 1 hour irradiation with a lens (Figure III-12) shows that most of the effects of irradiation occur very rapidly and then change slowly with time. This confirms the conclusion that only a very thin layer of irradiated material is formed which prevents the subsurface frost from being irradiated to any extent.

Only a preliminary attempt has been made to determine the composition of the UV irradiated frosts. As has been stated previously, all the H_2S-bearing frosts that have been irradiated have blue and ultraviolet absorption bands and an additional absorption band at about 0.6μ. Several classes of compounds must be considered that may be important in the formation of colored sulfur frosts:

(1) Sulfur radical cations: Sulfur in oleum forms a blue solution. Investigators are in disagreement as to the exact nature of the sulfur component that is causing the coloration, but it is agreed that an absorption feature at about 0.59μ and several other absorption features in the region of 0.2-0.4μ are due to sulfur cations (S_4^+, S_5^+, S_7^+, etc.). (See Ingram and Symons, 1957: Symons, 1957; Gillespie, et al., 1971;

Stillings, et al., 1971a,b; Beaudet and Stephens, 1971;
Gillespie and Ummat, 1972; Symons and Wilkinson, 1972).

(2) Sulfur radical anions: Sulfur in amine solvents have
been shown to be blue to green in color. Absorption bands
have been observed at 0.62μ, 0.59μ, 0.4μ and several bands in
the 0.2-0.4μ region. Again there has been some disagreement
among the investigators as to the actual sulfur components
causing the absorption features, but it has been generally
concluded that the green color (bands 0.59-0.62μ and 0.2-0.4μ)
is probably due to S_2^- and S_3^- ions in the solution. (MacColl
and Windwer, 1970; McLaughlin and Marshall, 1970; Chivers and
Drummond, 1971, 1972; Giggenbach, 1968, 1971a,b, 1972, 1973.)

Early works on frozen colored sulfur (Rice and Sparrow,
1952; Rice and Ditter, 1953; Freund, Adler and Sparrow, 1953;
Radford and Rice, 1960) showed that purple and green sulfur
was probably due to sulfur radicals (unpaired electrons in
sulfur chains). They were unable to identify the radiacl types
involved.

The more recent work of Feher (1963); Feher and Münzner
(1963); Meyer and Spitzer (1972); Meyer, Oommen and Stroyer-
Hansen (1972); Meyer, Gouterman, Jensen, Oommen, Spitzer and
Sroyer-Hansen (1972) has shed significant light on the possible
sulfur products being formed in our experiments. The results
show that hydrogen polysulfides (H_2S_x), ammonium polysulfides
(($NH_4)_2S_x$) and sulfur rings are in general yellow to yellow-
orange in color implying a decrease in reflectivity shortward
of 0.4-0.5μ. Also, diradical sulfur chains (S_n, n=5-7) can be

expected to have absorption features between 0.55μ and 0.65μ. This is exactly what we observe, a decrease in reflectivity shortward of 0.5μ (H_2S_X, $(NH_4)_2S_X$, $C-S_X$) and an absorption feature centered at about 0.6 (sulfur free radicals).

These conclusions are confirmed by the laboratory experiment conducted at 195°K. The steady-state number of free radicals would be expected to be greater at a lower temperature when they are less mobile and therefore less likely to form stable sulfur rings. This would imply that the absorption band caused by the radicals would be stronger at lower temperatures as can be seen from a comparison of Figures III-12 and III-14.

The exact compositions of the frosts formed by irradiation are not known, so it is difficult to make any conclusive re- marks as to the components causing the reflection spectra that we observe. But it is clear from the great similarities between our reflection spectra and the spectra of other investigators that we are looking at very similar processes and therefore very similar absorbing species.

IV. STABILITY OF VOLATILES IN THE SOLAR SYSTEM

a) Introduction

The discussions in the previous chapters have shown that the Galilean satellites and Saturn's rings have ice-like surfaces. Their infrared reflection spectra are similar to the reflection spectrum of water frost (Pilcher, et al., 1970; Pilcher, et al., 1972; Fink, et al., 1973), but their visible spectra decrease toward the blue and ultraviolet, unlike water frost (Johnson and McCord, 1970; Lebofsky, et al., 1970; Irvine and Lane, 1973). Other satellites whose reflection spectra have been investigated have flat, featureless reflection spectra (McCord, Johnson and Elias, 1970).

The results so far presented indicate that UV irradiated H_2S-bearing frosts are likely candidates for the coloring agent on the surfaces of the Galilean satellites and in the particles of Saturn's rings. But, there are many other frosts that have flat featureless spectra in the visible region and so are possible candidates for the surfaces of the other satellites. Until IR spectra of these other satellites are obtained, we must depend on our present knowledge of their spectra to help us determine the composition of their surfaces.

Watson, Murray and Brown (1963) investigated the stability of volatiles in the solar system. The stability of a frost is determined by the evaporation rate of the frost (heated by solar radiation), the greater the evaporation rate, the more frost that is evaporated in a given time (say 10^9 years) and the lower its stability. Their study was limited to rapidly rotating bodies, implying a uniform temperature over the entire surface of the body. They discussed slowly rotating bodies, ie. surfaces not in thermal equilibrium, but did not consider this case in any of their calculations of frost

stabilities.

The discussion presented here considers a more complicated model for the stability of volatiles on the surfaces of solar system bodies (satellites, particles in Saturn's rings). We have also expanded the number of frosts being investigated to cover the gas hydrates and frosts being studied in our laboratory experiments. We have found that the simple model used by Watson, et al., is not valid for satellites. All satellites with known or assumed rotation rates have synchronous rotation rates and are therefore slowly rotating (greater than two days). The rotation rates of the particles in Saturn's rings are unknown but are probably rapid enough to put them in the rapidly rotating class. As will be shown, a frost on the surface of a slowly rotating satellite is several orders of magnitude less stable than the same frost on the surface of a rapidly rotating body.

b) <u>Method</u>

We shall consider the stability of various frosts on the surfaces of rotating spherical bodies at given distances from the sun. As stated by Watson, Murray and Brown (1963), the surface temperature distribution of a body will be determined by its solar distance, by the rate of rotation and by the albedo, latent heat of sublimation and emissivity of the frosts exposed at the surface of the body. Only distances greater than a few AU from the sun will be considered for our stability calculations so that only sublimation of the frost (not melting) need be considered since equilibrium temperatures will be below the melting temperatures of the frosts in question (see Watson, <u>et al.</u>).

The rate of solar energy absorbed by a unit surface area of a spherical body is:

$$dE_{in}/dt = ((1-A)S/R^2)\cos\theta \cos\phi$$

Where:

A surface albedo

S solar constant in ergs/cm^2/sec (@1AU)

R heliocentric distance of objects in AU

θ latitude distance from meridian

ϕ longitude distance from equator

dE_{in}/dt energy absorbed in ergs/sec/cm^2

The assumption has been made that the plane of satellite rotation, the plane of the satellite's orbit around its primary and the plane of the orbit of the primary around the sun all coincide. This assumption implies that the subsolar point moves along the equator of the satellite, greatly simplifying calculations. The subsolar point is also defined as the 0° longitude

point of the satellite so that the satellite surface moves with respect to the coordinate system. For a planet, the assumptions are the same, except that it is not assumed to be revolving around a primary, which does not effect the calculations. For most solar system bodies (Neptune being an exception, having its rotation axis in the plane of its orbit) these assumptions lead to only very small errors which can be ignored.

For an equilibrium, ie. energy conservation, this absorbed energy must equal the sum of the surface flow inward, the energy reradiated by the surface and the energy removed by evaporation:

$$\therefore dE_{in}/dt = ((1-A)S/R^2)\cos\theta \cos\phi$$

$$= Q + \varepsilon \sigma T^4 + H\dot{E} \tag{2}$$

Where:

Q surface heat flow in ergs/cm^2/sec

ε emissivity of surface at the surface temperature (assumed = 1)

σ Stefan-Boltzmann constant

H latent heat of sublimation of the ice at T °K

$\dot{E}$ evaporation rate of the frost at T°K

The surface heat flow is considered small and will therefore be ignored (see Watson, et al., 1963).

$$\therefore ((1-A)S/R^2)\cos\theta \cos\phi = \sigma T^4 + H\dot{E} \tag{3}$$

The vapor pressure of various frosts have been determined experimental. In most cases, a linear fit is made to the experimental vapor pressure vs. temperature data which can be extrapolated to lower temperatures. In a few cases, a more complicated curve is fit to the data which can again be extrapolated to lower temperatures (see Appendix A).

Since the vapor pressures we are considering are low, we assume a perfect gas so that we can apply the Clausius-Clapyron equation to determine the heats of sublimation from the vapor pressure equations. The evaporation rate, $\dot{E}$, is calculated from the vapor pressure using the equation:

$$\dot{E} = p\sqrt{\mu/\pi R'T} \qquad (4)$$

Where:

P   vapor pressure

μ   molecular weight of gas

R'   gas constant

(Watson, et al., 1961; Estermann, 1955)

To facilitate the calculations of the evaporation rates of the frosts for specific distances from the sun, equation (3) was solved assuming T to be the independent variable and solved for R, ie.:

$$R = \left(\frac{(1-A)S \cos\theta \cos\phi}{\sigma T^4 + H\dot{E}}\right)^{1/2} \qquad (5)$$

See Figure IV-1 for solutions of temperature vs. distance for the ices being investigated. In this case we have assumed $\theta = \phi = 0$, ie. the subsolar point and an albedo of 50%. Note how the higher evaporation rates of some frosts tend to reduce the equilibrium temperatures of the frosts. For comparison, Figure IV-2 shows the temperature vs. distance for the same frosts but assuming the planet is in thermal equilibrium. Since the planet receives energy as a disk (πr^2) and radiates over its entire surface ($4\pi r^2$), equation (5) becomes:

$$R = \left(\frac{(1-A)S}{4(\sigma T^4 + H\dot{E})}\right)^{1/2} \qquad (6)$$

Figure IV-1A. Temperature vs. Distance curves for the frosts being investigated. The temperatures are for the subsolar point with an assumed albedo of 50%.
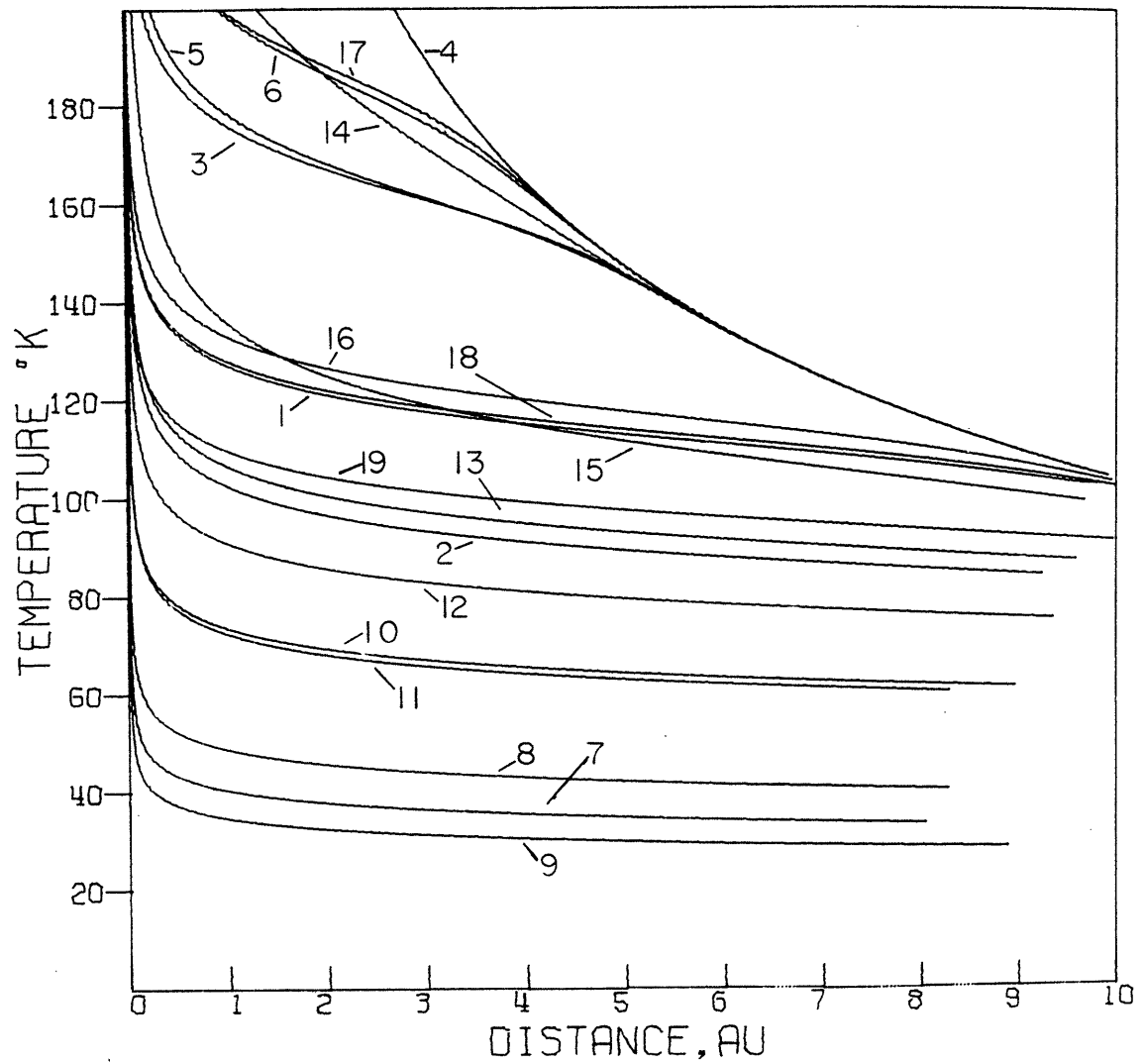
Figure IV-1B. The curves are expanded in distance for clarity. The numbers refer to the frosts in Table B-2.
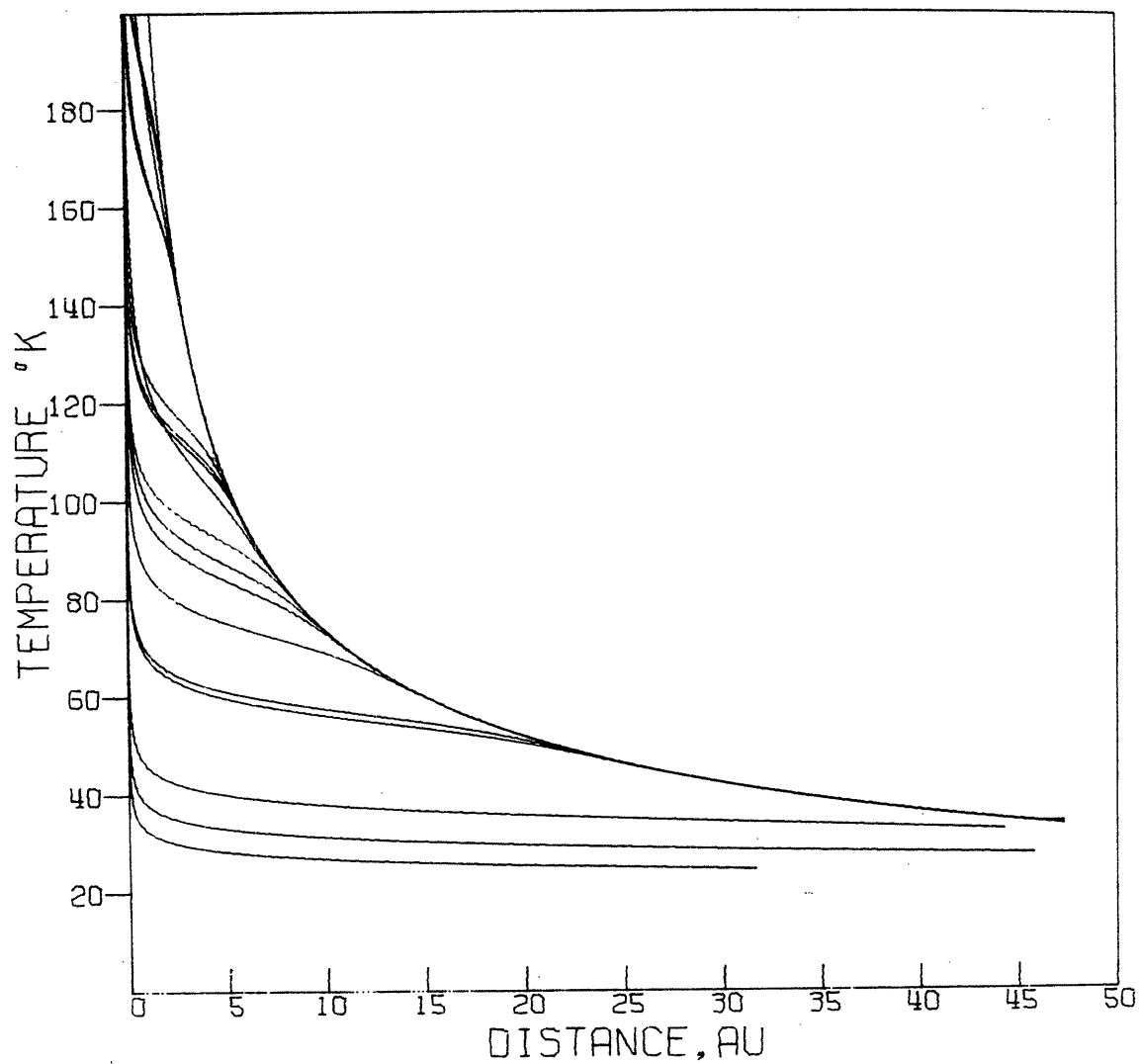
Figure IV-2A. Temperature vs. Distance curves for the frosts being investigated. The object is considered to be in thermal equilibrium (rapidly rotating). The albedo of the frost is assumed to be 50%.
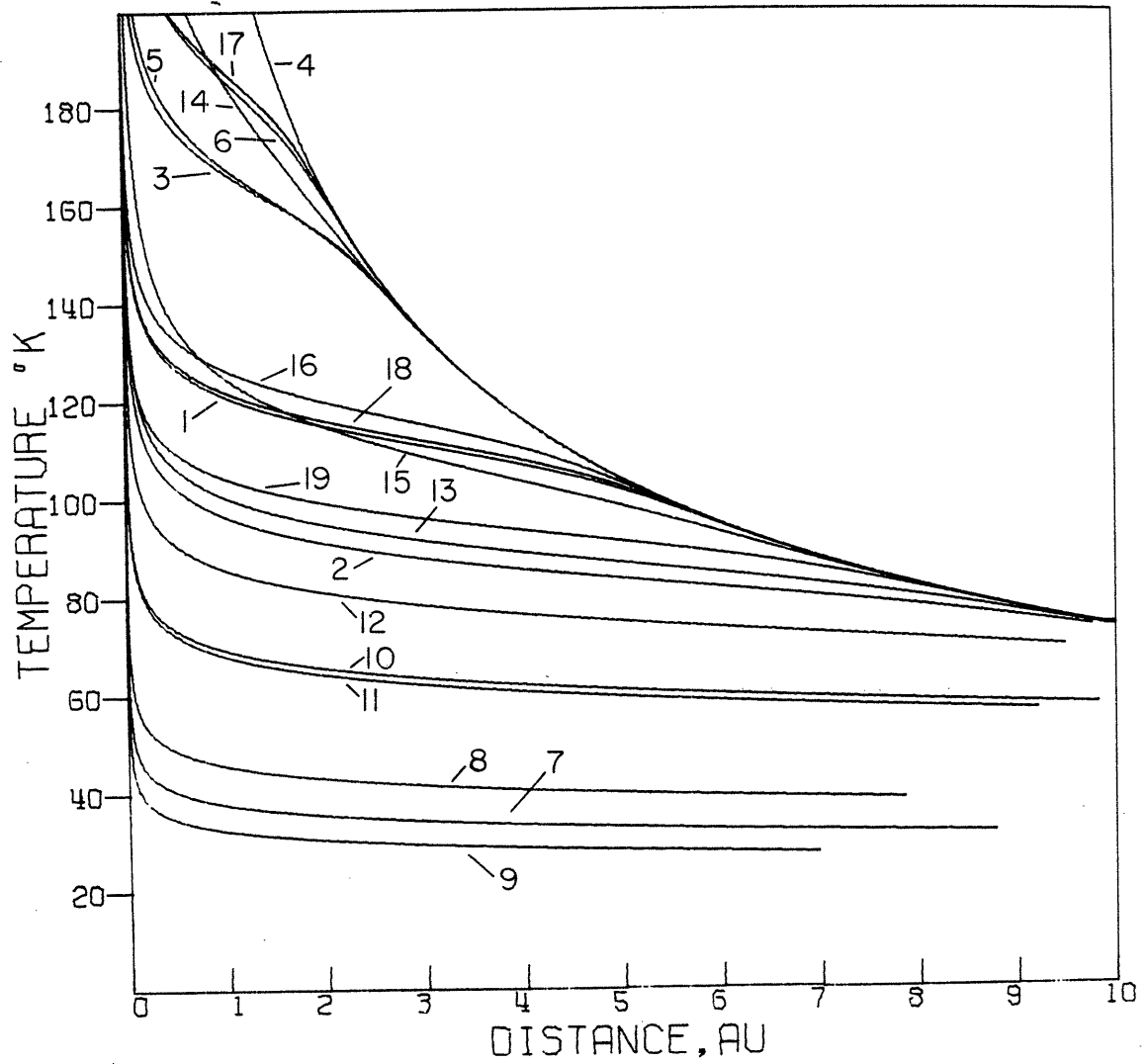
Figure IV-2B. The curves are expanded in distance for clarity. The numbers refer to the frosts in Table B-2.

Appendix B contains the temperature vs. distance curves for water frost, varying θ, ϕ and albedo. A desired value of R (the distance of a planet from the sun) can then be chosen and thus the equilibrium temperature and evaporation rate for a given frost at a given albedo at a given θ and ϕ can be found. The results of these calculations for several frosts for the distances of Jupiter, Saturn, Uranus and Neptune can also be found in Appendix B.

As can be seen from these results, most of the evaporation occurs around $\theta = 0°$. So, to a good approximation, the evaporation rate of a frost over a rotation of the planet about its axis can be approximated by 0.05 to 0.3 times the maximum evaporation rate. But, for the region of stability, ie. for evaporation rates less than 10-100 km/ 10^9 years the average rates are about 0.10 ± 0.05 times the maximum rate. So for an approximation in our evaluations of the stabilities of the frosts we will use 0.1 times the maximum rate as the average rate of evaporation of the frosts under consideration.

An analysis of the results of our calculations for the frosts under investigation (Appendix A) can be found in Table B-1. The distances of interest are: Jupiter (satellites), Saturn (rings and satellites) and Uranus and Neptune (satellites).

c) Conclusions

The following can be concluded from the results of Appendix B:

Sulfur-bearing compounds (except pure H_2S) would be stable on the surfaces of satellites at the distance of Jupiter and beyond. For the satellites of Jupiter, the sulfur-bearing frosts may not be stable near the equators of the satellites, but become much more stable as the poles are approached. There is essentially no loss of these frosts for Saturn and beyond so that these frosts would be stable even in the rings of Saturn where the particles may only be meters in diameter. H_2S itself does not reach stability until the distance of Uranus, and then only near the poles, though the hydrate of H_2S fits into the previously mentioned group. Solar UV irradiation of the sulfur-bearing frosts produces polysulfides (see Chapter III) which tend to be more stable than the parent frosts (as in the case of H_2S and H_2S_2).

Water frost is stable throughout this region of the solar system. Ammonia and its hydrates become stable on the surfaces of the satellites of Saturn and possibly in Saturn's rings (see section d). Methane hydrate, but not methane becomes stable near the poles of the satellites of Uranus and at the distance of Neptune. Carbon dioxide and its hydrate (if they exist) also become stable at Uranus and beyond. One would not expect to find frozen argon or nitrogen, except possibly for the hydrates at large distances from the sun and only near the poles.

d) Scope and Limitations

The results that have been presented are very approximate. Vapor pressures have been extrapolated many orders of magnitude and may lead to errors of an order of magnitude or more in the resulting evaporation rates. This error seems to be most apparent for the ammonia hydrates which would be expected to be more stable than pure ammonia. This is not the case in Table A-1. The error in this case is probably due to the fact that the vapor pressures used to determine the vapor pressure equations were read off of a graph and may not be very accurate.[1]

We have also assumed that each point on the surface is completely isolated from the rest of the surface and at any instant is in equilibrium with the solar energy received. In reality, satellites tend slightly toward the thermal equilibrium of a fast rotating body (see Hansen, 1972; Morrison and Cruikshank, 1973). This would tend to reduce somewhat the evaporation of the frosts near the subsolar point, but would also probably increase the rate far from the subsolar point. Overall, considering the differences between the two extremes, the rate of evaporation would probably decrease.

One of our original assumptions, Equations (2) and (3), was the heat flow into the planet was small and could therefore be ignored. It is possible, in fact, that there is internal heat production by radioactive decay (Lewis, 1971). This would tend to increase the rates of evaporation of frosts.

---

1 A recent revision of the work by Lewis, (1971) (Weidenschilling and Lewis, 1974) has been used by us to recalculate the vapor pressure equation for $NH_3 + H_2O$. The results show that the ammonia hydrate is about as stable as NH_4SH.

Another effect which has not been considered that may greatly reduce the loss of volatiles from the surfaces of satellites in the ability of the satellite to retain an atmosphere. As a frost approaches stability, the vapor pressure of the gas above the frost is very low (see Appendix B). If the planet is able to retain an atmosphere at this level, then there will be an equilibrium between the gas and the frost such that the frost will evaporate only to replenish the loss of the atmosphere (due to photolysis or escape). Calculations of this type are dependent on the size of the planet, the atmospheric temperature, the distance from the sun and the types of frosts and atmospheric gases involved. This is beyond the scope of this thesis.

V. CONCLUSIONS

The results of the previous chapters can be summarized for a preliminary determination of the composition of icy satellite surfaces and the particles in the rings of Saturn.

Saturn's satellites have been observed only in the visible (0.3-1.1μ) (McCord, Johnson and Elias, 1970), see Figure V-1. These satellites have flat, featureless reflection spectra so that no positive determination of composition is possible. From the results of the frost stability calculations and laboratory spectral reflectivity data, the possible frosts present on the satellites are ammonia, ammonia hydrate and water frosts. The sulfur-bearing frosts have reflection spectra which are featureless when unirradiated, but because there is no way to prevent the irradiation of the frosts on the surfaces of Saturn's satellites, we must make our conclusions based on UV irradiated frosts. Since the sulfur-bearing UV irradiated frosts have blue and UV decreases in their reflectivity, they can be eliminated as possible major surface components of Saturn's satellites. Both laboratory and telescopic infrared (1-4μ) spectra are needed to determine more accurately the composition of these satellites.

Saturn's rings and the Galilean satellites J2 and J3 have infrared reflection spectra (1-4μ) consistent with the presence of water frost (Pilcher, et al., 1970; Pilcher, et al., 1972; Fink, et al., 1973), but their visible spectra (0.3-1.1μ) are inconsistent with the presence of water frost (Johnson and McCord, 1970; Lebofsky, Johnson and McCord, 1970). Therefore the surfaces of these objects are probably composed of contaminated water frost (Lebofsky, Johnson and McCord, 1970). The Galilean satellites J1 and J4 may also have water frost present (based on their infrared spectra) and their visible spectra are similar to the spectra of J2 and J3, so it is
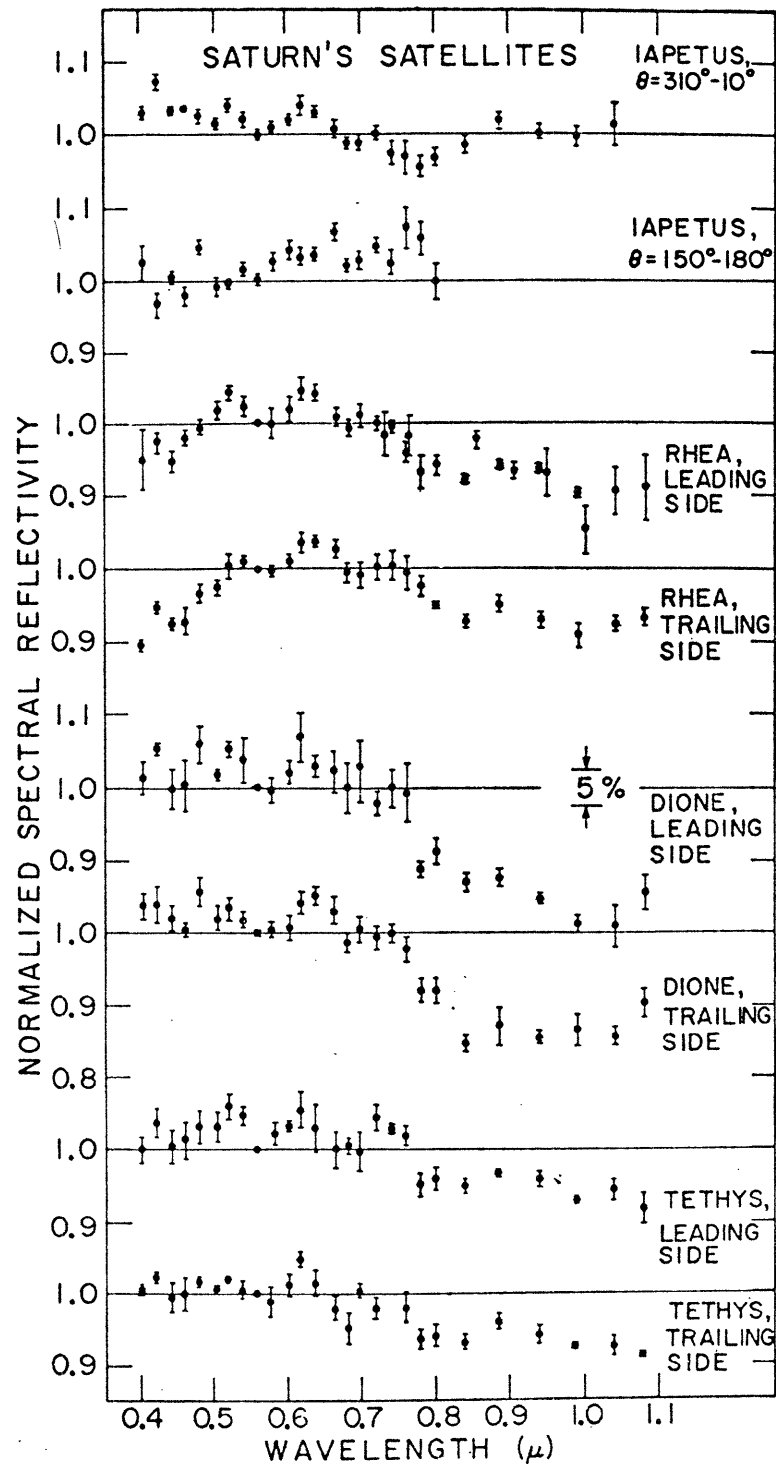
FIG. 1.—Reflectivities as a function of wavelength of four of Saturn's satellites, scaled to unity at 0.56 μ. Trailing- and leading-side spectra are shown separately. Error bars represent the standard deviation of the average of several measurements. Points with no error bars are from a single measurement. Satellite orbital phase angle is defined in the prograde sense with 0° at superior geocentric conjunction, i.e., on the Earth-planet line behind the planet. The leading side is that facing the observer when the satellite is moving in its orbit from behind Saturn to in front of Saturn as viewed from the Earth.

Figure V-1. Spectral reflectivity of Saturn's satellites.

From McCord, Johnson and Elias (1971).

possible thatJl and J4 have surface compositions similar to J2 and J3 and

Saturn's rings.

Figures V-2 and V-3 compare the visible reflection spectra of J1, J2

and Saturn's ring B with laboratory reflection spectra of $H_2S + NH_3 + H_2O$

(Figure V-2, from Figure III-19C) and $H_2S + 10H_2O$ (Figure V-3, from Figure

III-18C). The match between the $NH_4SH + H_2O$ and the solar system bodies is

fairly good except for the existance of the 0.6μ feature in the laboratory

ice spectrum. The spectra all show decreases toward the UV and toward the

infrared. The match of $H_2S + 10H_2O$ with the solar system bodies is much

better. The 0.6μ feature appears only as a shoulder. This matches very

well the shoulder in the spectra of the solar system bodies. Again the

match in the region of the UV feature and the IR feature is very good. The

similarity of the structure of all the spectra in the IR feature is pro-

bably coincidental. The 0.6μ feature has been shown to be temperature de-

pendent (Chapter III). Therefore the exact strength of the 0.6μ feature

relative to the UV feature will depend greatly on the temperature of the

surface. Also, the amount of H_2S and NH_3 the water frost will affect the

strength of the feature as can be seen by a comparison of $NH_4SH + H_2O$ and

$H_2S + 10H_2O$.

NH_4SH and H_2S hydrate and their UV irradiated products are probably

stable enough to exist on the surfaces of the Galilean satellites and in

the rings of Saturn (see Table B-2). Based on these stability consider-

ations and on the comparisons of visible and infrared reflection spectra

we can conclude that the UV irradiated products of H_2S and NH_4SH are likely

contaminants of the water frost present on the surfaces of the Galilean

satellites and in the rings of Saturn.
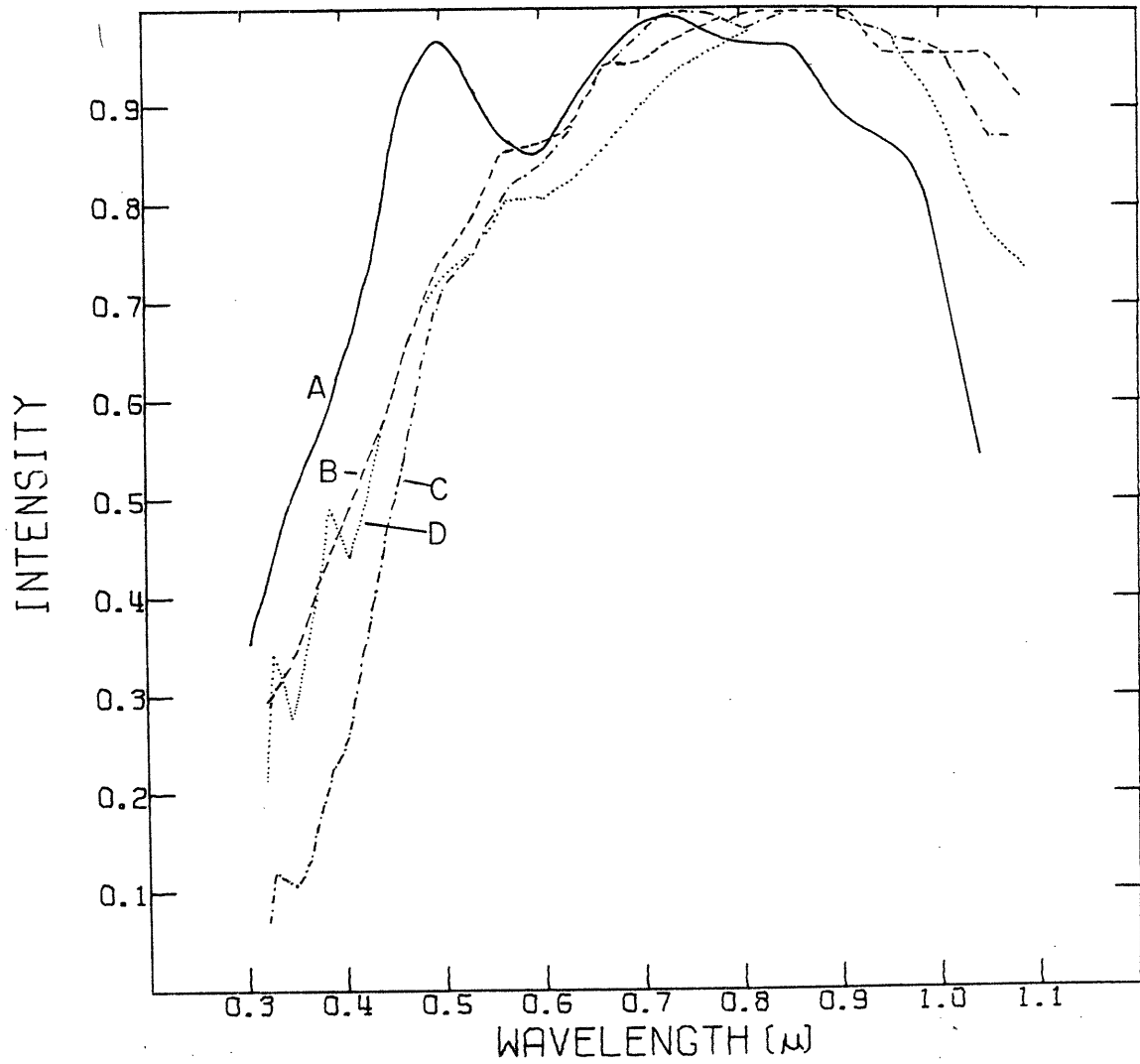
Figure V-2. Reflectivity of $NH_4SH + H_2O$ compared with solar system objects.

A. $NH_4SH + H_2O$, 3 hours irradiation
B. ring B
C. J1
D. J2
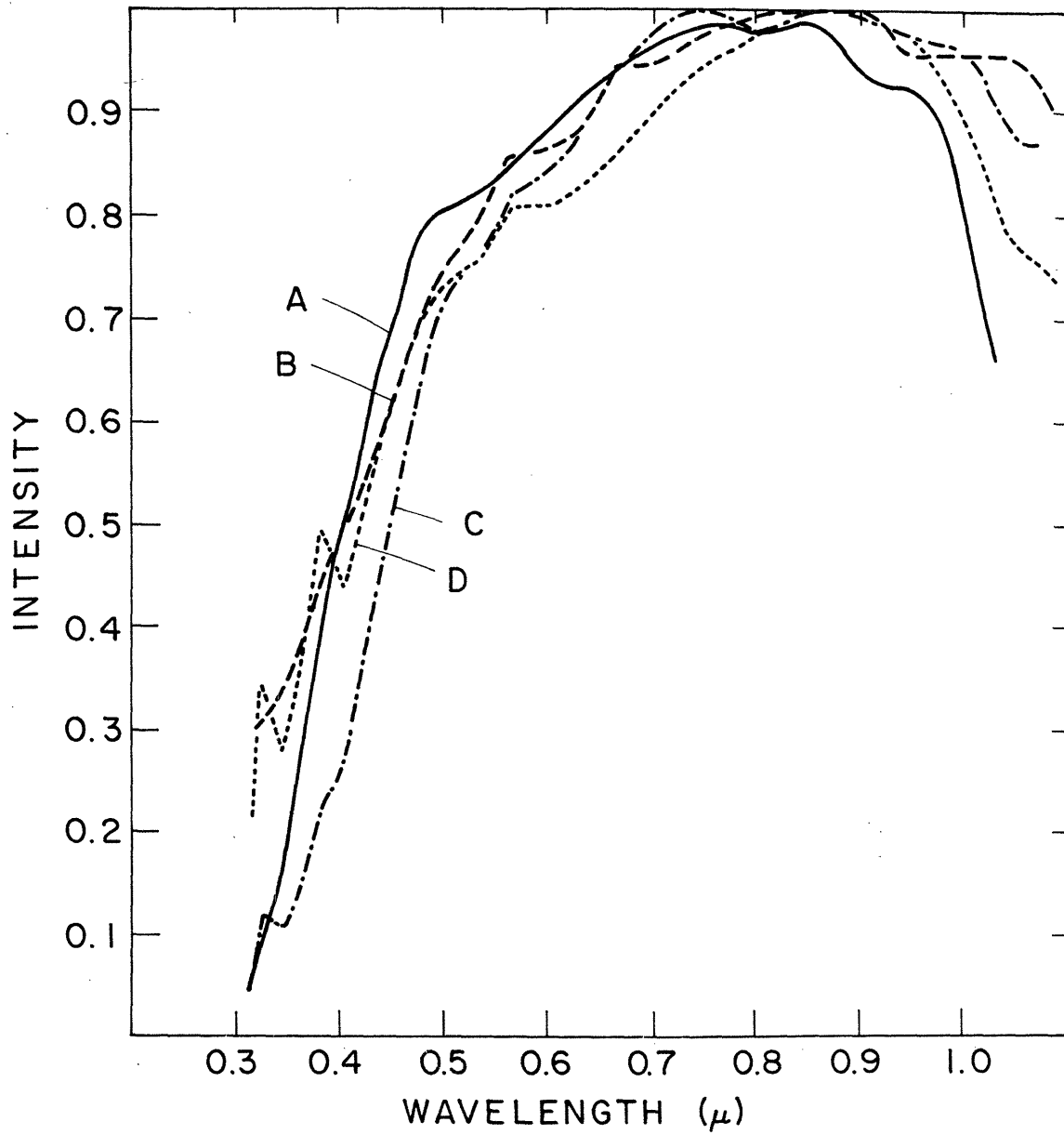
Figure V-3. Reflectivity of H_2S + $10H_2O$ compared with solar system objects.

A. H_2S + $10H_2O$, 3 hours irradiation
B. ring B
C. J1
D. J2

A very interesting phenomenon is possible on the surfaces of the Galilean satellites. As can be seen from Table B-2, it would appear that NH_4SH and NH_3+H_2O (and probably the poly-sulfides) are very stable near the poles of the satellites, but not in the equatorial regions. This brings up the possibility of having yellow polar caps and white equatorial regions (water frost). Kuiper has supposedly observed "red" polar caps on J1 (Lewis and Chapman, 1973), but because of the crude method used and the very small angular diameter of the satellite, it is probable that all that can be concluded is that the poles are darker than the equatorial region. This is still consistent with our conclusions.

The identification of these contaminants is not conclusive. No investigations have been carried out to determine the infra-red ($1-4\mu$) spectral reflectivity of unirradiated and irradiated contaminated water frost. From Figure III-16, it can be seen that the contaminant can be diluted at least 10:1 with water frost. Greater dilution may be possible without affecting the overall reflection spectra of the contaminated frosts. It is unknown, though, what the infrared reflection spectra of these contaminated and irradiated water frosts look like or how much contaminant can be added to water frost without affecting the infrared reflection spectrum of the water frost. Until infrared spectra of contaminated and irradiated water frosts can be investigated and compared with the spectra of Saturn's rings and the Galilean satellites, we cannot make any

firmer conclusions as to the composition of these objects.

It should be noted that we have been dealing here with pure frosts. No attempt has been made to study the effects of mixing silicates with the frosts or dusting the surfaces of the frosts with silicate materials. As has been previously stated, the reflectivities of most of the satellites and Saturn's rings are high and so the surfaces of these objects are composed predominantly of frosts. The addition of small amounts of silicate material will have little effect on the spectral reflectivities of frosts and so would have little effect in our comparisons of laboratory frosts and icy surfaces.

In this thesis we have tried to determine the composition of the surfaces of icy bodies in the solar system. We have been able to eliminate many materials (silicates, etc.) as major components of the surfaces of these bodies and have come up with certain frosts whose spectra and stability make them by far the most likely major components of the surfaces of the objects we have investigated.

APPENDIX A

Most of the data used for the calculations of evaporation rates of frosts has been obtained from the Handbook of Chemistry and Physics, 52nd Edition, 1971 (CRC). For these data:

$$\log_{10} P = (-0.2185A/T) + B \qquad (A1)$$

Where:

    P   vapor pressure of gas over solid in Torr

    T   temperature in °K

    A   molar heat of vaporization (see below)

    B   constant

The data for most of the gas hydrates comes from Miller (1961). In these cases:

$$\log_{10} P = A'/T + B'$$

Where P is in atmospheres.

Or if P is in Torr:

$$\log_{10} P = A'/T + B' + 2.881$$

$$\log_{10} P = A'/T + B \qquad (A2)$$

One gas hydrate ($H_2S \cdot 6H_2O$) comes from the International Critical Tables (1926-1933) (ICT) and is of the same form as equation (A2).

Two hydrates ($NH_3 \cdot H_2O$ and $2NH_3 \cdot H_2O$) have been calculated by the author (LAL) from $NH_3 - H_2O$ system in Lewis (1969), and with these results, the author has also calculated the vapor pressure equation for $NH_4SH + H_2O$.

Given the following equilibrium equations:

$$NH_3 \cdot H_2O(s) = NH_3(g) + H_2O(g) \tag{A3}$$

$$K_{A3} = \frac{p(NH_3) \cdot p(H_2O)}{a(NH_3 \cdot H_2O)}$$

$$\log K_{A3} = \log\left(\frac{p(NH_3) \cdot p(H_2O)}{a(NH_3 \cdot H_2O)}\right) = A_{A3}/T + B_{A3}$$

$$NH_3 \cdot H_2O(s) = NH_3(g) + H_2O(s) \tag{A4}$$

$$K_{A4} = p(NH_3)\left(\frac{a(H_2O)}{a(NH_3 \cdot H_2O)}\right)$$

$$\log K_{A4} = \log\left(p(NH_3)\left(\frac{a(H_2O)}{a(NH_3 \cdot H_2O)}\right)\right) = A_{A4}/T + B_{A4}$$

$$H_2O(s) = H_2O(g) \tag{A5}$$

$$K_{A5} = \frac{p(H_2O)}{a(H_2O)}$$

$$\log K_{A5} = \log\left(\frac{p(H_2O)}{a(H_2O)}\right) = A_{A5}/T + B_{A5}$$

$$2NH_3 \cdot H_2O(s) = NH_3 \cdot H_2O(s) + NH_3(g) \tag{A6}$$
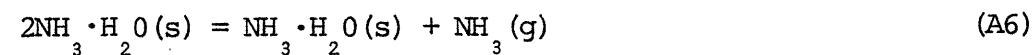
$$K_{A6} = p(NH_3)\left(\frac{a(NH_3 \cdot H_2O)}{a(2NH_3 \cdot H_2O)}\right)$$

$$\log K_{A6} = \log\left(p(NH_3)\left(\frac{a(NH_3 \cdot H_2O)}{a(2NH_3 \cdot H_2O)}\right)\right) = A_{A6}/T + B_{A6}$$

$$2NH_3 \cdot H_2O(s) = 2NH_3(g) + H_2O(g) \qquad \text{(A7)}$$

$$K_{A7} = \frac{(p(NH_3))^2 \cdot p(H_2O)}{a(2NH_3 \cdot H_2O)} = A_{A7}/T + B_{A7}$$

$$\log K_{A7} = \log\left(\frac{(p(NH_3))^2 \cdot p(H_2O)}{a(2NH_3 \cdot H_2O)}\right) = A_{A7}/T + B_{A7}$$

$$NH_4SH(s) + H_2O(s) = NH_3 \cdot H_2O(s) + H_2S(g) \qquad \text{(A8)}$$
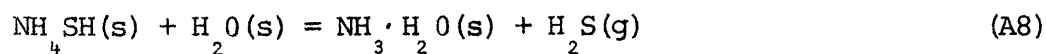
$$K_{A8} = \frac{p(H_2S) \cdot a(NH_3 \cdot H_2O)}{a(NH_4SH) \cdot a(H_2O)}$$

$$\log K_{A8} = \log\left(\frac{p(H_2S) \cdot a(NH_3 \cdot H_2O)}{a(NH_4SH) \cdot a(H_2O)}\right) = A_{A8}/T + B_{A8}$$

$$NH_4SH(s) = NH_3(g) + H_2S(g) \qquad \text{(A9)}$$
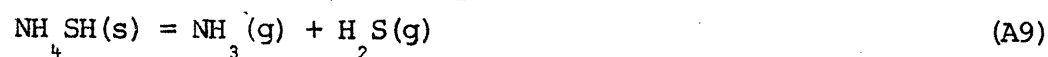
$$K_{A9} = \frac{p(NH_3) \cdot p(H_2S)}{a(NH_4SH)}$$

$$\log K_{A9} = \log\left(\frac{p(NH_3) \cdot p(H_2S)}{a(NH_4SH)}\right) = A_{A9}/T + B_{A9}$$

Where:

p( )   partial pressure of gas

a( )   activity of the solid

Equations A3 and A7 have been calculated from the phase diagram of the NH_3-H_2O system of Lewis (1969). A5 and A9 are known from the Handbook of Chemistry and Physics (1971).

And:

$$\log K_{A4} = \log(K_{A3}/K_{A5}) = (A_{A3} - A_{A5})/T + (B_{A3} - B_{A5}) \qquad \text{(A10)}$$

$$\log K_{A6} = \log(K_{A7}/K_{A3}) = (A_{A7} - A_{A3})/T + (B_{A7} - B_{A3}) \qquad \text{(A11)}$$

$$\log K_{A8} = \log(K_{A9}/K_{A4}) = (A_{A9} - A_{A4})/T + (B_{A9} - B_{A4}) \qquad \text{(A12)}$$

If the activities of the solids are considered to be 1, then log K = log p which is then the vapor pressure of the gas over the solid.

For the $NH_3 - H_2O$ system we are interested in the vapor pressure of the NH_3 gas over the solid, ie. Equations A4 and A6. For the $NH_3-H_2S-H_2O$ system we are interested in the stability of NH_4SH in H_2O. Since both NH_4SH and H_2O have such low vapor pressures and the vapor pressure of H_2S is, in comparison, very high, it is probable that the NH_4SH is stable in the presence of H_2O. So no data will be included on Equation A8.

The values for A and B for the frosts discussed above are found in Table A-1.

Finally, several frosts have vapor pressure equations that are non-linear fits to the experimental data, ie. they have higher order terms involving the temperature. These equations are from the Internation Critical Tables (1929) and are:

$$H_2O: \quad \log P = -2445.5646/T + 8.2312 \log T - 0.0167706T + 1.20514 \times 10^{-5} T^2 - 6.757169 \tag{A13}$$

$$NH_3: \quad \log P = 1790.0T - 1.81630 \log T + 14.97593 \tag{A14}$$

$$CO_2: \quad \log P = -1275.62/T + 0.006833T + 8.3071 \tag{A15}$$

Equation A13 is valid for $-90 < T < 400$ °C

Equation A14 is valid for low T

Equation A15 is valid for $-183 < T < -135$ °C

T in °K (except where region of validity is stated).

The Clausius Clapyron equation states that:

$$\frac{d(\ln P)}{dT} = \frac{\Delta H}{RT^2} \tag{A16}$$

Where:

ΔH heat of sublimation (evaporation)

$$\therefore \Delta H - RT^2 \cdot \ln(10) \frac{d}{dT} (\log P) \qquad (A17)$$

For the CRC equations we have:

$$\Delta H = RT^2 \cdot \ln(10) \frac{d}{dT} (-0.2185A/T + B)$$

$$= RT^2 \ln(10) \cdot (0.2185)A/T^2$$

$$= R \ln(10) \cdot (0.2185)A$$

$$\therefore \Delta H = A \quad \text{as stated previously}$$

For the other linear equations:

$$\Delta H = R \ln(10)A'$$

The nonlinear equations are somewhat more complicated and H is not independent of T.

TABLE A-1

ICE	A	B	μ	SOURCE
NH_3	7459.6	9.997400	17.0307	CRC
H_2S	4814.5	7.735135	34.076	CRC
NH_4SH	10609.3	10.472153	51.1067	CRC
S	16609.6	8.015165	32.06	CRC
H_2S_2	9488.9	9.028026	66.136	CRC
H_2O	10999.4	9.183837	18.0154	CRC
Ar	1739.1	7.131953	39.948	CRC
CH_4	2128.8	7.027729	16.043	CRC
$N_2 \cdot ?H_2O$	-763	7.877	28.0134	M
$Ar \cdot ?H_2O$	-719	7.535	39.948	M
$CH_4 \cdot 7H_2O$	-947.4	7.7519	16.043	M
$CO_2 \cdot ?H_2O$	-1121	8.0332	44.01	M
$H_2S \cdot 6H_2O$	-1333	3.8585	34.076	ICT
$NH_3 \cdot H_2O$	-1006	4.82	17.0307	LAL
$2NH_3 \cdot H_2O$	-1677	9.78	17.0307	LAL
N_2	1489.7	7.050410	28.0134	CRC

APPENDIX B
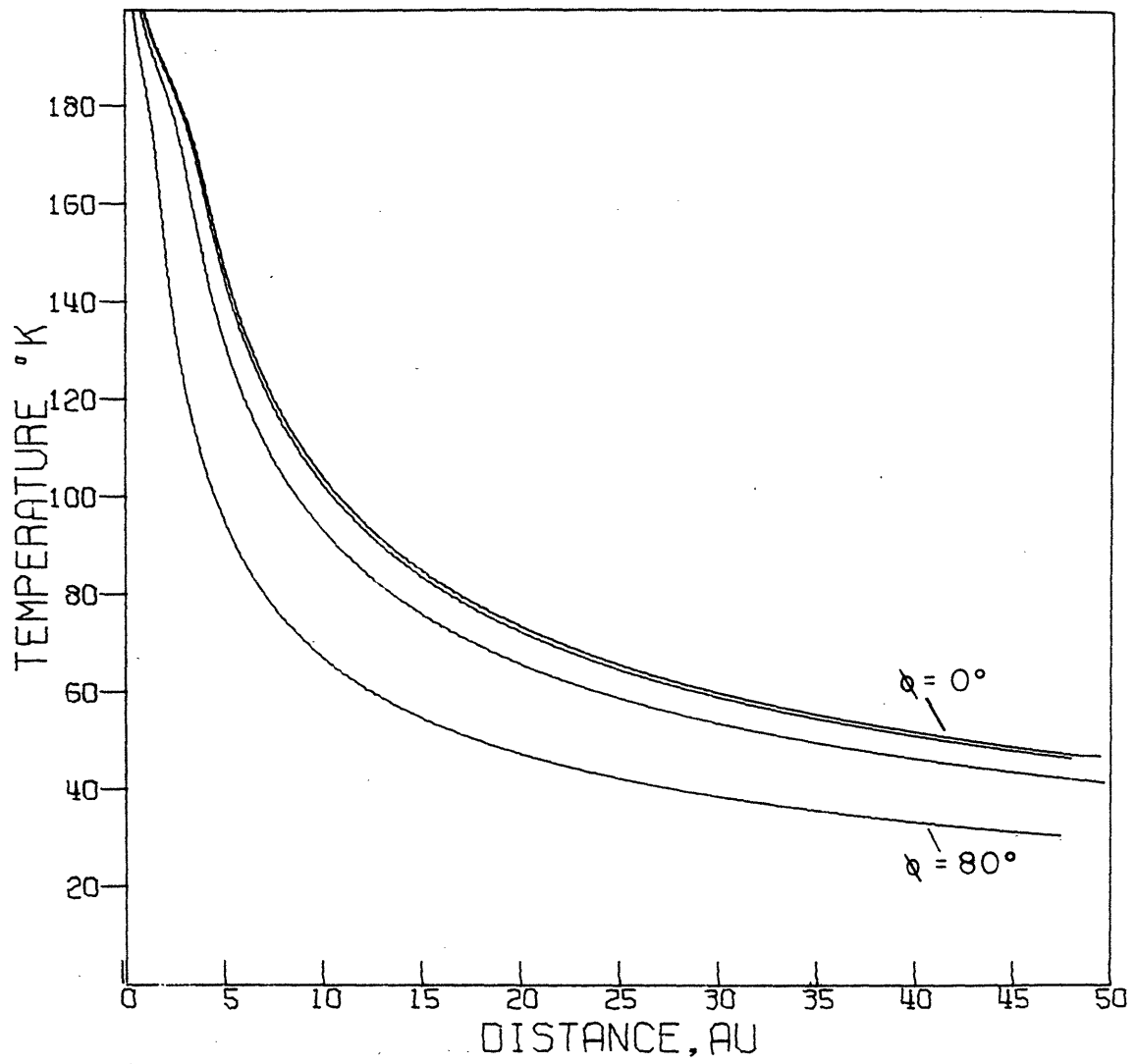
Figure B-1. Water frost, albedo = 50%, $\theta = 0^{\circ}$, $\phi = 0^{\circ}$, 20°, 50°, 80°
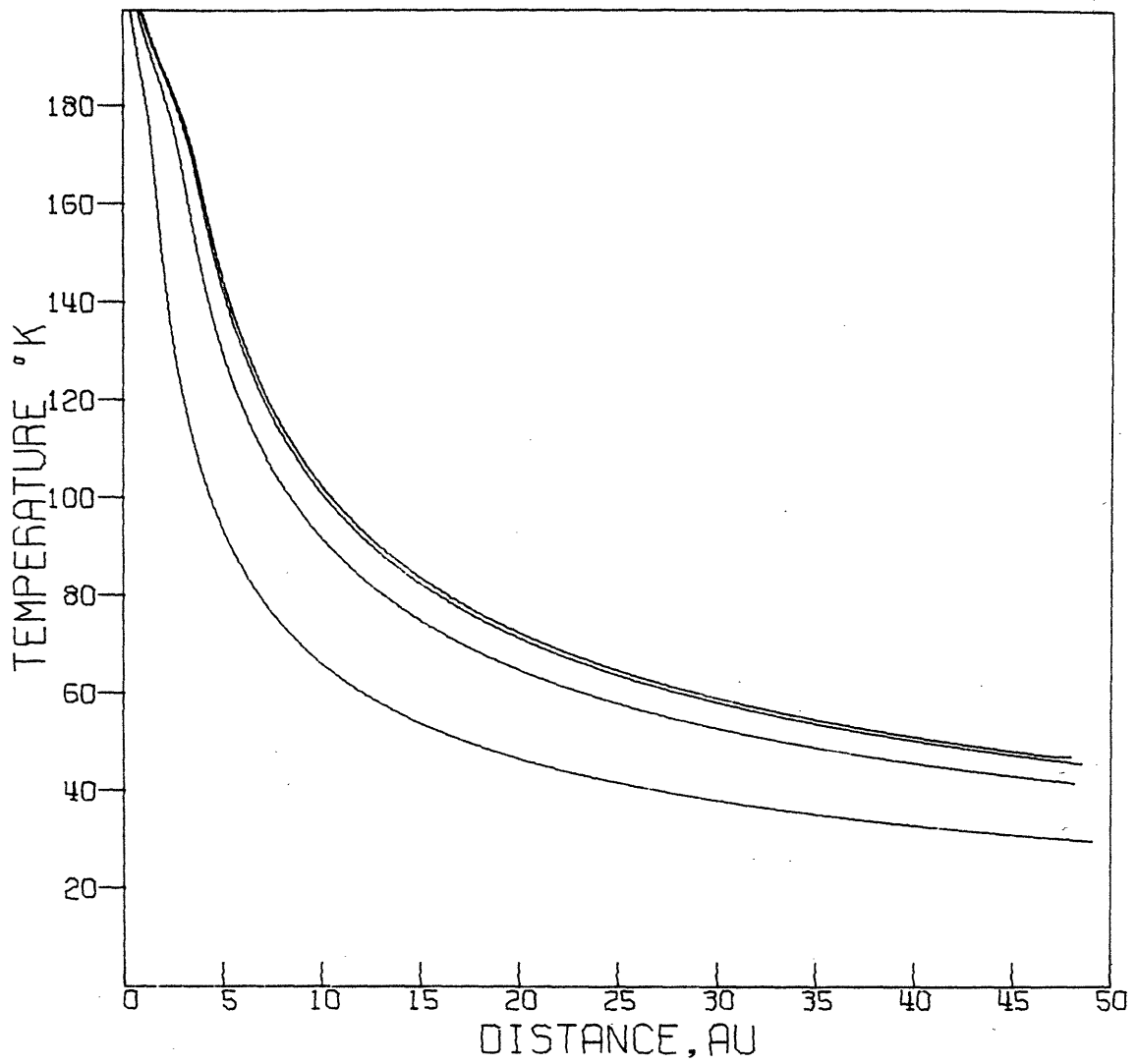
Figure B-2. Water frost, albedo = 50%, $\theta = 20°, \phi = 0°, 20°, 50°, 80°$
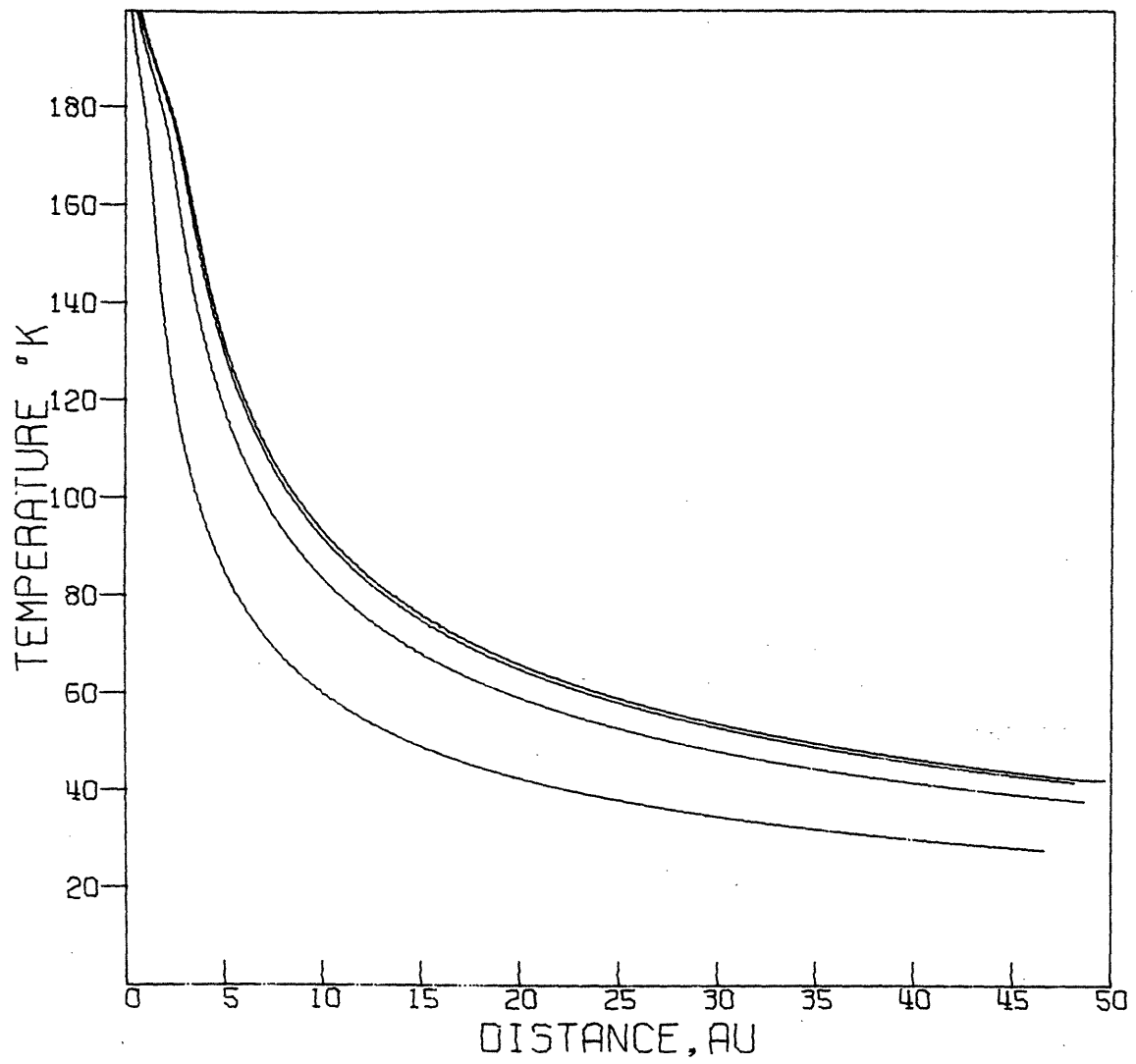
Figure B-3. Water frost, albedo ≈ 50%, θ = 50°, ø = 0°, 20°, 50°, 80°
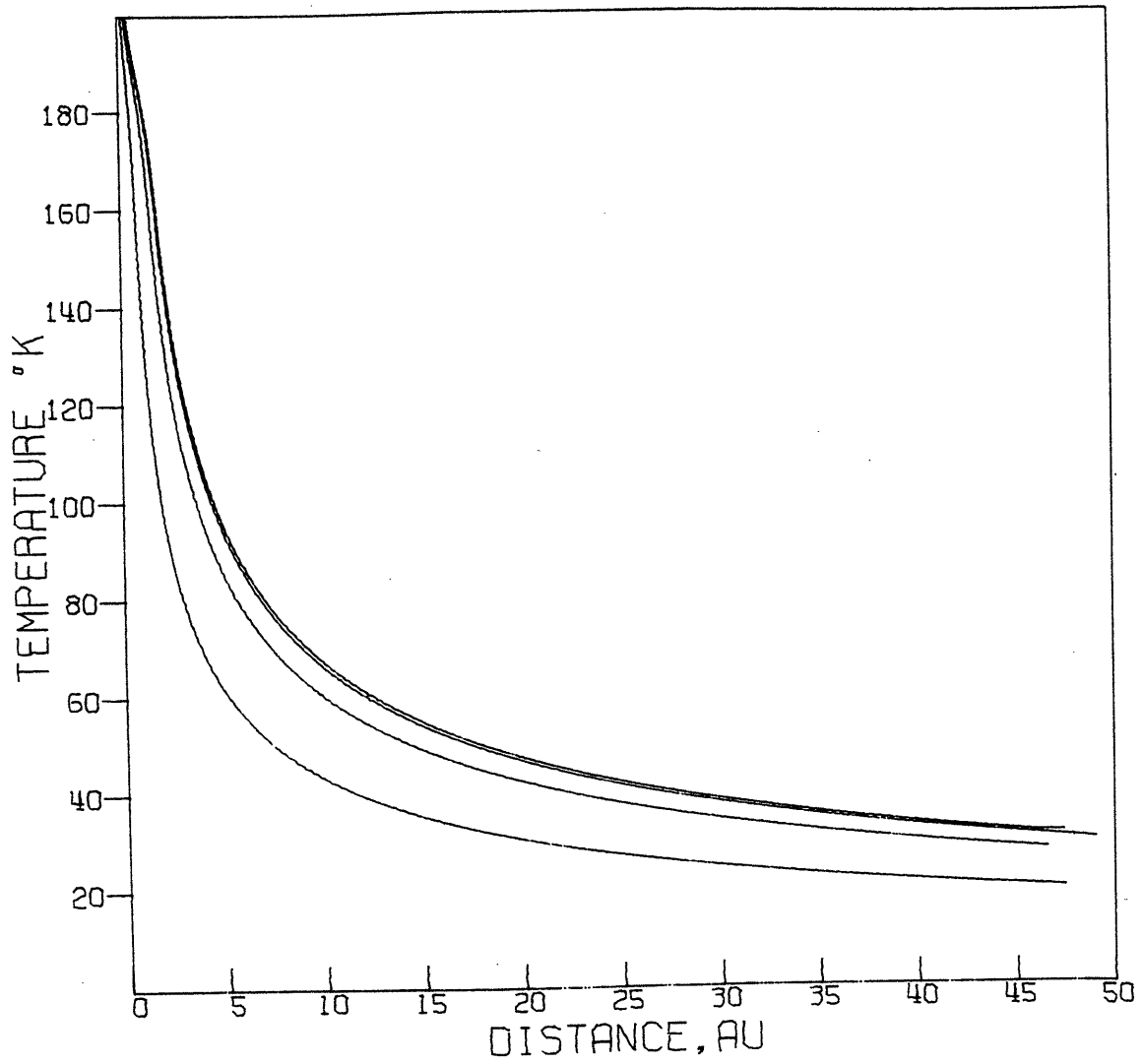
Figure B-4. Water frost, albedo = 50%, $\theta = 80°$, $\phi = 0°$, $20°$, $50°$, $80°$
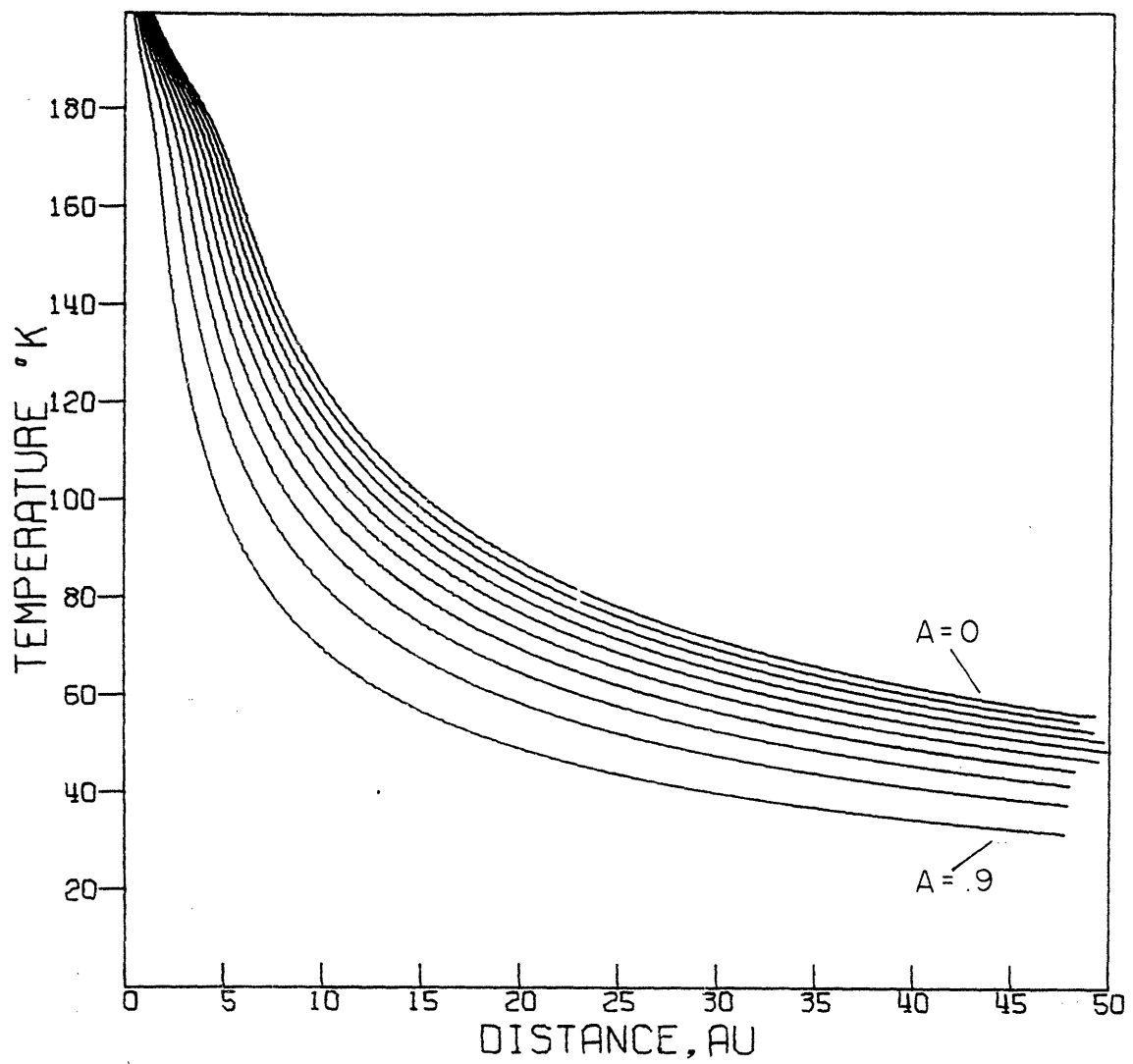
Figure B-5. Water frost, $\theta = \phi = 0^\circ$

Albedo = 0%, 10%, 20%, 30%, 40%, 50%, 60%, 70%, 80%, 90%

TABLE B-1

TEMPERATURE

WATER

PHI= 0.0   ALBEDO= 0.5

PLANET	THEDA= 0.	10.	20.	30.	40.	50.	60.	70.	80.	85.
JUP	145.00	144.40	142.70	139.90	135.60	129.80	121.90	110.90	93.60	79.80
SAT	107.10	106.60	105.40	103.30	100.20	95.90	90.00	81.90	69.10	58.20
URAN	75.50	75.20	74.40	72.90	70.70	67.60	63.50	57.80	48.80	41.10
NEPT	60.30	60.10	59.40	58.20	56.40	54.00	50.70	46.10	39.00	32.80

VAPOR PRESSURE, TORR

WATER

PHI= 0.0   ALBEDO= 0.5

PLANET	THEDA= 0.	10.	20.	30.	40.	50.	60.	70.	80.	85.
JUP	0.406333 -7.00	0.346746 -7.00	0.219650 -7.00	0.101076 -7.00	0.288324 -8.00	0.465480 -9.00	0.293721 -10.00	0.325346 -12.00	0.321236 -16.00	0.483223 -21.00
SAT	0.553688 -13.00	0.434677 -13.00	0.240702 -13.00	0.827804 -14.00	0.157806 -14.00	0.152631 -15.00	0.301817 -17.00	0.269730 -20.00	0.252824 -25.00	0.774188 -32.00
URAN	0.224462 -22.00	0.167552 -22.00	0.759447 -23.00	0.164369 -23.00	0.154861 -24.00	0.427614 -26.00	0.216528 -26.00	0.400930 -32.00	0.859971 -40.00	0.510173 -49.00
NEPT	0.212315 -30.00	0.156439 -30.00	0.528553 -31.00	0.774186 -32.00	0.372324 -33.00	0.475350 -35.00	0.602726 -38.00	0.112210 -42.00	0.362247 -52.00	0.313596 -64.00

EVAPORATION RATE CM/BILLION YEARS

WATER

PHI= 0.0   ALBEDO= 0.5

PLANET	THEDA= 0.	10.	20.	30.	40.	50.	60.	70.	80.	85.
JUP	0.026365 9.00	0.022545 9.00	0.014366 9.00	0.006677 9.00	0.019345 8.00	0.031922 7.00	0.020785 6.00	0.024133 4.00	0.025942 0.0	0.042540 -5.00
SAT	0.041317 3.00	0.032894 3.00	0.018318 3.00	0.063636 2.00	0.012317 2.00	0.010582 1.00	0.024857 -1.00	0.059547 -4.00	0.023763 -9.00	0.079298 -16.00
URAN	0.020183 -6.00	0.015096 -6.00	0.068792 -7.00	0.015041 -7.00	0.014390 -8.00	0.040635 -10.00	0.021230 -12.00	0.041203 -16.00	0.096193 -24.00	0.062276 -33.00
NEPT	0.021362 -14.00	0.015766 -14.00	0.053582 -15.00	0.079286 -16.00	0.038735 -17.00	0.050541 -19.00	0.066136 -22.00	0.012912 -26.00	0.045321 -36.00	0.110995 -48.00

TABLE B-1 (Cont.)

AMMONHYDROSULFIDE PHI = 0.0 ALBEDO = 0.5

TEMPERATURE

PLANET	THETA= 0.	10.	20.	30.	40.	50.	60.	70.	80.	85.
JUP	144.00	143.50	142.10	139.50	135.50	129.80	121.90	110.90	93.60	78.80
SAT	107.10	106.60	105.40	103.30	100.20	95.90	90.00	81.90	69.10	58.20
URAN	75.50	75.20	74.40	72.90	70.70	67.60	63.50	57.80	48.80	41.10
NEPT	60.30	60.10	59.40	58.20	56.40	54.00	50.70	46.10	39.00	32.80

AMMONHYDROSULFIDE PHI = 0.0 ALBEDO = 0.5

VAPOR PRESSURE, TORR

PLANET	THETA= 0.	10.	20.	30.	40.	50.	60.	70.	80.	85.
JUP	0.236601 -5.00	0.207934 -5.00	0.144135 -5.00	0.75685 -6.00	0.231297 -6.00	0.410105 -7.00	0.285432 -8.00	0.370897 -10.00	0.507913 -14.00	0.113205 -18.00
SAT	0.672357 -11.00	0.552204 -11.00	0.300950 -11.00	0.107494 -11.00	0.217324 -12.00	0.199420 -13.00	0.518941 -15.00	0.147142 -17.00	0.840741 -23.00	0.438043 -29.00
URAN	0.586709 -20.00	0.442522 -20.00	0.205686 -20.00	0.471374 -21.00	0.482914 -22.00	0.151449 -23.00	0.925004 -26.00	0.233231 -29.00	0.932086 -37.00	0.117449 -45.00
NEPT	0.106857 -27.00	0.795997 -28.00	0.279491 -28.00	0.438241 -29.00	0.234708 -30.00	0.349774 -32.00	0.561870 -35.00	0.153923 -39.00	0.107846 -48.00	0.627702 -60.00

AMMONHYDROSULFIDE PHI = 0.0 ALBEDO = 0.5

EVAPORATION RATE CM/BILLION YEARS

PLANET	THETA= 0.	10.	20.	30.	40.	50.	60.	70.	80.	85.
JUP	0.025946 11.00	0.022842 11.00	0.015912 11.00	0.079740 10.00	0.026148 10.00	0.047370 9.00	0.034019 8.00	0.046348 6.00	0.069086 2.00	0.016796 -2.00
SAT	0.085496 5.00	0.067833 5.00	0.038576 5.00	0.013918 5.00	0.028570 4.00	0.026798 3.00	0.071987 1.00	0.021396 -1.00	0.133096 -7.00	0.075505 -13.00
URAN	0.088857 -4.00	0.067153 -4.00	0.031472 -4.00	0.072651 -5.00	0.075579 -6.00	0.024240 -7.00	0.152756 -10.00	0.040021 -13.00	0.175585 -21.00	0.074113 -29.00
NEPT	0.018110 -11.00	0.135119 -12.00	0.047722 -12.00	0.075595 -13.00	0.041127 -14.00	0.067638 -16.00	0.103842 -19.00	0.029833 -23.00	0.072730 -32.00	0.144116 -44.00

TABLE B-1 (Cont.)

HYDROGEN SULFIDE   PHI= 0.0   ALBEDO= 0.5   TEMPERATURE

PLANET	THETA= 0.	10.	20.	30.	40.	50.	60.	70.	80.	85.
JUP	89.70	89.60	89.50	89.20	88.70	88.00	87.00	85.40	82.00	76.60
SAT	84.70	84.70	84.50	84.10	83.50	82.60	81.10	78.20	69.00	58.70
URAN	74.50	74.30	73.60	72.40	70.50	67.60	63.50	57.80	48.20	43.10
NEPT	60.30	60.10	59.40	58.20	56.40	54.00	50.70	46.10	39.00	20.80

HYDROGEN SULFIDE   PHI= 0.0   ALBEDO= 0.5   VAPOR PRESSURE, TORR

PLANET	THETA= 0.	10.	20.	30.	40.	50.	60.	70.	80.	85.
JUP	0.101744 -3.00	0.987234 -4.00	0.957860 -4.00	0.874523 -4.00	0.750399 -4.00	0.603883 -4.00	0.440097 -4.00	0.261221 -4.00	0.805854 -5.00	0.102642 -5.00
SAT	0.206636 -4.00	0.206636 -4.00	0.193112 -4.00	0.158499 -4.00	0.136998 -4.00	0.998721 -5.00	0.580616 -5.00	0.191804 -5.00	0.306476 -7.00	0.457179 -9.00
URAN	0.411848 -6.00	0.377354 -6.00	0.276752 -6.00	0.160394 -6.00	0.651032 -7.00	0.149100 -7.00	0.147472 -8.00	0.342764 -10.00	0.150864 -13.00	0.137977 -17.00
NEPT	0.947719 -9.00	0.270415 -9.00	0.105983 -9.00	0.457175 -10.00	0.121121 -10.00	0.179575 -11.00	0.968854 -13.00	0.823894 -15.00	0.577750 -19.00	0.446009 -24.00

HYDROGEN SULFIDE   PHI= 0.0   ALBEDO= 0.5   EVAPORATION RATE CM/BILLION YEARS

PLANET	THETA= 0.	10.	20.	30.	40.	50.	60.	70.	80.	85.
JUP	0.011844 13.00	0.112071 12.00	0.108797 12.00	0.099498 12.00	0.095616 12.00	0.069173 12.00	0.050701 12.00	0.030374 12.00	0.095876 11.00	0.012022 9.00
SAT	0.024126 12.00	0.024126 12.00	0.022574 12.00	0.019744 12.00	0.016110 12.00	0.118081 11.00	0.069280 11.00	0.023307 11.00	0.079905 9.00	0.064394 5.00
URAN	0.051275 10.00	0.047042 10.00	0.034664 10.00	0.020256 10.00	0.083317 9.00	0.019486 9.00	0.019836 8.00	0.048446 6.00	0.023197 3.00	0.065077 -1.00
NEPT	0.026954 7.00	0.023622 7.00	0.014776 7.00	0.054394 6.00	0.017730 6.00	0.026259 5.00	0.146211 3.00	0.130791 1.00	0.099578 -3.00	0.065343 -8.00

TABLE B-1 (Cont.)

AMMONIA PHI= 0.0 ALBEDO= 0.5

TEMPERATURE

PLANET	THEDA= 0.	10.	20.	30.	40.	50.	60.	70.	80.	85.
JUP	113.10	113.00	112.80	112.30	111.70	110.60	109.00	105.60	93.50	78.80
SAT	103.80	103.60	103.00	101.70	99.40	95.70	90.00	81.90	69.10	58.20
URAN	75.50	75.20	74.40	72.90	70.70	67.60	63.50	57.80	48.80	41.10
NEPT	60.30	60.10	59.40	56.20	56.40	54.00	50.70	46.10	39.00	33.60

AMMONIA PHI= 0.0 ALBEDO= 0.5

VAPOR PRESSURE, TORR

PLANET	THEDA= 0.	10.	20.	30.	40.	50.	60.	70.	80.	85.
JUP	0.385234 −4.00	0.374377 −4.00	0.352967 −4.00	0.304368 −4.00	0.254353 −4.00	0.182099 −4.00	0.110658 −4.00	0.365199 −5.00	0.367347 −7.00	0.205640 −10.00
SAT	0.197185 −5.00	0.183891 −5.00	0.148906 −5.00	0.934614 −6.00	0.397016 −6.00	0.924313 −7.00	0.771174 −8.00	0.124747 −9.00	0.256757 −13.00	0.98?427 −18.00
URAN	0.256463 −11.00	0.210330 −11.00	0.122982 −11.00	0.435582 −12.00	0.877681 −13.00	0.769349 −14.00	0.213468 −15.00	0.628134 −18.00	0.395688 −23.00	0.21337? −29.00
NEPT	0.977213 −17.00	0.753752 −17.00	0.361103 −17.00	0.981437 −18.00	0.125334 −18.00	0.651109 −20.00	0.706369 −22.00	0.437691 −25.00	0.160148 −31.00	0.201772 −39.00

AMMONIA PHI= 0.0 ALBEDO= 0.5

EVAPORATION RATE CM/BILLION YEARS

PLANET	THEDA= 0.	10.	20.	30.	40.	50.	60.	70.	80.	85.
JUP	0.027539 12.00	0.026754 12.00	0.025246 12.00	0.021819 12.00	0.018282 12.00	0.013154 12.00	0.008052 12.00	0.026997 11.00	0.028860 9.00	0.01759? 6.00
SAT	0.014703 11.00	0.013725 11.00	0.011146 11.00	0.070403 10.00	0.030319 10.00	0.071776 9.00	0.061752 8.00	0.010471 7.00	0.023464 3.00	0.097729 −2.00
URAN	0.022422 5.00	0.018425 5.00	0.010831 5.00	0.038755 4.00	0.079295 3.00	0.071083 2.00	0.020350 1.00	0.062764 −2.00	0.043029 −7.00	0.025919 −13.00
NEPT	0.090707 −1.00	0.073860 −1.00	0.035592 −1.00	0.097728 −2.00	0.012678 −2.00	0.067309 −4.00	0.075361 −6.00	0.048971 −9.00	0.019481 −15.00	0.026750 −23.00

TABLE B-2

ICE	JUPITER		SATURN			URANUS		NEPTUNE	
	0°	60°	0°	60°	EQ	0°	60°	0°	60°
NH_3	U	8-U	6-8	3-6	0-3	0-2	0	0	0
H_2S	U	U	U	8-U	7-U	6-8	3-5	2-4	0-1
NH_4SH	6-8	3-5	0-3	0	0	0	0	0	0
S	0	0	0	0	0	0	0	0	0
H_2S_2	7-8	4-6	1-4	0	0	0	0	0	0
H_2O	4-6	1-3	0-1	0	0	0	0	0	0
Ar	U	U	U	U	U	U	U	U	8-U
CH_4	U	U	U	U	U	8-8	8-8	8-8	8-8
$N_2 \cdot H_2O$	U	U	U	U	U	8-U	8-8	7-8	5-7
$Ar \cdot H_2O$	U	U	U	U	U	U	U	U	8-U
$CH_4 \cdot H_2O$	U	U	U	8-U	8-U	7-8	5-7	4-6	0-3
$CO_2 \cdot H_2O$	U	U	U	8-U	6-8	5-7	2-4	1-3	0
$H_2S \cdot H_2O$	7-8	5-7	4-5	1-3	0-1	0	0	0	0
$NH_3 \cdot H_2O$	U	8-U	8-8	6-7	4-6	3-5	1-3	0-2	0
$2NH_3 \cdot H_2O$	U	8-U	6-8	3-5	0-2	0-1	0	0	0
N_2	U	U	U	U	U	U	U	U	8-U
H_2O	3-6	0-2	0	0	0	0	0	0	0
NH_3	U	8-U	6-8	3-5	0-3	0-2	0	0	0
CO_2	U	U	U	7-8	5-7	4-6	0-3	0-2	0

APPENDIX C

a) <u>Spectral Reflectivity Measurements</u>

A single beam Heath UV-Visible scanning monochromator (EU700) (350mm focal length) is used in conjunction with a Heath light source (EU 701-50) and detectors to measure the spectral reflectivity of the samples being investigated. The monochromator has a usable range of 0.18 to 1.03μ with a resolution of 10 to 20°A. In the spectral region 0.18 to 0.45μ, the Heath lightsource (using a deuturium lamp) is used with a Heath photomultiplier (EU701-30), an RCA 1P-28A phototube with an S-5 surface. For the region 0.30 to 1.03μ the Heath lightsource (using a tungsten lamp) is used with an ITT FW-118 (S-1 surface) phototube. The output signal of the Heath photomultiplier is recorded on a stripchart recorder and the putput of the ITT FW-118 phototube is recorded digitally on magnetic tape.

The data from the strip chart recorder is digitized and then reduced to produce reflectivity curves of the frost relative to the MgO standard. The magnetic tape output is already in digitized form. Since the light path is the same when making the reflectivity measurements on both the standard and the frost, dividing the output of the frost spectrum by that of the MgO standard eliminates the system characteristics (lamp output, phototube response, etc.) and results in $R_{frost}(\lambda)/R_{MgO}(\lambda)$, the spectral reflectivity if the frost relative to the MgO standard. The reflection spectrum of MgO is relatively flat in the spectral region being investigated, so that the relative reflectivity closely approximates the absolute reflectivity of the frost.

b) <u>Sample Purity</u>

The following gases are used in the experiments. H_2S: Matheson C.P. Grade.

Component	ppm
propane	810
oxygen	30
nitrogen	75
propylene	2700
water	31
dimethyl sulfide	31

NH_3: Matheson Anhydrous.

Component	ppm
water	<50
oil	< 5

c) Experiment Procedure

The basic system is shown in Figure III-1. All tubing is stainless

steel. The main chamber and the water chamber are glass and the windows

are UV grade quartz. The "cold finger" is also made of stainless steel.

About 12-16 hours before the beginning of an experiment, the system is

set up, MgO is smoked onto the surface of the "cold finger" and the finger

is placed into the cold chamber. The system is evacuated to about 10^{-2} torr,

using a fore pump. Pumping is continued until the start of the final setup

for an experiment. If water is to be used in the experiment, the water is

introduced into the evacuated water chamber and pumped on for several hours

before the start of the experiment to remove dissolved volatiles. Just be-

fore the start of the experiment, argon is passed through the system to

purge it. The system is then reevacuated and then closed off from the pump.

Several runs (a single scan over the spectral region being investigated)

are made on the MgO standard after which the finger is cooled down with liquid nitrogen (LN_2) as the coolant (77°K). Several experiments were conducted using a dry ice-acetone mixture as a coolant (195°K).

The gases are then introduced into the system. NH_3 and H_2S are introduced into separate stainless steel gas chambers of known volume and at known pressure. The gases are then slowly leaked together in the mixing chamber and then into the cold chamber where the mixture condenses out on the cold finger. The pressure of the mixed gases is kept below 100 torr to prevent the condensation of NH_4SH in the mixing chamber. This procedure is repeated several times until the desired thickness of frost is attained (2-5mm).

In the experiments with H_2O, the procedure is somewhat different. Because H_2O is liquid at room temperature, it is very difficult to get a known volume of water frost condensed on the cold finger. From the experiments with NH_3 and H_2S, it was found that equal amounts of gas produced approximately equal amounts of condensate, so it was assumed that this was also true for the water, so an approximate estimate of the total amount of water condensed out could be made by noting the thickness of the frost deposit. The water chamber is heated to evaporate some of the water in it. The vapor passes through the mixing chamber and is condensed on the cold finger. If other gases are to be used in the experiment, they are mixed with the water vapor in the mixing chamber before entering the cold chamber. Again the process is continued until the desired thickness of frost is formed on the cold finger.

For the NH_3 and H_2S experiments, the amount of each are known to about 5%, the accuracy of the pressure readings in the gas chambers. Because of the inaccuracies in the amount of water frost deposited, the contaminated

water frost experiments are probably accurate to only about

50%

Several runs are made on the unirradiated frost. A xenon

arc lamp (Christie CXL-300HL) is then used to irradiate the

sample[1]. The frosts can then be rescanned and further irra-

diated and rescanned.

---

[1]The 300 watt xenon are lamp has a spectral energy distribution
similar to the solar energy distribution, but with a cutoff at
about 0.22μ (Figure III-2). A quartz lens is used to focus
the lamp on a circular area on the cold finger about one inch
in diameter. One hour of ultraviolet irradiation approximately
equals 15 and 58 days of solar irradiation at the mean distances
of Jupiter and Saturn respectively.

REFERENCES

Adams, J. B. and Filice, A. L. (1967). Spectral reflectance 0.4 to 2.0
microns of silicate powders. J. Geophys. Res. 72, 5705-5715.

Alexander, A. F. (1967). The planet Saturn. (Faber and Faber, London).

Allen, D. A. and Murdock, T. L. (1971). Infrared photometry of Saturn,
Titan and the rings. Icarus 14, 1-2.

American Petrolium Institute (1959). Infrared Spectral Data, Research
Project 44, Serial No. 2148.

Beaudet, R. A. and Stephens, P. J. (1971). Identification of S_4^+ in
sulfur-oleum solutions. Chem. Comm., 1093.

Berge, G. L. and Read, R. B. (1968). The microwave emission of Saturn.
Ap. J. 152, 755-764.

Bobrov, M. S. (1970). Physical properties of Saturn's rings. Surfaces
and Interiors of Planets and Satellites. (Permagon Press, New York).

Chapman, C. R. (1971). Doctoral Thesis, Massachusetts Institute of
Technology.

Chapman, C. R., McCord, T. B. and Johnson, T. V. (1973). Asteroid spectral
reflectivities. Astron. J. 78, 126-140.

Chivers, T. and Drummond, I. (1971). Blue solutions of sulfur in
hexamethylphosphoramide. Chem. Comm., 1623.

Chivers, T. and Drummond, I. (1972). Characterization of the trisulfur
radical anion S_3^- in blue solutions of alkali polysulfides in
hexamethylphosphoramide. Inorg. Chem. 11, 2525.

Cook, A. F., Franklin, F. A. and Palluconi, F. D. (1973). Saturn's rings-
A survey. Icarus 18, 317-337.

Delsemme, A. H. and Miller, D. C. (1970). Physico-Chemical phenomena in
comets - II: Gas absorption in the snows of the nucleus. Planet.

Space Sci. 18, 717-730.

Delsemme, A. H. and Wenger, A. (1970). Physico-Chemical phenomena in
comets - I: Experimental study of snows in a cometary environment.
Planet. Space Sci. 18, 709-715.

Elias, J. H. (1972). Masters Thesis, Massachusetts Institute of Technology.

Estermann, I. (1955). Gases at low densities. Thermodynamics and Physics
of Matter, 2. High Speed Aerodynamics and Jet Propulsion.

Feher, F. (1963). Handbook of Preparative Inorganic Chemistry. 1, 2nd
ed., G. Brauer, editor.

Feher, F. and Münzer, H. (1963). Ber, 96, 1131.

Fink, U., Dekkers, N. H. and Larson, H. P. (1973). Infrared spectra of the
Galilean satellites of Jupiter. Astrophys. J. 179, #3, pt. 2, L155.

Franklin, F. A. and Cook, A. F. (1965). Optical properties of Saturn's
rings, II: Color phase curves of the two bright rings. Astron. J. 70,
704-720.

Fredrick, L. W. (1963). On the infrared reflectivity of Saturn's rings.
(abstract) PASP 75, 414.

Freund, T., Adler, S. and Sparrow, C. (1953). A preliminary magnetic study
of purple sulfur. J. Chem. Phys. 21, 180.

Gaffey, M. J. (1973). Doctoral Thesis, Massachusetts Institute of Technology.

Giggenbach, W. (1968). On the nature of the blue solutions of sulfur. J.
Inorg. Nuclear Chem. 30, 3189-3201.

Giggenbach, W. (1971a). The blue solutions of sulfur in water at elevated
temperatures. Inorg. Chem. 10, 1306.

Giggenbach, W. (1971b). The blue solutions of sulfur in salt melts. Inorg.
Chem. 10, 1308.

Giggenbach, W. (1972). Optical spectra and equilibrium distribution of

polysulfide ions in aqueous solutions at 20°. *Inorg. Chem.* <u>11</u>, 1201.

Giggenbach, W. (1973). The blue supersulfide ion, S_2^-. *JSC Dalton*, 729-731.

Gillespie, R. J., Passmore, J., Ummat, P. K., and Vaidya, O. C. (1971). Polyatomic cations of sulfur. I. Preparation and properties of S_{16}^{2+}, S_8^{2+} and S_4^{2+}. *Inorg. Chem.* <u>10</u>, 1327.

Gillespie, R. J. and Ummat, P. K. (1972). Polyatomic cations of sulfur. III. the solutions of sulfur in oleum. *Inorg. Chem.* <u>11</u>, 1674.

Handbook of Chemistry and Physics (1971). The Chemical Rubber Co., Cleveland, Ohio.

Hansen, O. L. (1972). Doctoral Thesis, California Institute of Technology.

Hertzberg, G. (1966). Infrared and Raman Spectra. (D. Van Nostrand Co., Inc., Princeton, New Jersey).

Huguenin, R. L. (1973). Doctoral Thesis, Massachusetts Institute of Technology.

Hunt, G. R. and Salisbury, G. W. (1970). Visible and near infrared spectra of minerals and rocks: Silicate minerals. *Mod Geol.* 1, 283-300.

Ingram, D. J. E. and Symonds, M. C. R. (1957). Solution of sulfur in oleum. Part I. Electron-spin resonance of solutions of sulfur in oleum. *J. Chem. Soc.* 2437.

International Critical Tables of Numerical Data, Physics, Chemistry and Technology (1926-1933). National Research Council.

Irvine, W. M. and Lane, A. P. (1973). Photometric properties of Saturn's rings. Icarus 18, 171-173.

Johnson, T. V. (1969). Doctoral Thesis, California Institute of Technology.

Johnson, T. V. and McCord, T. B. (1970). Galilean satellites: The spectral reflectivity 0.30-1.10 microns. Icarus 13, 37-42.

Kieffer, H. H. (1968). Doctoral Thesis, California Institute of Technology.

Kieffer, H. H. (1970). Spectral reflectance of CO_2-H_2O frosts. J. Geophys. Res. 75, 501-509.

Kieffer, H. H. and Smythe, W. (1974). Icarus, in press.

Krinov, E. L. (1947). Spectral reflectance properties of natural surfaces. Tech. Translations, 439.

Kuiper, G. P., Cruikshank, D. P. and Fink, U. (1970). As reported in Sky and Telescope 39.

Lebofsky, L. A., Johnson, T. V. and McCord, T. B. (1970). Saturn's rings: Spectral reflectivity and compositional implications. Icarus 13, 226-230.

Lewis, J. S. (1969). The clouds of Jupiter and the NH_3-H_2O and NH_3-H_2S systems. Icarus 10, 365.

Lewis, J. S. (1971a). Satellites of the outer planets: Thermal models. Science 172, 1127.

Lewis, J. S. (1971b). Satellites of the outer planets: Their physical and chemical nature. Icarus 15, 174-185.

Lewis, J. S. (1972). Low-temperature condensation from the Solar Nebula. Icarus 16, 241-252.

Lewis, J. S. (1973). Chemistry of the outer solar system. Space Science Reviews 14, 401.

Lewis, J. S. and Prinn, R. G. (1970). Jupiter's clouds: Structure and composition. Science 169, 472.

Lewis, J. S. and Chapman, C. R. (1973). Personal communication.

Lumme, K. (1970). On the photometric properties of Saturn's rings. Astrophys. Space Sci. 8, 90-101.

MacColl, R. and Windwer, S. Spectroscopy of sulfur in ethylenediamine. J. Phys. Chem. 74, 1261.

McLaughlin, S. D. and Marshall, D. J. (1970). Paramagnetic resonance of sulfur radicals in synthetic sodalites. J. Phys. Chem. 74, 1359.

McCord, T. B. (1968). A double beam astronomical photometer. Appl. Optics 7, 475-478.

McCord, T. B. and Adams, J. B. (1969). Spectral reflectivity of Mars. Science 163, 1058-1060.

McCord, T. B., Adams, J. B. and Johnson, T. V. (1970). Asteroid Vesta: Spectral reflectivity and compositional implications. Science 168, 1445-1447.

McCord, T. B. and Johnson, T. V. (1970). The spectral reflectivity of the Lunar surface (0.30-2.50 microns) and implications for remote mineral analysis. Science 169, 855-858.

McCord, T. B., Johnson, T. V. and Elias, J. H. (1971). Saturn and its satellites: Spectrophotometry 0.3-1.1 microns and compositional implications. Ap. J. 165, 413-424.

Meyer, B., Gouterman, M., Jensen, D., Donmen, T. V., Spitzer, K. and Stroyer-Hansen, T. (1972). Advan Chem. Ser. No. 110, 53.

Meyer, B., Oommen, T. V. and Stroyer-Hansen, T. (1972). J. Mol. Spectrosc. 42, 335.

Meyer, B. and Spitzer, K. (1972). Extended huckel calculations in the color of sulfur chains and rings. J. Phys. Chem. 76, 2274.

Miller, S. L. (1961). The occurence of gas hydrates in the solar system. Proc. NAS 47, 1798-1808.

Moroz, V. I. (1968). Physics of planets. NASA Tech. Trans. 518.

Morrison, D. and Cruikshank, D.P. (1973). Thermal properties of the Galilean satellites. Icarus 18, 224-236.

Münch, G. (1971). Personal communication.

Ockman, N. (1957). Doctoral Thesis, University of Michigan.

Ockman, N. (1958). The infrared and raman spectra of ice. Astron. Phys. 7, 199-220.

Owen, T. (1965). Saturn's rings and the satellites of Jupiter: Interpretations and infrared spectra. Science 149, 974-975.

Pilcher, C. B., Chapman, C. R., Lebofsky, L. A. and Kieffer, H. H. (1970). Saturn's rings: Identification of water frost. Science 167, 1372-1373.

Pilcher, C. B., Ridgeway, S. T. and McCord, T. B. (1972). Galilean satellites: Identification of water frost. Science 178, 1087.

Radford, H. E. and Rice, F. O. (1960). Green and purple sulfur: electron spin resonance studies. J. Chem. Phys. 33, 774.

Rice, F. O. and Ditter, J. (1953). Green sulfur, a new allotropic form. JACS 75, 6066-6068.

Rice, F. O. and Sparrow, C. (1953). Purple sulfur, a new allotropic form. JACS 75, 848-850.

Schultz, E. D. and Holland, A. C. Planetary aeronomy VII. The solar flux incident at the top of atmospheres of Earth and neighboring planets

for the spectral region 50 Å to 3000 Å. Geophysics Corporation of
America. GCA Technical Report No. 62-14-N. NASA Contractor report
CR-11.

Shain, G. A. (1935). On the intensity distribution of the spectrum of
Saturn and its rings. Obs. Cir. 9-16.

Stillings, M., Symons, M. C. R. and Wilkinson, J. G. (1971a). Electron
spin resonance studies of sulfur in oleum. The ion S_8^+. Chem. Comm.,
372.

Stillings, M., Symons, M. C. R. and Wilkinson, J. G. (1971b). Unstable
intermediates. Part CII. Electron spin resonance studies of solutions
of sulfur in oleum: the S_8^+ cation. J. Chem. Soc. (A), 3201.

Symons, M. C. R. (1957). Solutions of sulfur in oleum. Part II. Visible
and ultraviolet absorption spectra. J. Chem. Soc. 2440.

Symons, M. C. R. and Wilkinson, J. G. (1972). Nature of the paramagnetic
cation in solutions of sulfur in oleum. Nature Phys. Sci. 236, 126.

Vanderberg (1954). Doctoral Thesis, University of California at Los
Angeles.

Veverka, J. F. (1970). Doctoral Thesis, Harvard University.

Veverka, J. F. (1971). Polarization measurements of the Galilean satellites
of Jupiter. Icarus 14, 355-359.

Watson, K., Murray, B. C., and Brown, H. (1961). The behavior of volatiles
on the lunar surface. J. Geophys. Res. 66, 3033-3045.

Watson, K., Murray, B. C., and Brown, H. (1963). Stability of volatiles in
the solar system. Icarus 1, 317-327.

Younkin, R. L. and Münch, G. (1966). Visible and near infrared spectro-
photometry of Saturn's rings. (abstract) Ap. J. 71.